CHARACTERIZATION OF NOVEL CANNABINOID LIGANDS AND RECEPTOR-RECEPTOR INTERACTIONS WITH A FOCUS ON THE TYPE 2 CANNABINOID RECEPTOR

A Thesis Submitted to the
College of Graduate and Postdoctoral Studies
In Partial Fulfillment of the Requirements
For the Degree of Master of Science
In the College of Pharmacy and Nutrition
University of Saskatchewan
Saskatoon

By

Kawthar Ahmed Mohamed

Permission to Use

In presenting this thesis/dissertation in partial fulfillment of the requirements for a Postgraduate degree from the University of Saskatchewan, I agree that the Libraries of this University may make it freely available for inspection. I further agree that permission for copying of this thesis/dissertation in any manner, in whole or in part, for scholarly purposes may be granted by the professor or professors who supervised my thesis/dissertation work or, in their absence, by the Head of the Department or the Dean of the College in which my thesis work was done. It is understood that any copying or publication or use of this thesis/dissertation or parts thereof for financial gain shall not be allowed without my written permission. It is also understood that due recognition shall be given to me and to the University of Saskatchewan in any scholarly use which may be made of any material in my thesis/dissertation.

DISCLAIMER

Reference in this thesis/dissertation to any specific commercial products, process, or service by trade name, trademark, manufacturer, or otherwise, does not constitute or imply its endorsement, recommendation, or favoring by the University of Saskatchewan. The views and opinions of the author expressed herein do not state or reflect those of the University of Saskatchewan, and shall not be used for advertising or product endorsement purposes.

Requests for permission to copy or to make other uses of materials in this thesis/dissertation in whole or part should be addressed to:

Head of the College of Pharmacy and Nutrition
University of Saskatchewan
Health Sciences Building, 107 Wiggins Road
Saskatoon, Saskatchewan S7N 5E5 Canada

OR

Dean
College of Graduate and Postdoctoral Studies
University of Saskatchewan
116 Thorvaldson Building, 110 Science Place
Saskatoon, Saskatchewan S7N 5C9 Canada

Abstract

Cannabis and cannabinoids are currently being investigated for their potential utility as therapeutics in various illnesses. Of the two cannabinoid receptors that have been identified thus far, the type 2 cannabinoid receptor (CB2R) is of growing interest due to its potential immunomodulatory and anti-inflammatory activities. Similarly, the orphan receptor G protein-coupled receptor 55 (GPR55) is known to interact with cannabinoids and has potential for its anti-inflammatory activity. CB2R- and GPR55-mediated therapeutics may provide safer side effect profiles and avoid central nervous system (CNS)-mediated psychoactivity associated with the activation of the type 1 cannabinoid receptor (CB1R). The identification of CB2R-specific ligands has been challenging given the high degree of similarity between CB1R and CB2R. Exploiting novel paradigms in G protein-coupled receptor (GPCR) signaling, such as biased agonism, bitopic ligands, and receptor dimerization, may provide a new avenue for the development of clinically effective CB2R-selective ligands. Characterizing a diverse array of ligands, including orthosteric agonists, allosteric modulators, bitopic ligands, and compound metabolites may improve our ability to identify novel drug candidates. In this study, we explored the *in vitro* pharmacological properties of novel GPR55 and CB2R ligands, cannabinoid-orexin receptor heterodimers and phytocannabinoid metabolites using Chinese hamster ovary (CHO)-K1 cells expressing human CB1R, CB2R, GPR55, orexin receptor type 1 (OX1R), or orexin receptor type 2 (OX2R) plasmids. Our study revealed that novel cannabinoids can be characterized using pharmacological data and drug design. Relatively little is known about the specific pharmacological properties and mechanisms of ligands and receptor interactions at CB2R. A better understanding of these pharmacodynamics may be useful in the development of CB2R-selective therapeutics for illnesses associated with inflammation and/or pain.

Acknowledgements

There are many people who have supported me on this journey. First and foremost, I would like to thank my supervisor, Dr. Robert Laprairie. When I was an undergraduate student looking to get hands-on experience in the world of research, you took me under your wing and afforded me more opportunities than I could have imagined. Over the years, your continuous support, guidance, and immense knowledge have shaped me into the scientist that I am today. I am forever grateful to have you as a mentor.

I would also like to extend my deepest gratitude to my advisory committee members Dr. Jane Alcorn, Dr. Ildiko Badea, and Dr. Erique Lukong. I am extremely appreciative of their insightful feedback and expertise which were invaluable to the creation of this thesis.

I would also like to thank the Natural Sciences and Engineering Research Council of Canada and the University of Saskatchewan's College of Pharmacy and Nutrition for financial support during my studies.

Finally, none of this would have been possible without the love and encouragement of my family. To my parents, thank you for believing in me and supporting my endeavors. My accomplishments are a testament to the values and work ethic you instilled in me. To my sisters, thank you for always being there for me and inspiring me to achieve my dreams.

Table of Contents

List of Tables

List of Figures

List of Abbreviations

Δ^9-THC	Δ^9-tetrahydrocannabinol
11-OH-THC	11-hydroxy-THC
2-AG	2-arachidonoylglycerol
5-HT_{1A}R	Serotonin 5-HT_{1A} receptor
5-HT_{2A}R	Serotonin 5-HT_{2A} receptor
6-OH-CBD	6-hydroxy-CBD
7-OH-CBD	7-hydroxy-CBD
7TMR	Seven transmembrane receptor
A_{2A}R	Adenosine A_{2A} receptor
AC	Adenylate cyclase
AEA	*N*-arachidonoylethanolamine
ANOVA	Analysis of variance
AT1R	Angiotensin II type 1 receptor
βAR	β-adrenergic receptor
β2AR	β2-adrenergic receptor
β-gal	β-galactosidase
BAM	Biased allosteric modulator
BBB	Blood brain barrier
BRET	Bioluminescence resonance energy transfer
C. sativa	*Cannabis sativa*
cAMP	Cyclic adenosine monophosphate
CasR	Calcium-sensing receptor
CB1R	Type 1 cannabinoid receptor
CB2R	Type 2 cannabinoid receptor
CB3R	Type 3 cannabinoid receptor
CBD	Cannabidiol
CHO	Chinese hamster ovary
CI	Confidence interval
CNS	Central nervous system
Co-IP	Co-immunoprecipitation
COOH-CBD	7-carboxy-CBD
COOH-THC	11-carboxy-THC
CRC	Concentration-response curve
CREB	cAMP response-element binding protein
CCR5	C-C chemokine receptor type 5
CXCR4	C-X-C chemokine receptor type 4

CYP450	Cytochrome P450
D_1	Dopamine 1 receptor
D_2	Dopamine 2 receptor
Da	Dalton
DAG	Diacylglycerol
DAGL	Diacylglycerol lipase
DMEM	Dulbecco's Modified Eagle Medium
DMSO	Dimethyl sulfoxide
DORA	Dual orexin receptor antagonist
EFC	Enzyme fragment complementation
ECS	Endocannabinoid system
ERK1/2	Extracellular signal-regulated kinase 1/2
FAAH	Fatty acid amine hydrolase
FBS	Fetal bovine serum
FDA	Food and Drug Administration
FRET	Fluorescence resonance energy transfer
FSK	Forskolin
GABA	γ-aminobutyric acid
GAP	GTPase-activating protein
GDP	Guanosine diphosphate
GEF	Guanine exchange factor
GPCR	G protein-coupled receptor
GPR119	G protein-coupled receptor 119
GPR18	G protein-coupled receptor 18
GPR55	G protein-coupled receptor 55
GRK	GPCR kinase
GTP	Guanosine triphosphate
HIV	Human immunodeficiency virus
ICV	Intracerebroventricular
IL	Interleukin
INF	Interferon
IP_3	Inositol trisphosphate
JNK	c-Jun N-terminal kinase
LPI	Lysophosphatidylinositol
mAChR	Muscarinic acetylcholine receptor
MAGL	Monoacylglycerol lipase
MAPK	Mitogen-activated protein kinase
MD	Molecular dynamics

MOR	μ-opioid receptor
n.c	Not converged
NAL	Neutral allosteric ligand
NAM	Negative allosteric modulator
NAPE-PLD	N-acyl phosphatidylethanolamine phospholipase D
NF-κB	Nuclear factor kappa B
NSAID	Non-steroidal anti-inflammatory drug
OX1R	Orexin receptor type 1
OX2R	Orexin receptor type 2
OXA	Orexin A
OXB	Orexin B
PAM	Positive allosteric modulator
PBS	Phosphate-buffered saline
Pen/Strep	Penicillin-streptomycin
pERK1/2	Phosphorylated ERK1/2
PI3K	Phosphoinositide-3 kinase
PKA	Protein kinase A
PKB	Protein kinase B
PKC	Protein kinase C
PLC	Phospholipase C
SBDD	Structure-based drug design
SEM	Standard error of the mean
SORA	Single orexin receptor antagonist
SSR5	Somatostatin receptor 5
TEAE	Treatment-emergent adverse event
TGF	Transforming growth factor
TNF	Tumor necrosis factor

Chapter 1: Introduction

The type 1 and type 2 cannabinoid receptors (CB1R, CB2R) have come to be seen as highly promising drug targets. Characterizing novel cannabinoid ligands may lead to the development of new drug candidates for inflammation and pain, among other conditions. The focus of this thesis was the *in vitro* pharmacological characterization of an array of cannabinoid modulators, agonists, and receptor-receptor interactions.

Over the past two decades, Cannabis and cannabinoid-based medicines have emerged as a promising avenue for the development of novel therapeutics for various conditions[1,2]. Cannabinoids are compounds whose structure and/or function are similar to that of Δ^9-tetrahydrocannabinol (Δ^9-THC), a plant-derived cannabinoid (i.e. phytocannabinoid) and primary psychoactive constituent of *Cannabis sativa* (*C. sativa*)[3]. Cannabinoids mediate their physiological actions through a complex biological system termed the endocannabinoid system (ECS) [4,5]. The ECS consists of three main components: cannabinoid receptors, endogenous cannabinoids (i.e. endocannabinoids), and enzymes responsible for the synthesis and degradation of endocannabinoids[6,7]. Cannabinoid receptors are a group of at least two G protein-coupled receptors (GPCRs), with CB1R and CB2R having been validated as targets of cannabinoids, though research suggests the existence of additional cannabinoid receptors[8–13]. Endocannabinoids, the endogenous ligands for CB1R and CB2R, are synthesized "on demand" from cell membrane lipids, such as arachidonic acid [14–17]. Although various endocannabinoids have been identified, *N*-arachidonoylethanolamine (AEA)/anandamide, and 2-arachidonoylglycerol (2-AG) represent the most intensively studied endocannabinoids[4,16,18]. Lastly, biosynthetic enzymes, such as N-acyl

phosphatidylethanolamine phospholipase D (NAPE-PLD) and diacylglycerol lipase (DAGL), and catabolic enzymes, such as fatty acid amine hydrolase (FAAH) and monoacylglycerol lipase (MAGL), play a key role in the initiation and termination of endocannabinoid signaling[8,19–22].

The ECS is implicated in the modulation of various physiological processes such as synaptic plasticity, appetite, energy balance, pain, memory and emesis[6,10,14,23,24]. Furthermore, cannabinoids are being investigated as potential treatments for a wide array of conditions including chronic pain, inflammatory bowel diseases, obesity, diabetes, neurodegenerative diseases (e.g. Huntington's disease, Alzheimer's disease, multiple sclerosis), osteoporosis, cancer and epilepsy[4,7,8,23,25–27]. Though these indications appear encouraging, only 4 cannabinoid-based therapies (Sativex, Marinol/Syndros, Cesamet, and Epidiolex) have been approved for clinical use[19,28–31]. The ECS and cannabinoid receptor signaling are both highly complex. These complexities speak to why the development of cannabinoid medicines has proven to be so difficult.

1.1 G protein-coupled receptors (GPCRs)

Cannabinoid receptors are G protein-coupled receptors (GPCRs)[32]. GPCRs, also known as seven transmembrane receptors (7TMRs), are a superfamily of more than 800 membrane proteins implicated in various physiological processes [33–36]. GPCRs are critical in cellular signaling, acting as "physical conduits" by responding to various external stimuli such as photons, ions, odorants, hormones and neurotransmitters[37–40]. At least 30% of all drugs approved by the United States Food and Drug Administration (FDA) target GPCRs, further exemplifying the importance of this class of proteins[41–43].

There are 6 groups of GPCRs: rhodopsin-like (class A), secretin-like (class B), metabotropic glutamate (class C), fungal mating pheromone (class D), cyclic AMP receptors (class E), and frizzled/smoothened (class F)[44]. Class A GPCRs, which include the cannabinoid receptors, represent the largest group of GPCRs [16,40,45]. Nevertheless, all GPCRs share a common structural motif consisting of a seven transmembrane α-helices with alternating extracellular and intracellular loops[38,46,47].

1.1.1 GPCR activation

GPCR activation is a multi-step process. Following the binding of a ligand at an extracellular site on the receptor, a conformational change is induced in the cytoplasmic portions of the receptor, exposing an intracellular pocket critical for interacting with signaling proteins such as heterotrimeric G proteins, GPCR kinases (GRKs), and βarrestins[36,43,48]. G proteins consist of α, β, and γ subunits and when inactive, the Gα subunit is bound to the Gβγ subunit and to guanosine diphosphate (GDP)[46]. Ligand binding results in the activation of guanine exchange factors (GEFs) which promotes the exchange of GDP for guanosine triphosphate (GTP) on the Gα subunit[49,50]. This subsequently leads to the dissociation of the Gβγ subunit from the Gα subunit; both subunits are now free to initiate signaling cascades involving different downstream proteins (Figure 1-1)[40,48,51]. Depending on which Gα isoform is present, Gα subunits may activate adenylate cyclase (AC) ($G\alpha_s$), inhibit AC ($G\alpha_{i/o}$), activate phospholipase C (PLC) ($G\alpha_{q/11}$), or modulate the activity of small GTPases such as Ras and Rho and mitogen-activated protein kinase (MAPK) cascades ($G\alpha_{12/13}$, $G\alpha_{q/11}$)[46,52]. Gβγ subunits are also implicated in GPCR signal transduction by regulating ion channels, AC activity, MAPK cascades and interacting with GRKs[48,53,54]. Downstream

signaling by G protein subunits is terminated through GTPase-activating proteins (GAPs)[55]. GAPs facilitate G protein inactivation by ameliorating the intrinsic GTP hydrolysis activity of Gα subunits, resulting in the conversion of GTP to GDP[48,56].

1.1.2 GPCR signaling

CB1R and CB2R primarily couple to $G\alpha_{i/o}$ G proteins (Figure 1-1)[16,57]. Consequently, their activation results in the inhibition of AC, the enzyme responsible for the production of cyclic adenosine monophosphate (cAMP)[58]. Cannabinoid receptor activation is thus associated with reduced levels of cAMP[59]. As a second messenger, cAMP is a critical effector of downstream signaling pathways[48,50]. Reduced levels of cAMP impair the activity of protein kinase A (PKA), which has greater implications on signal transduction due to the regulatory role of PKA on Raf-1 kinase[8,16,60].

Cannabinoid receptors are also known to promote the phosphorylation of extracellular signal-regulated kinases 1 and 2 (ERK1/2), a member of the serine-threonine MAPK family (Figure 1-1)[11,46]. ERK1/2 is implicated in various physiological processes such as cell cycle progression, cell migration, apoptosis, and cytokine production[57,61]. Additionally, cannabinoid receptors regulate the activity of other MAPKs such as p38 kinase and c-Jun N-terminal kinase (JNK)[7,62,63]. Though not widely researched, additional signaling cascades of cannabinoid receptors may involve phosphoinositide-3 kinase (PI3K)/Akt, Akt kinase/protein kinase B (PKB), cAMP response-element binding protein (CREB), and nuclear factor kappa B (NF-κB)[8,24,57,64–66].

1.1.3 Regulation of GPCR signaling

Activated GPCRs are downregulated by a class of proteins called arrestins[51]. Four isoforms [arrestin-1, arrestin-2 (i.e. βarrestin1), arrestin-3 (i.e. βarrestin2), and arrestin-4] have been identified, though only βarrestin1 and βarrestin2 are implicated in cannabinoid receptor signaling (Figure 1-1)[48,49,58]. βarrestin recruitment is facilitated by GRK-dependent phosphorylation of the GPCR on its C-terminus and intracellular loops[36,41,67]. Binding of βarrestin to the GPCR ultimately facilitates receptor desensitization, trafficking and internalization by targeting GPCRs to clathrin-coated pits for endocytosis[50,68–70]. βarrestin can also initiate downstream signaling cascades involving Src kinases, MAPKs, NF-κB, and PI3K in a G protein-independent manner, thus representing unique scaffolding proteins with dualistic roles in the initiation and termination of signaling[36,39,50,65,70].

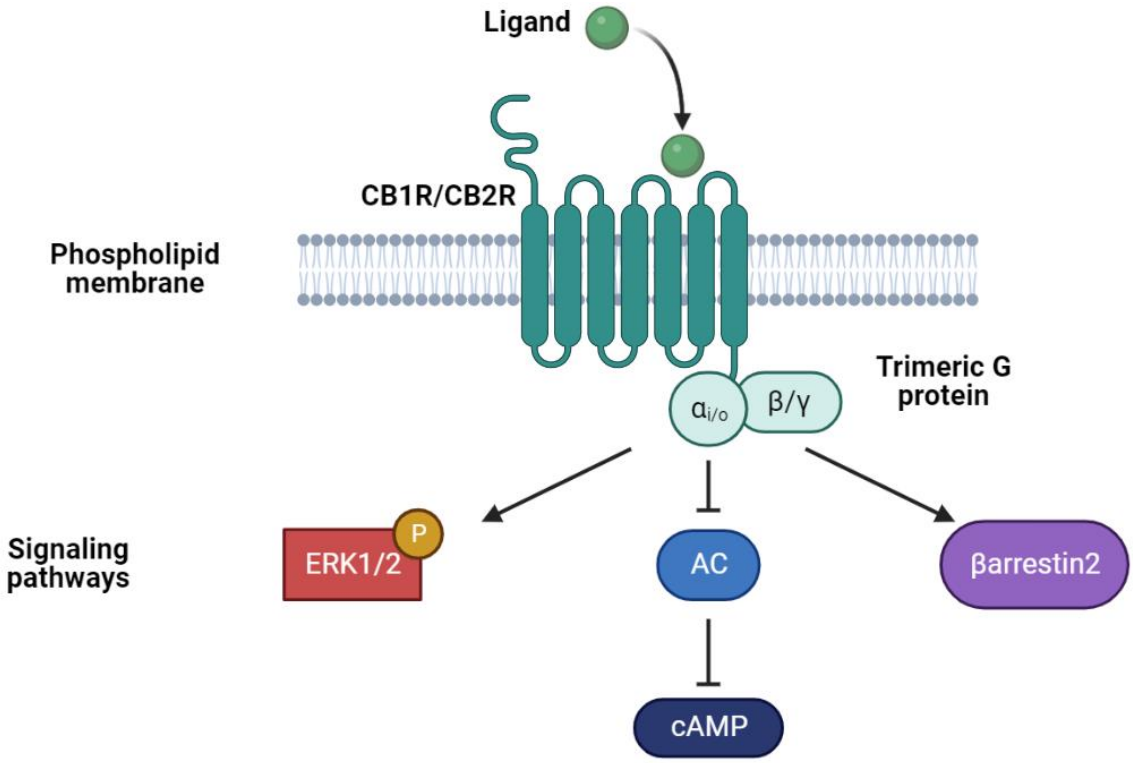

Figure 1-1. Main signaling pathways implicated in cannabinoid receptor-dependent signaling. Following ligand binding and subsequent receptor activation, cannabinoid receptors (e.g. CB1R, CB2R) mediate various downstream signaling cascades. By coupling to $G\alpha_{i/o}$ G proteins, cannabinoid receptors inhibit adenylate cyclase (AC), leading to reduced levels of the second messenger cyclic adenosine monophosphate (cAMP). Cannabinoid receptor activation also leads to increased phosphorylation of extracellular signal-regulated kinases 1 and 2 (ERK1/2). Cannabinoid receptors are downregulated following the recruitment of βarrestin2, an intracellular protein which facilitates receptor desensitization, trafficking, and internalization. Adapted from "GPCR Effector Pathways", by BioRender.com (2023). Retrieved from https://app.biorender.com/biorender-templates

1.2 Cannabinoid receptors

1.2.1 CB1R

CB1R is among the most abundant GPCRs in the central nervous system (CNS), with prominent expression in the hippocampus, basal ganglia, brainstem, cerebellum, cortex, substantia nigra, amygdala and striatum[5,8,14,71]. Though less prevalent in the periphery, CB1R expression has also

been identified in the heart, liver, pancreas, small intestine, adipocytes, skeletal muscle, uterus, and testis[4,12,17]. Its high CNS expression implicates CB1R in most of the psychoactive and behavioural effects associated with cannabinoids like Δ^9-THC[13,14,32,72,73].

In general, CB1R functions as a neuromodulatory receptor, preventing neurotransmitter release at presynaptic terminals by regulating the activity of voltage-gated calcium channels and inwardly rectifying potassium channels[3,4,16,17]. CB1R activation is involved in nociception, anxiety, memory, motor activity, reward, appetite, and energy homeostasis[6,8,11,23,24,74]. As such, CB1R has become an attractive target for novel treatments for seizures, neurodegenerative disorders, smoke cessation, obesity, and pain management[14,72,75,76].

Unfortunately, the therapeutic utility of CB1R appears to be limited, a caveat first exposed by the CB1R antagonist/inverse agonist SR141716A (rimonabant) [7,77,78]. Rimonabant effectively promoted weight loss and improved lipid and glucose metabolism, thus representing a promising novel treatment for obesity[15,23,79]. However, within two years of approval, rimonabant's clinical use was suspended owing to adverse effects (e.g. anxiety, depression, and suicide) propagated by blockade of centrally located CB1R [39,80–83]. The development of CB1R antagonists/inverse agonists which lack blood brain barrier (BBB) penetrance may be a useful approach in avoiding CNS-mediated psychoactivity, though the modifications required to peripherally restrict these ligands may impair their effectiveness and applicability as anti-obesity agents[15,80].

1.2.2 CB2R

CB2R has limited expression throughout the CNS, and is generally restricted to the periphery, predominantly throughout the immune system[8,84]. Peripheral CB2R expression has been observed

in various tissues and cell types including T cells, B cells, NK cells, eosinophils, macrophages, spleen, tonsils, thymus, adipose tissue, intestine, testis, skeletal muscle, pancreatic islet cells, pulmonary endothelial cells, bone, and the trabecular meshwork of the eyes[4,23,32,62,71,85,86]. CB2R expression may be limited to immune cells of the CNS (e.g. microglia, astrocytes), though some studies noted the presence of CB2R in the brainstem, cortex, and spinal cord[66,85,87]. Furthermore, it appears that pathological states drive CNS CB2R expression as CB2R is reportedly absent from healthy brain microglia but is present in neuroinflammatory conditions, such as in the microglia of Alzheimer's brain tissue and in astrocytes and microglia of multiple sclerosis plaques[12,62,71,86,88]. Induction of CB2R expression is not restricted to the CNS, as CB2R expression has also been observed in hepatic myofibroblasts during cirrhosis but not in a healthy liver[62].

CB2R is an immunomodulatory receptor. It is involved in the regulation of cytokine release and its activation prevents the release of pro-inflammatory cytokines [e.g. interleukin (IL)-2, IL-12, IL-17, interferon (INF)-γ, tumor necrosis factor (TNF)-α] and enhances the release of anti-inflammatory cytokines [e.g IL-4, IL-10, transforming growth factor (TGF)-β][4,23,57,61,84,89]. Unlike CB1R, no clear consensus exists on whether CB2R couples to voltage-gated calcium channels or inwardly rectifying potassium channels[7,59,90].

The anti-inflammatory capacities of CB2R, coupled with its diverse pattern of expression, make CB2R an attractive target for various conditions such as pain (e.g. acute, chronic, inflammatory, neuropathic, etc.), cancer, osteoporosis, hyperinsulinemia, hypertriglyceridemia, diabetic neuropathy and nephropathy, hypertension, liver cirrhosis, inflammatory bowel diseases, atherosclerosis, stroke, and neurodegenerative disorders (e.g. multiple sclerosis, amyotrophic lateral sclerosis, Alzheimer's disease, Parkinson's disease, Huntington's disease)[8,19,23,27,62,65,86].

The anti-nociceptive and anti-inflammatory effects of CB2R ligands have been previously explored in preclinical studies[7,74,77,91,92].

Given the concerns regarding undesirable psychiatric side effects by CB1R-acting ligands, targeting CB2R may present a novel avenue for producing safe yet effective cannabinoid therapies[19,29,81,82]. It is thought that the activation of CB2R is not associated with psychoactivity due to the low level of CB2R expression in the CNS[4,28,62]. The finding that CB2R agonists fail to elicit centrally-mediated cannabimimetic effects, such as catalepsy, hypoactivity, and hypothermia, gives credence to this[87,93]. Additionally, the inducible nature of CNS CB2R during neuroinflammation further highlights the attractiveness of CB2R, especially as a "disease-associated target"[4,6,29,66].

A major caveat in exploiting the therapeutic potential of CB2R is the challenge of developing ligands which activate CB2R and not CB1R. Though the overall receptor homology of CB1R and CB2R is only 44%, the homology increases to 68% in the region containing their ligand binding domains, which contributes to the difficulties in designing CB2R-selective ligands[27,32]. Synthetic cannabinoids like CP55,940, WIN 55,212-2, and HU-210 are potent agonists of CB2R but also have affinity for CB1R; as such they are considered non-selective cannabinoid receptor agonists[62,94]. Ligands with greater selectivity for CB2R were eventually developed. This includes both agonists (e.g. AM-1241, GW405833, HU-308, JWH-015, JWH-133) and antagonists (e.g. AM-630, SR144528) of CB2R[11,59,62,90]. Additionally, numerous pharmaceutical companies have developed CB2R-selective agonists that have reached phase 1 and 2 clinical trials[88,93]. Nevertheless, the translation of compelling preclinical results into desirable clinical outcomes has failed for many of these ligands[95,96].

With the overall aim of developing clinically effective CB2R-selective ligands, it may be advantageous to exploit novel paradigms in GPCR signaling, namely biased agonism, bitopic ligands, and receptor dimerization. In addition to CB2R, there may be other putative cannabinoid receptors whose activity could be modulated for therapeutic benefit without the psychoactivity of CB1R ligands.

1.3 Orphan cannabinoid receptors

G protein-coupled receptor 55 (GPR55) is an orphan receptor undergoing investigation as a potential cannabinoid receptor[11,74]. Its classification as a type 3 cannabinoid receptor (i.e. CB3R) has been challenged by findings that GPR55 exhibits low receptor homology with CB1R (13.5%) and CB2R (14.4%) and couples to $G\alpha_{12/13}$ proteins, leading to a different signaling paradigm than commonly observed for cannabinoid receptors[13,52,61]. Nevertheless, various cannabinoids have been shown to act at GPR55[10,11,17,62,97]. Lysophosphatidylinositol (LPI) is the proposed endogenous ligand of GPR55[9,98]. GPR55 is expressed in the CNS (e.g. hypothalamus, striatum, hippocampus, olfactory bulb), bone marrow, spleen, vascular endothelial cells, and immune cells and thus may be a useful target for treating osteoporosis, pain, cancer, and sepsis[11,61,74,75,98].

Additional orphan receptors, namely G protein-coupled receptor 18 (GPR18) and G protein-coupled receptor 119 (GPR119), are implicated in cannabinoid signaling[75]. GPR18 is expressed throughout the immune system and in organs such as the lungs and testis and has been proposed to be a useful prognostic tool in cancer as it is involved in cell migration, proliferation, and apoptosis[10,99–101]. GPR119 is expressed in the pancreas and gastrointestinal tract and appears to be a promising target for novel therapeutics treating obesity and diabetes [102–105]. Further research is required to fully elucidate the roles of these receptors and uncover their true classification.

1.4 Biased agonism

Biased agonism, also known as biased signaling, functional selectivity, or stimulus trafficking, refers to the ability of different ligands to preferentially activate certain signaling pathways over others at the same GPCR[35,106,107]. Unlike balanced ligands, which activate all signaling pathways to similar extents, biased ligands stabilize specific receptor conformations that facilitate receptor interactions with intracellular proteins and are critical for the activation or inhibition of specific downstream signaling pathways (Figure 1-2)[7,17,45,69,83]. Biased signaling can occur at either the ligand-, receptor-, or system-level[50,74]. A common approach to assessing whether a ligand displays biased agonism is to compare the levels of G protein-dependent and G protein-independent signaling induced by the ligand via G proteins and βarrestins, respectively[41,108,109]. Assays quantifying cAMP inhibition or [^{35}S]-GTPγS binding are often used to monitor G protein-dependent signaling while βarrestin recruitment is used as a measure of G protein-independent signaling[110].

The concept of biased agonism provides opportunity to develop agonists with safer side effect profiles by selectively activating therapeutically beneficial signaling pathways while avoiding those responsible for undesirable effects[35,91,111]. Biased agonists targeting μ-opioid receptors (MOR), β-adrenergic receptors (βAR) and the angiotensin II type 1 receptor (AT1R) have shown promising results. It has been suggested that the analgesic effects of opioids at MOR are mediated through the $G\alpha_{i/o}$ G protein whereas detrimental effects, namely respiratory depression and constipation, are mediated by βarrestin2 signaling[35,112]. Preclinical studies in mice and rats with the G protein-biased MOR agonist TRV130 allowed for a proof of concept as TRV130 mediated analgesia and produced less respiratory depression and constipation than morphine[113]. However, in a recent study with morphine, methadone, buprenorphine, fentanyl, oxycodone, and TRV130,

βarrestin2 engagement with MOR did not enhance respiratory depression and βarrestin2 may actually reduce analgesic tolerance through its interactions with MOR[114]. In another study, morphine and fentanyl produced respiratory depression and constipation in βarrestin2 knockout mice suggesting that these effects are mediated independently from βarrestin2 signaling[115]. These conflicting results demonstrate the need for additional research into the specific roles of G proteins and βarrestin2 on MOR-mediated effects, and whether these effects can be explained by bias, or if other factors (e.g. intrinsic efficacy) are at play[116,117]. Bias at βAR has been explored with antagonists, which can be used to treat heart failure[106]. Carvedilol, a βAR antagonist approved for the treatment of congestive heart failure, may mediate its cardioprotective effects through its bias towards βarrestin signaling[36,50,118]. AT1R is an attractive target in treating conditions such as hypertension, myocardial hypertrophy, and chronic heart failure[119]. βarrestin-biased ligands of AT1R, such as TRV120023 and TRV120027, stimulate the contractility of cardiac myocytes and avoid side effects associated with $G\alpha_{q/11}$ G protein activation (e.g. vasoconstriction, cardiac hypertrophy)[68,110,113,118]. In addition to these receptors, biased agonism has also been observed in cannabinoid, chemokine, and serotonin receptors[17,106,120]. Numerous phytocannabinoids, endocannabinoids, and synthetic cannabinoids have demonstrated G protein- and βarrestin2-biased agonism at CB1R and CB2R[110,111,121,122].

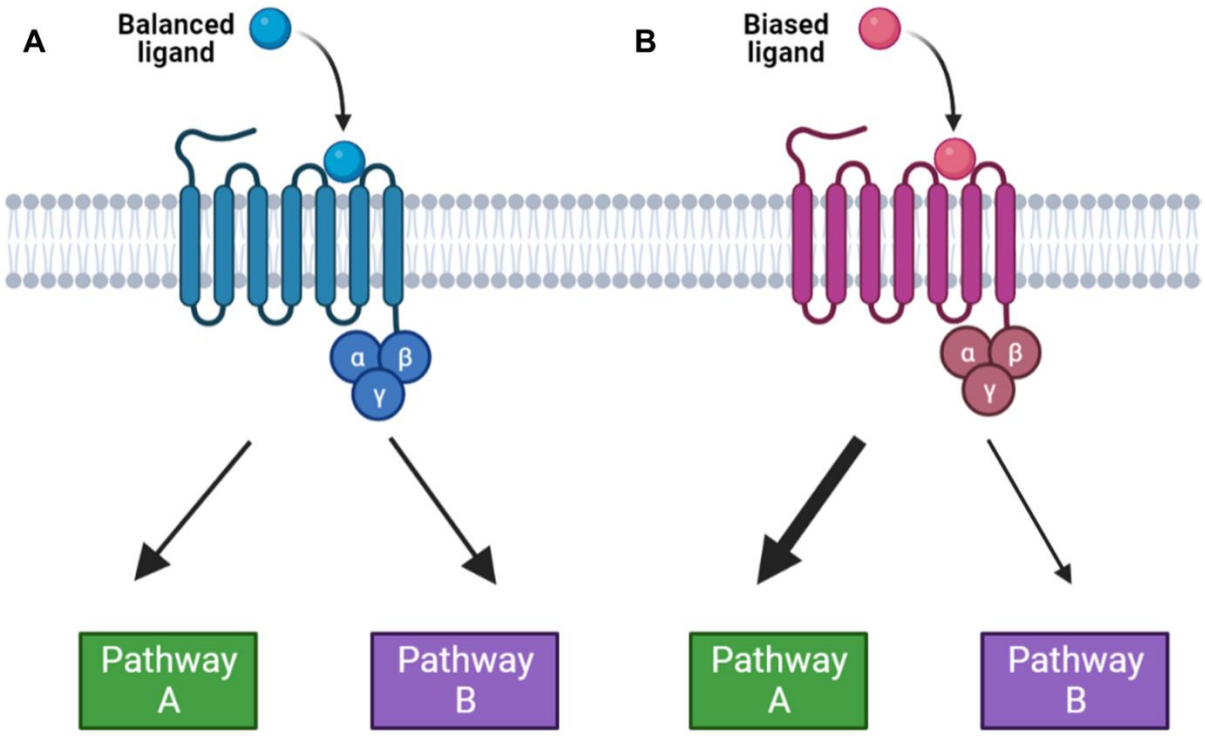

Figure 1-2. Biased agonism at GPCRs. While a balanced ligand (A) binds to a GPCR and activates pathway A and pathway B to similar extents, a biased ligand (B) binds to a GPCR and preferentially activates one pathway (pathway A) over the other (pathway B). Adapted from "GPCR Effector Pathways", by BioRender.com (2023). Retrieved from https://app.biorender.com/biorender-templates

1.5 Bitopic ligands

GPCRs are often targeted by drugs acting at the orthosteric binding site[25]. This site, where endogenous ligands bind to, often displays a high degree of similarity among receptor subtypes, thus complicating the process of developing subtype selective ligands[123,124]. A possible solution is to target the allosteric binding site, that is, a site which is distinct from the orthosteric binding site[125]. Compounds which bind to the allosteric site are called allosteric modulators. Such modulators affect the affinity, potency, and/or efficacy of an orthosteric ligand at the receptor[25,74]. Furthermore, allosteric modulators can either enhance orthosteric agonist activity [i.e. positive

allosteric modulators (PAMs)], decrease orthosteric agonist activity [i.e. negative allosteric modulators (NAMs)], or occupy the allosteric binding site without directly affecting the response of the orthosteric agonist [i.e. neutral allosteric ligands (NALs)][43,126]. Some allosteric modulators are capable of activating receptors in the absence of an orthosteric ligand while retaining the ability to enhance orthosteric agonist activity (i.e. ago-PAMs)[125,127].

Allosteric modulation has several advantages. Firstly, allosteric binding sites are generally less conserved among receptor subtypes, thus targeting these sites allows for greater subtype selectivity, for example, between CB1R and CB2R [8,35]. Secondly, since allosteric modulators like PAMs and NAMs lack intrinsic activity, their effects can only occur in the presence of an endogenous ligand or a co-administered orthosteric agonist[25,128]. Lastly, allosteric sites demonstrate a "ceiling" effect, where saturation of allosteric sites produces a maximal response and higher concentrations of the allosteric modulator yield no further increase in allosteric effect, thereby reducing the risk for drug overdose[8,129]. Several allosteric modulators are currently approved for clinical use: benzodiazepines are used to treat anxiety and sleep disorders, and act as PAMs of the γ-aminobutyric acid $(GABA)_A$ receptor; cinacalcet is used in the treatment of hyperparathyroidism, and is a PAM of the calcium-sensing receptor (CasR); and maraviroc is used to treat human immunodeficiency virus (HIV), and is a C-C chemokine receptor type 5 (CCR5) NAM[124,130].

Unfortunately, allosteric modulators tend to have lower affinity when compared to orthosteric ligands and their therapeutic utility is limited in conditions where endogenous tone is reduced[128,131]. Ligands with an orthosteric and allosteric component (i.e. bitopic ligands) may resolve these limitations[47,132]. Bitopic ligands, also known as bivalent ligands or dualsteric ligands, consist of two pharmacophores joined together by a linker molecule (Figure 1-3)[106,131,133]. It is

essential that the linker molecule is appropriately sized as deviations in either direction (i.e. too short or too long) would impact the ligand's ability to bind to the targeted sites[134]. Bitopic ligands can be homobivalent (i.e. composed of two identical pharmacophores) or heterobivalent (i.e. composed of two distinct pharmacophores)[135]. By targeting both the highly-conserved orthosteric site and the less-conserved allosteric site, bitopic ligands exhibit improved receptor affinity and enhanced receptor subtype selectivity[47,131–133,136]. The therapeutic potential of bitopic ligands has primarily been studied at the M_1 muscarinic acetylcholine receptor (mAChR), where orthosteric activation is beneficial in treating Alzheimer's disease and schizophrenia while engagement with the allosteric site is desired to avoid side effects mediated by other muscarinic receptors[132,137].

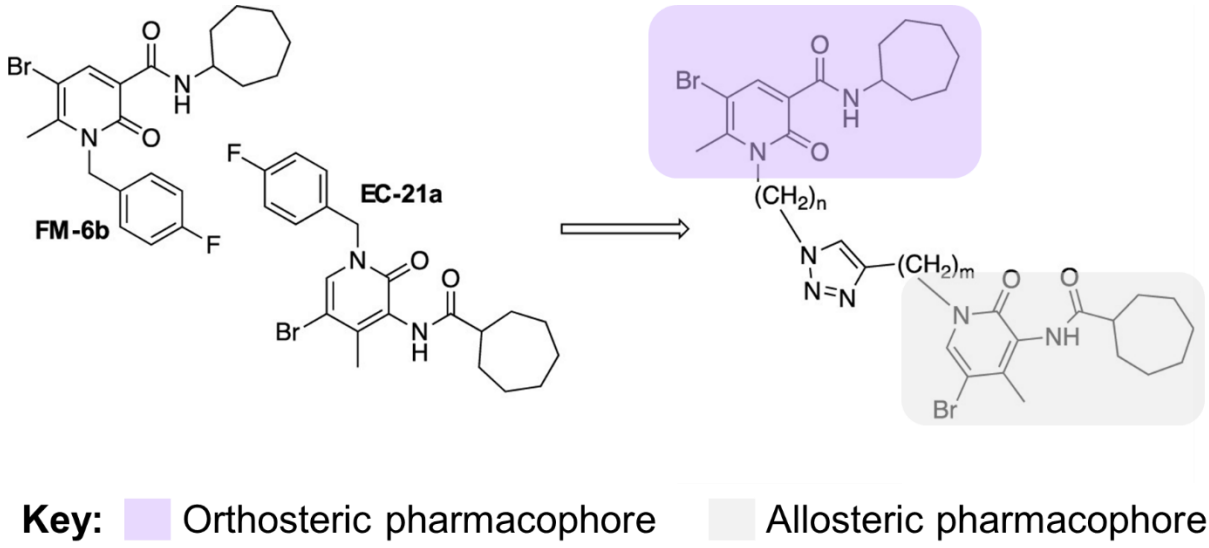

Figure 1-3. General structure of a bitopic ligand. Bitopic ligands consist of an orthosteric pharmacophore and an allosteric pharmacophore joined together by a linker molecule. As such, bitopic ligands can target both orthosteric and allosteric binding sites of a given receptor. The FD series of bitopic ligands were synthesized by joining the pharmacophoric portions of the CB1R/CB2R orthosteric agonist FM-6b and the CB2R PAM EC-21a. Figure generated by author in PowerPoint. Compound structures generated in ChemDraw® (PerkinElmer, Waltham, MA, USA) by Rebecca Ferrisi (University of Pisa).

1.6 Receptor dimerization

GPCRs can exist as individual receptors (i.e. monomers) and as receptors joined together (i.e. dimers)[7,37]. Dimer formation may involve two identical receptors (i.e. homodimers) or two distinct receptors (i.e. heterodimers)[138]. Though dimerization is a requirement for proper function among other receptors (e.g. $GABA_B$), it is not obligatory for GPCR activation as monomeric GPCR units are sufficient in this regard[39,139]. Heterodimers confer two main advantages over their monomeric constituents. Firstly, heterodimers tend to display distinct pharmacological properties[33,140–143]. For example, SKF83959 is a dopamine receptor agonist which signals through $G\alpha_s$ and $G\alpha_{i/o}$ G proteins at the dopamine D_1 and D_2 receptors, respectively. However in D_1-D_2 heterodimeric complexes, SKF83959 binds both receptors and couples to $G\alpha_{q/11}$ G proteins instead, thus engaging a signaling cascade distinct from its monomeric parent receptors[144]. Secondly, heterodimers are believed to have a more restricted pattern of expression, which may be increased or decreased under specific conditions[133,139]. For example, women experiencing pre-eclampsia exhibit increased heterodimerization of AT1R and bradykinin B2 receptors while adenosine A_{2A} receptor ($A_{2A}R$) and D_2 receptor heterodimerization is upregulated in Parkinson's disease but downregulated in schizophrenia[133,143]. Exploiting these properties of heterodimers may yield novel therapeutics with improved selectivity and reduced side effects[33,42,76,145].

1.6.1 Cannabinoid receptor dimerization

Both CB1R and CB2R may form either homodimers or heterodimers. CB1R and CB2R may heterodimerize with each other[10,24]. Additionally, CB1R heterodimerization has been observed with various receptors including the orexin receptor type 1 (OX1R), orexin receptor type 2

(OX2R), β2-adrenergic receptor (β2AR), serotonin 5-HT_{2A} receptor (5-HT_{2A}R), somatostatin receptor 5 (SSR5), D_2 receptor, MOR, A_{2A}R, AT1R, and GPR55[75,76,78,142,146–150]. Much less is known about CB2R heterodimers and their physiological implications, though previous studies suggest dimer formation with the serotonin 5-HT_{1A} receptor (5-HT_{1A}R), C-X-C chemokine receptor type 4 (CXCR4), and GPR55[7,9,10,151].

1.6.2 Orexin receptor signaling and interactions with cannabinoid receptors

Orexin receptors OX1R and OX2R are known to interact with CB1R as observed using bioluminescence resonance energy transfer (BRET) and intracellular signaling assays[75,76,78]. In general, heterodimerization with CB1R appears to facilitate $G\alpha_{q/11}$-dependent signaling and OX1R may augment 2-AG synthesis[152]. Far less is known about CB2R-orexin receptor interactions. Here we will briefly summarize the physiological role of the orexinergic system as a preface to later observations of cannabinoid-orexin receptor interactions.

1.6.2.1 Orexinergic system

Orexins, also known as hypocretins, are hypothalamic neuropeptides that are formed following proteolytic processing of a common precursor polypeptide called prepro-orexin, giving rise to orexin A (OXA) and orexin B (OXB)[97,153,154]. They bind to a pair of GPCRs called orexin receptors (OX1R, OX2R), though OXA binds to both receptors with equal affinity while OXB displays much higher affinity for OX2R[155]. Both orexin receptors mediate intracellular signaling via $G\alpha_{q/11}$ G proteins[97]. As such, their activation leads to production of diacylglycerol (DAG) and inositol trisphosphate (IP_3) via PLC activation and the subsequent signal cascades initiated by these second

messengers [e.g. protein kinase C (PKC) activation, calcium release][16,46]. Additionally, OX2R may couple to $G\alpha_{i/o}$ G proteins[155].

Orexinergic neurons are present in the lateral, perifornical, and dorsomedial regions of the hypothalamus, with extensive projections throughout the CNS[16,156]. Additionally, orexins and orexin receptors have been detected in peripheral tissues such as the adrenal glands, adipose tissue, pancreas, and gastrointestinal tract[44].

Orexins are best known for being modulators of sleep and wakefulness. Deficiencies at either the receptor level or of the neuropeptides themselves result in disorders such as narcolepsy-catalepsy[76,97,157]. Furthermore, intracerebroventricular (ICV) injection of orexin in rats promotes food intake, establishing a role for orexins in the control of feeding and appetite, where orexin-deficient mice experience obesity, linking to energy metabolism[153,158]. Each orexin subtype contributes differently to these physiological processes: OX1R is primarily responsible for feeding while OX2R regulates sleep and arousal[97,157,159]. Additionally, orexins and orexin receptors have been implicated in pain regulation, neuroprotection and immunomodulation[44,160–162].

1.6.2.2 Therapeutic relevance of orexinergic system

Pharmacological interventions targeting the orexinergic system primarily focus on orexin receptor antagonists, namely single orexin receptor antagonists (SORAs) and dual orexin receptor antagonists (DORAs)[44,163]. Several DORAs, such as suvorexant (Belsomra) and lemborexant (Dayvigo), have received FDA approval in the treatment of insomnia[164,165]. Orexin antagonists may also prove to be useful as anti-obesity agents. Though none have been approved for clinical usage yet, orexin agonists may be useful in the treatment of narcolepsy, specifically through

OX2R-selective agonism[166]. Preclinical and clinical studies with danavorexton (TAK-925), a OX2R-selective agonist, revealed that danavorexton ameliorates symptoms of narcolepsy and was well tolerated and did not produce serious treatment-emergent adverse events (TEAEs)[167]. Danavorexton is administered intravenously, which may be a limitation to its clinical application[168].

1.7 Phytocannabinoids and their metabolites

Last within this introduction and beyond the signaling of cannabinoids and the interactions of cannabinoid receptors with other GPCRs, it is important to consider plant-derived cannabinoids.

At least 120 different phytocannabinoids have been identified among which Δ^9-THC and cannabidiol (CBD) are two of the most abundant and thoroughly investigated constituents of *C. sativa*[28,169–171]. While various studies have explored the pharmacokinetic properties of Δ^9-THC and CBD, the pharmacological activity of their metabolites remains largely unknown[172–176].

1.7.1 Metabolism of Δ^9-THC

Hepatic cytochrome P450 (CYP450) enzymes, mainly CYP2C9, CYP2C19, and CYP3A4, are responsible for the metabolism of Δ^9-THC[177,178]. Over 100 metabolites of Δ^9-THC have been identified, though 11-hydroxy-THC (11-OH-THC) and 11-carboxy-THC (COOH-THC) are considered to be the main metabolites[175,179]. 11-OH-THC is a short-lived metabolite that is formed following the oxidation of Δ^9-THC at the 11-position carbon and is subsequently further oxidized to yield COOH-THC (Figure 1-4A)[172,180,181]. It has been previously reported that 11-OH-THC is a psychoactive metabolite whereas COOH-THC lacks pharmacological activity[31,177].

1.7.2 Metabolism of CBD

Similar to Δ^9-THC, CBD is also metabolized by hepatic CYP2C9, CYP2C19, and CYP3A4 enzymes[178,182]. The main metabolites of CBD, 6-hydroxy-CBD (6-OH-CBD), 7-hydroxy-CBD (7-OH-CBD) and 7-carboxy-CBD (COOH-CBD), are formed following oxidation of the 6- and 7-position carbons (Figure 1-4B)[26,176,183]. It is currently unknown whether these metabolites have activity at the cannabinoid receptors[30,177].

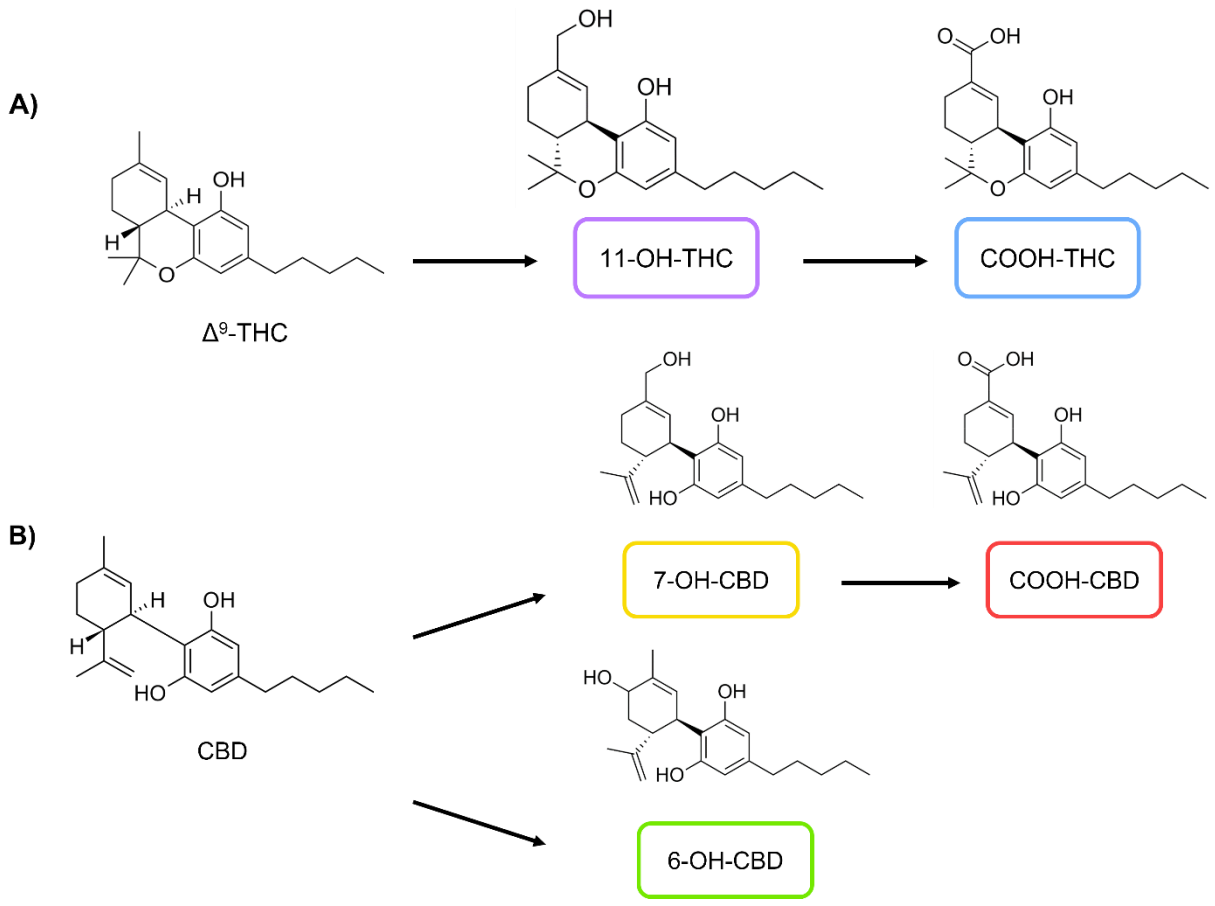

Figure 1-4. General scheme of metabolite formation for Δ^9-THC and CBD. Δ^9-THC (A) is oxidized at the 11-position carbon to yield 11-hydroxy-THC (11-OH-THC), which is subsequently oxidized to yield 11-carboxy-THC (COOH-THC). CBD (B) is oxidized at the 6- and 7-position carbons to yield 6-hydroxy-CBD (6-OH-CBD) and 7-hydroxy-CBD (7-OH-CBD). 7-OH-CBD is further oxidized to yield 7-carboxy-CBD (COOH-CBD). Figure generated by author in PowerPoint. Compound structures generated in ChemDraw® JS (PerkinElmer, Waltham, MA, USA) by author, based on previously published structures[184].

1.8 Objectives

The limited number of cannabinoid-based therapeutics highlights the need for further investigation of cannabinoid ligands and their signaling. Furthermore, CB2R's limited expression in the CNS, coupled with its anti-inflammatory and anti-nociceptive properties, makes it an attractive drug target for cannabinoid therapeutics with safer side effect profiles compared to CB1R-acting ligands. The high degree of similarity between the ligand binding domains of CB1R and CB2R has made the identification of CB2R-selective ligands challenging. Our understanding of cannabinoid receptor pharmacology is expanding rapidly to encompass standard agonists and antagonists as well as more novel allosteric ligands, bitopic ligands, orphan receptor-targeted ligands, and drug metabolites. In this research, there was an opportunity to cover a wide swath of cannabinoid chemotypes and identify which ligand classes displayed potentially beneficial signaling properties (Figure 1-5). Overall, the objectives of this research were:

1. To explore the pharmacological properties of novel synthetic cannabinoids at GPR55 and CB2R.
2. To determine how CB1R and CB2R are influenced by other GPCRs involved in modulating pain and inflammatory responses, such as the orexin receptors.
3. To investigate the pharmacological properties of Δ^9-THC and CBD metabolites at CB1R and CB2R.

1.9 Hypotheses

1. Novel synthetic cannabinoids developed using iterative pharmacological data and drug design will display measurable GPR55-specific or CB2R-specific *in vitro* pharmacological activity.
2. The potency and efficacy of CB1R and CB2R agonist-dependent signaling will be increased by the co-expression of OX1R or OX2R.
3. Metabolites of Δ^9-THC will be agonists of CB1R and CB2R signaling while metabolites of CBD will be inactive at both CB1R and CB2R.

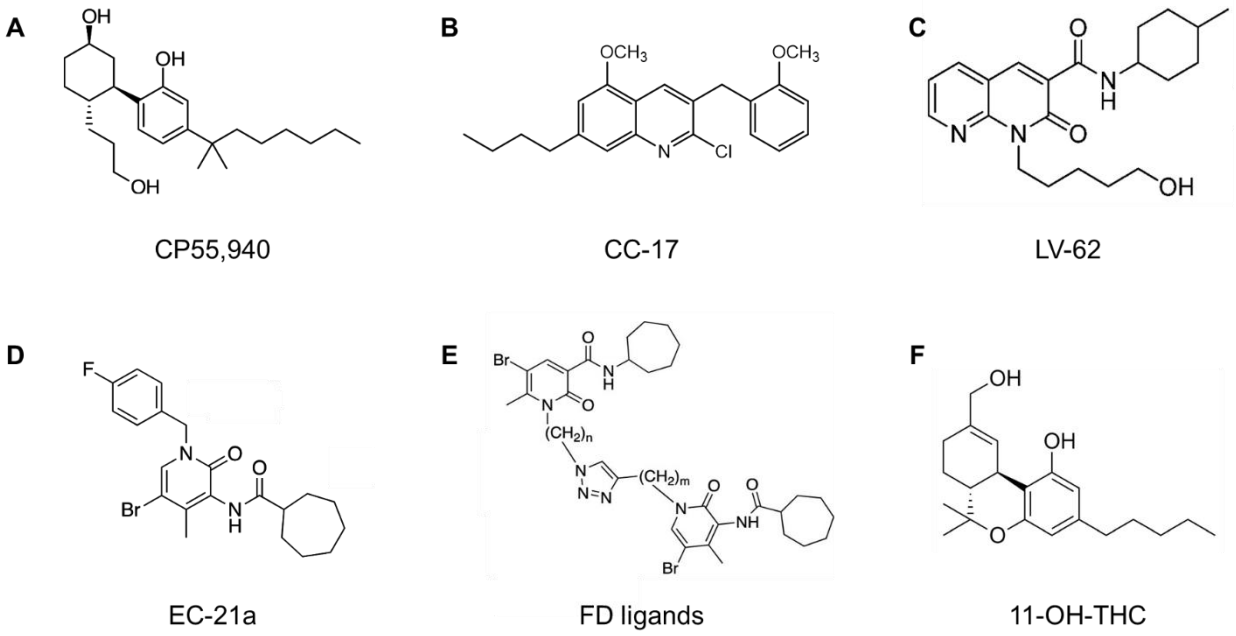

Figure 1-5. Select compounds assessed in the present study. (A) CP55,940, a non-selective orthosteric cannabinoid receptor agonist, (B) CC-17, a GPR55 ligand, (C) LV-62, a selective CB2R agonist, (D) EC-21a, a CB2R PAM, (E) general structure of the FD ligands, a series of CB2R bitopic ligands, (F) 11-OH-THC, a phytocannabinoid metabolite. Figure generated by author in PowerPoint. CP55,940 structure obtained from Wikimedia Commons. CC-17 structure generated in ChemDraw® by Costanza Ceni (University of Pisa). LV-62, EC-21a, and FD ligands structures generated in ChemDraw® by Rebecca Ferrisi (University of Pisa). 11-OH-THC structure generated in ChemDraw® JS by author.

Chapter 2: Materials & Methods

2.1 Compounds

CP55,940 [(-)-*cis*-3-[2-Hydroxy-4-(1,1-dimethylheptyl)phenyl]-*trans*-4-(3-hydroxypropyl)cyclohexanol] was purchased from Tocris Biosciences (Oakville, ON, Canada). SR144528 [5-(4-Chloro-3-methylphenyl)-1-[(4-methylphenyl)methyl]-N-[(1S,2S,4R)-1,3,3-trimethylbicyclo[2.2.1]hept-2-yl]-1H-pyrazole-3-carboxamide] was purchased from Sigma-Aldrich (Oakville, ON, Canada). GPR55 ligands (CC-17, CC-28, CC-38, CC-66, CC-67, CC-81a, and CC-81b) were synthesized in the laboratory of Dr. Simone Bertini at the University of Pisa (Pisa, Italy). CB2R ligands (EC-21a, FD-22a, FD-24a, FD-25a, FD-27a, FD-32a, FG-158a, FG-160a, FG-161a, FM-6b, JR-14a, JR-16a, JR-22a, JR-26a, JR-58a, JR-60a, JR-61a, JR-64a, and LV-62) were synthesized in the laboratory of Dr. Clementina Manera at the University of Pisa. A general description of the syntheses and structures of both GPR55 and CB2R ligands is provided in this thesis for context, but this chemistry was not part of the experimental work of the present thesis. 11-OH-THC, COOH-THC, 6-OH-CBD, 7-OH-CBD, and COOH-CBD were obtained from Cayman Chemical (Ann Arbor, MI, USA). Compounds were dissolved in dimethyl sulfoxide (DMSO) with a final concentration of 0.1% DMSO in assay media for all assays. Compounds were added directly to media at the concentrations and times indicated.

2.1.1 Synthesis of GPR55 ligands

2.1.1.1 CC series

Structural modifications to a class of 3-benzylcoumarins derivatives yielded the variously substituted 3-benzylquinolin-2(1*H*)-ones CC-17, CC-28, CC-38, CC-66, CC-67, CC-81a, and CC-81b (Figure 2-1; Table 2-1). Detailed synthesis of these compounds has been previously described[185].

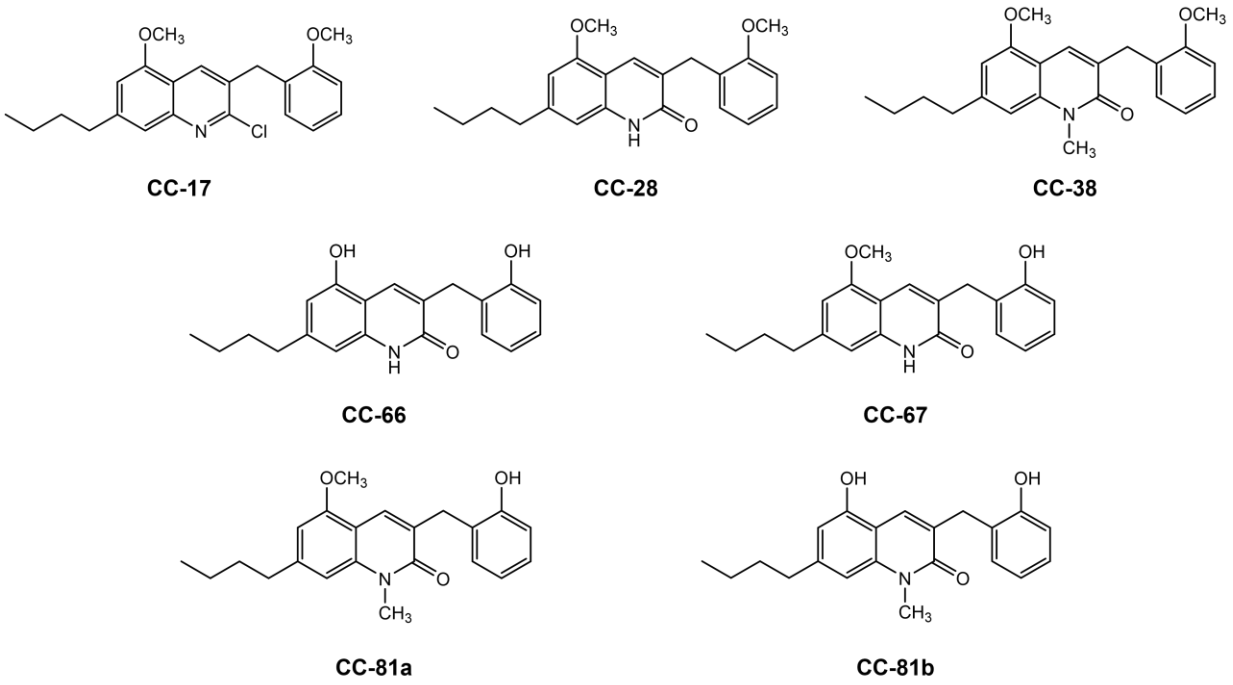

Figure 2-1. Chemical structures of the CC series of GPR55 ligands. The CC series of GPR55 ligands consists of the following compounds: CC-17, CC-28, CC-38, CC-66, CC-67, CC-81a, and CC-81b. Figure generated by author in PowerPoint. Compound structures generated in ChemDraw® by Costanza Ceni (University of Pisa).

Compound	Molecular weight (Da)
CC-17	369.89
CC-28	351.45
CC-38	365.47
CC-66	323.39
CC-67	337.42
CC-81a	351.45
CC-81b	337.42

Table 2-1. Molecular weights of the CC series of GPR55 ligands.

2.1.2 Synthesis of CB2R ligands

2.1.2.1 FD series

FD-22a, FD-24a, FD-25a, FD-27a, and FD-32a were designed by joining the pharmacophoric portions of the 2-oxo-pyridine derivative and dualsteric CB1R/CB2R agonist FM-6b and the 2-oxopyridine-3-carboxamide derivative and CB2R PAM EC-21a (Figure 2-2; Figure 2-3; Table 2-2). FM-6b and EC-21a were joined together by a linker molecule consisting of a di-substituted 1,2,3-triazole ring connected to two alkyl chains of variable length at position N(1) and C(4). Detailed synthesis of these compounds has been previously described[186].

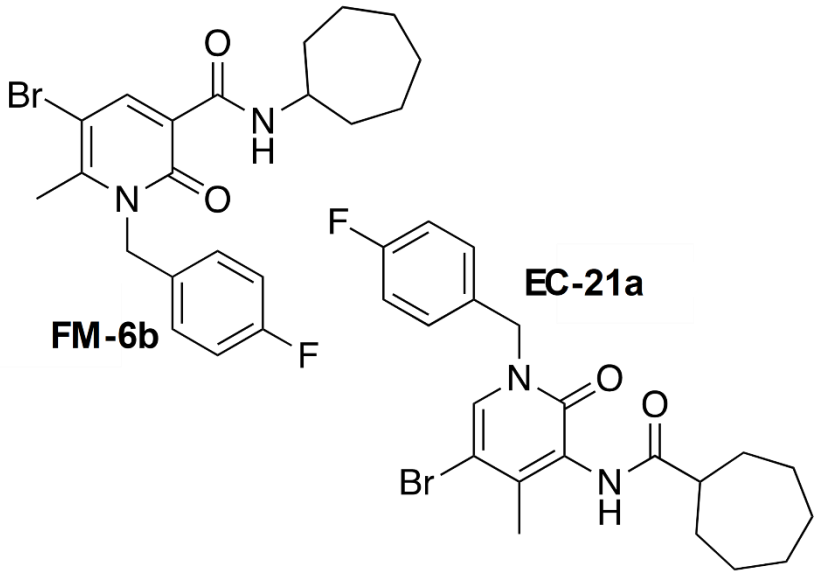

Figure 2-2. Chemical structures of FM-6b and EC-21a. The CB1R/CB2R orthosteric agonist FM-6b and the CB2R PAM EC-21a represent the orthosteric and allosteric parent ligands of the FD series of CB2R bitopic ligands. Figure generated in ChemDraw® by Rebecca Ferrisi (University of Pisa).

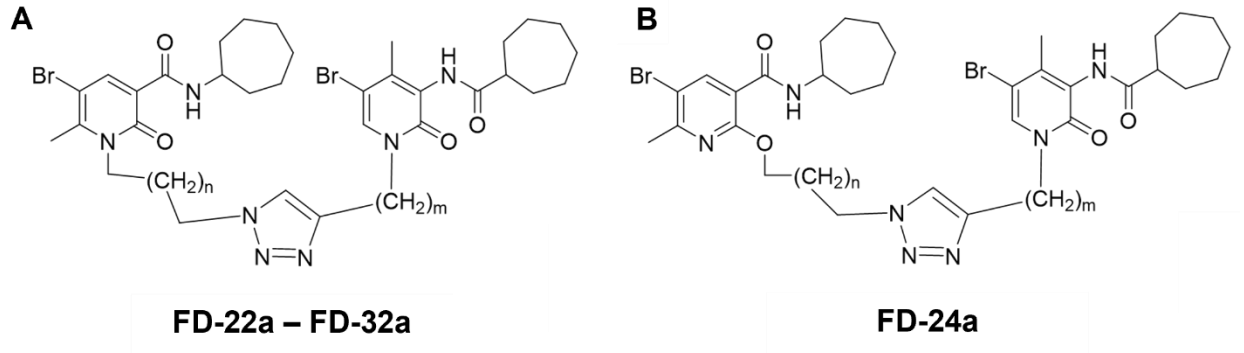

Figure 2-3. General chemical structures of the FD series of CB2R bitopic ligands. General chemical structure for FD-22a, FD-25a, FD-27a, FD-32a (A) and FD-24a (B). Figure generated in ChemDraw® by Rebecca Ferrisi (University of Pisa).

Compound	Molecular weight (Da)
EC-21a	440
FM-6b	440
FD-22a	590
FD-24a	535
FD-25a	562
FD-27a	562
FD-32a	535

Table 2-2. Molecular weights of the FD series of CB2R ligands.

2.1.2.2 FG series

The 1,8-naphthyridin-2(1*H*)-one-3-carboxamide derivatives FG-158a, FG-160a, and FG-161a were designed based on structural modifications to the selective CB2R agonist and N1-hydroxypentyl derivative LV-62 (Figure 2-4; Table 2-3). Detailed synthesis of these compounds has been previously described[187].

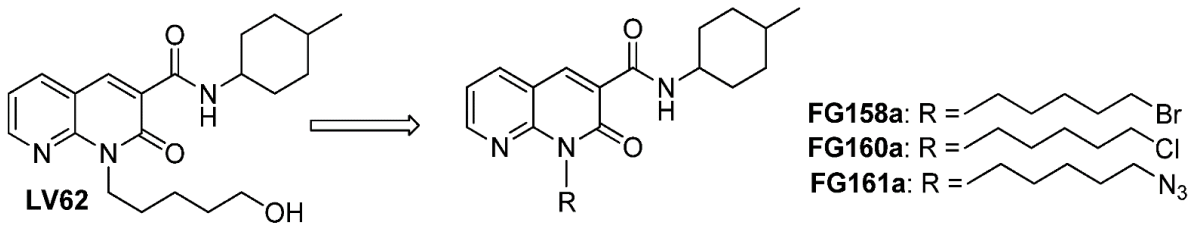

Figure 2-4. Chemical structures of the FG series of CB2R ligands. The FG series of CB2R ligands were derived from the selective CB2R agonist LV-62 and consists of the following compounds: FG-158a, FG-160a, and FG-161a. Figure generated in ChemDraw® by Rebecca Ferrisi (University of Pisa).

Compound	Molecular weight (Da)
LV-62	371
FG-158a	450
FG-160a	406
FG-161a	413

Table 2-3. Molecular weights of the FG series of CB2R ligands.

2.1.2.3 JR series

JR-14a, JR-16a, JR-22a, JR-26a, JR-58a, JR-60a, JR-61a, and JR-64a were synthesized by joining the pharmacophoric portions of the selective CB2R agonist LV-62 and the CB2R PAM EC-21a (Figure 2-5; Table 2-4). LV-62 and EC-21a were joined together by a linker molecule consisting of a varying-chain length hydrocarbon between 5-8 carbons in length. Two compounds of the JR series, JR-58a and JR-60a, have an ether substitution at positions 3 (JR-58a) or 5 (JR-60a) of the hydrocarbon chain. Detailed synthesis of these compounds has been previously described[188].

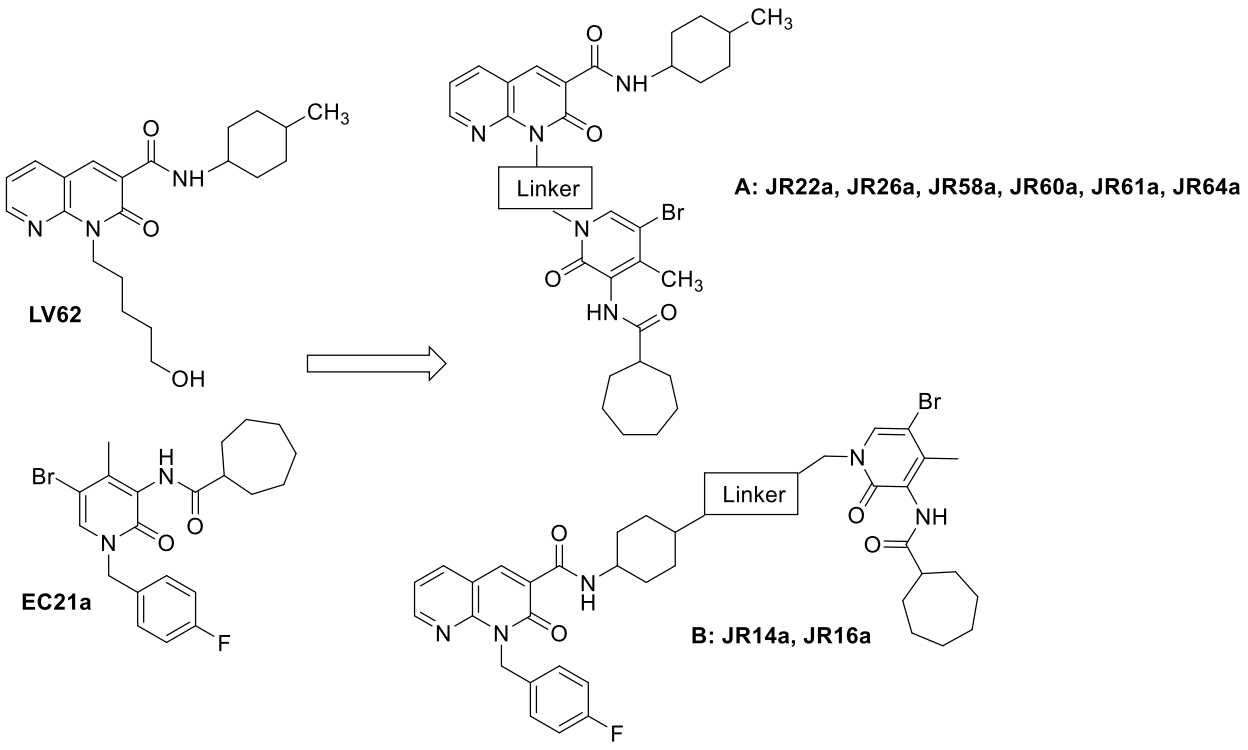

Figure 2-5. Chemical structures of the JR series of CB2R ligands. The selective CB2R agonist LV-62 and the CB2R PAM EC-21a represent the orthosteric and allosteric parent ligands of the JR series of CB2R bitopic ligands. The JR series can be divided into series A (JR-22a, JR-26a, JR-58a, JR-60a, JR-61a, and JR-64a) and series B (JR-14a, JR-16a), with members of each sub-series sharing a common linker molecule. Figure generated in ChemDraw® by Rebecca Ferrisi (University of Pisa).

Compound	Molecular weight (Da)
EC-21a	440
JR-14a	899
JR-16a	871
JR-22a	764
JR-26a	736
JR-58a	643
JR-60a	671
JR-61a	669
JR-64a	697
LV-62	371

Table 2-4. Molecular weights of the JR series of CB2R ligands.

2.1.3 Phytocannabinoid metabolites

Five phytocannabinoid metabolites were assessed in this study. They can be classified as: a) Δ^9-THC metabolites: 11-OH-THC and COOH-THC and b) CBD metabolites: 6-OH-CBD, 7-OH-CBD, and COOH-CBD (Figure 2-6; Figure 2-7; Table 2-5).

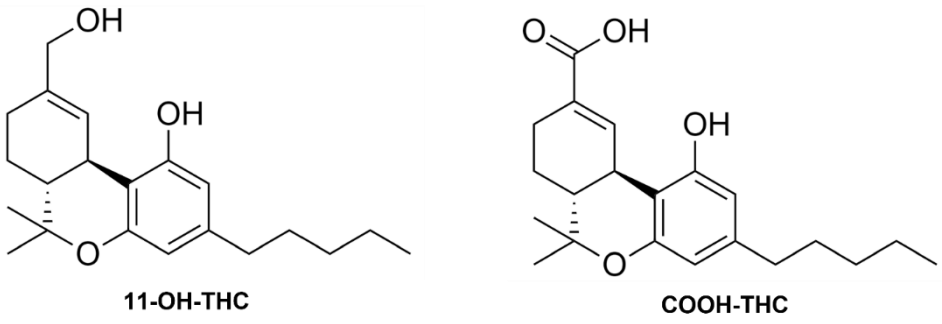

Figure 2-6. Chemical structures of Δ^9-THC metabolites. 11-OH-THC and COOH-THC are metabolites of Δ^9-THC that were assessed in this study. Compound structures generated in ChemDraw® JS by author.

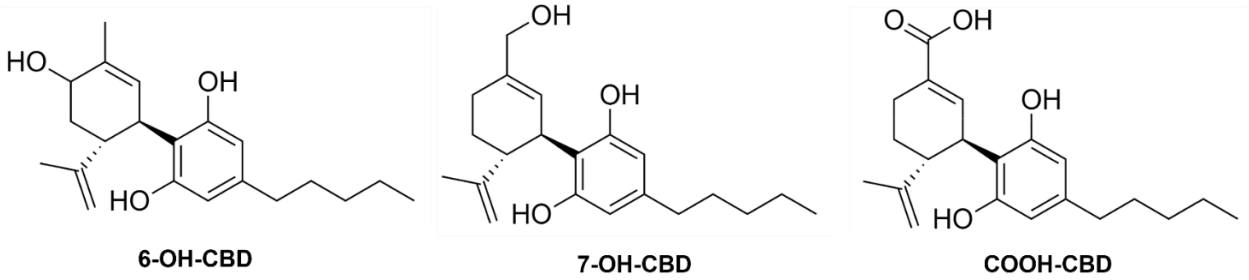

Figure 2-7. Chemical structures of CBD metabolites. 6-OH-CBD, 7-OH-CBD, and COOH-CBD are metabolites of CBD that were assessed in this study. Compound structures generated in ChemDraw® JS by author.

	Compound	Molecular weight (Da)
Δ^9-THC metabolites	11-OH-THC	330.5
	COOH-THC	344.4
CBD metabolites	6-OH-CBD	330.5
	7-OH-CBD	330.5
	COOH-CBD	344.4

Table 2-5. Molecular weights of Δ^9-THC and CBD phytocannabinoid metabolites assessed in this study.

2.2 Cell culture

Chinese hamster ovary (CHO)-K1 cells were obtained from the American Type Culture Collection (ATCC, Manassas, VA, USA). CHO-K1 cells transfected with and stably expressing human CB1R, CB2R, or GPR55; or transiently expressing human OX1R or OX2R, were maintained at 37°C and 5% CO_2 in F-12/Dulbecco's Modified Eagle Medium (DMEM) containing 1 mM L-glutamine, 10% fetal bovine serum (FBS), and 1% penicillin-streptomycin (Pen/Strep). CHO-K1 GPR55 cells were supplemented with ampicillin (100 µg/mL). Additional cell lines described as HitHunter® (cAMP) and PathHunter® (βarrestin2) CHO-K1 cells stably expressing human CB1R or CB2R were obtained from DiscoverX (Eurofins, Fremont, CA, USA) and maintained at 37°C

and 5% CO_2 in F-12/DMEM containing 1 mM L-glutamine, 10% FBS and 1% Pen/Strep. These HitHunter® CHO-K1 CB1R and CB2R cAMP cells were supplemented with geneticin (800 µg/mL); whereas PathHunter® CHO-K1 CB1R and CB2R βarrestin2 cells were supplemented with geneticin (800 µg/mL) and hygromycin B (300 µg/mL)[122,170,189].

2.3 Cell signaling assays

2.3.1 In-cell western

Phosphorylation of ERK1/2 was measured using the in-cell western assay (Figure 2-8). Compared to traditional western blots, in-cell westerns allow a greater number of samples to be quantified with higher thru-put to assess ligand potency and efficacy; however, the assay cannot show antibody specificity and relies on total measured signal between phosphorylated and total target protein within the timepoint being studied[190]. Cells were dissociated from 10 cm tissue culture plates using 2 mL 0.5% trypsin-EDTA and replated into clear, flat-bottom 96-well tissue culture plates at a density of 20,000 cells/well. Plates were incubated overnight in F-12/DMEM containing 1 mM L-glutamine, 10% FBS, and 1% Pen/Strep at 37°C and 5% CO_2. Plates were incubated for 2-3 days. Following this, cell culture media was removed and cells were incubated in serum-free media for 30 min at 37°C. Cells were then treated with 0.1 nM – 10 µM ligands for 10 min at 37°C. Ten minutes was chosen based on previous studies from our group with cannabinoid receptors in the same assay[191]. Afterwards, cells were fixed for 10 min at room temperature with 4% paraformaldehyde as a fixative. The fixative was subsequently aspirated and cells were washed with 1X phosphate-buffered saline (PBS) 3 times, 5 min each. Cells were incubated with blocking solution (1X PBS/20% Odyssey® Blocking Buffer containing 0.3% Triton X-100) for 45 min at room temperature. Cells were incubated with primary antibody solutions directed against ERK1/2

and phosphorylated ERK1/2 (pERK1/2) (Y205/185) (Santa Cruz Biotechnology, Santa Cruz, CA, USA) diluted in blocking solution overnight at 4°C. The next day, cells were washed 3 times with 1X PBS for 5 min each. Cells were incubated in IRDye® 680RD and 800CW secondary antibodies (LI-COR Biosciences, Lincoln, NE, USA) diluted in blocking solution for 60 min at room temperature protected from light. Cells were washed 3 times with 1X PBS for 5 min each and dried overnight. Plates were visualized and optical density data was acquired using the LI-COR Odyssey® Imaging system and software (v. 3.0, LI-COR Biosciences, Lincoln, NE, USA)[192].

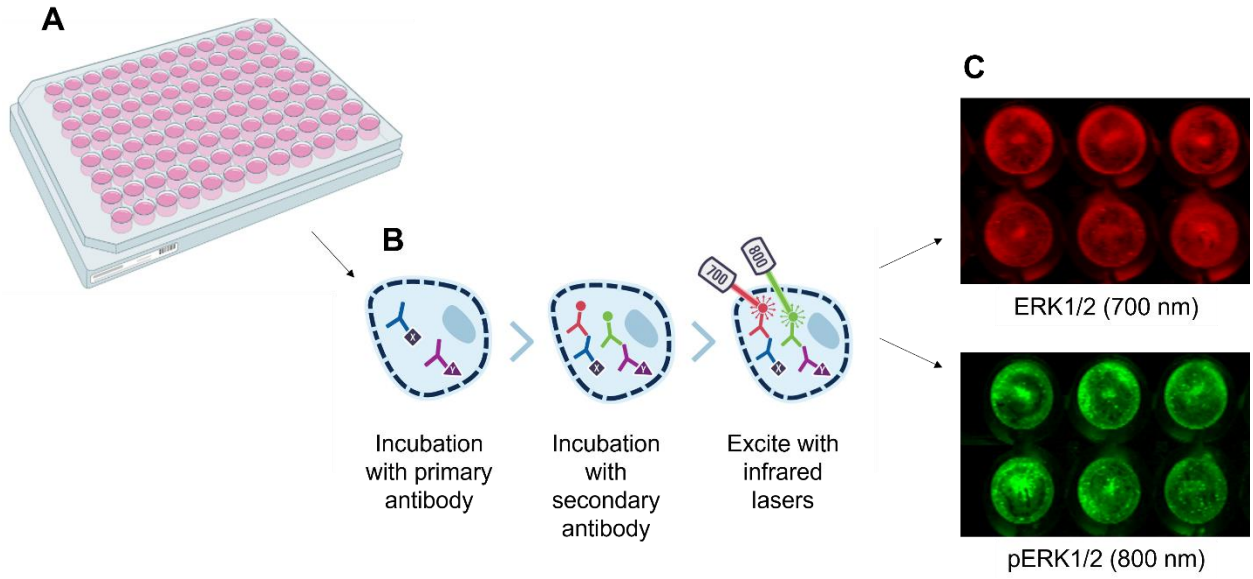

Figure 2-8. Schematic of in-cell western protocol. In the in-cell western assay, cells are plated into 96-well plates (A). Following ligand treatment and cell fixation, cells are incubated with primary antibodies targeting extracellular signal-regulated kinases 1 and 2 (ERK1/2) and phosphorylated ERK1/2 (pERK1/2) followed by incubation with infrared secondary antibodies targeting the primary antibodies. Cells are excited with infrared lasers in order to quantify the levels of ERK1/2 and pERK1/2 (B, C). Figure generated by author in PowerPoint using images from BioRender.com (A) and LI-COR In-Cell Western Assay Application (B)[190]. (C) is the author's own work.

2.3.2 HitHunter® cAMP assay

$G\alpha_{i/o}$-mediated inhibition of forskolin (FSK)-stimulated cAMP production was assessed using the DiscoverX HitHunter® assay in CHO-K1 CB1R and CB2R cAMP cells (Figure 2-9). Cells were dissociated from 10 cm tissue culture plates using 2 mL 0.5% trypsin-EDTA and replated into white-walled, white-bottom, flat-bottom 96-well tissue culture plates at a density of 160,000 cells/well. Plates were incubated overnight in Opti-MEM™ containing 1% FBS at 37°C and 5% CO_2. The next day, Opti-MEM™ media was removed and replaced with cell assay buffer (1X PBS). Subsequently, cells were treated with 10 µM FSK and 0.1 nM – 10 µM ligands for 90 min at 37°C. cAMP antibody solution and cAMP working detection solution were then added to cells according to the manufacturer's directions (DiscoverX). Cells were incubated with these solutions for 60 min at room temperature protected from light. cAMP solution A was added according to the manufacturer's directions (DiscoverX) and cells were incubated for an additional 3 h at room temperature protected from light. Chemiluminescence was measured on a BioTek Synergy™ HT microplate reader (BioTek Instruments, Winooski, VT, USA) with the following settings: top read, gain 200, integration time 1,000 ms[122,170,189].

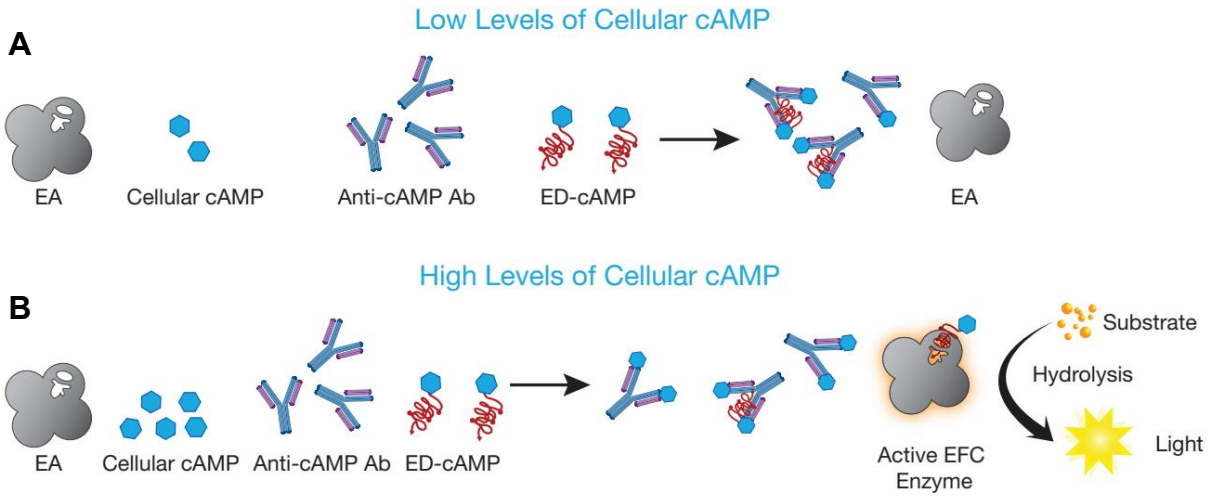

Figure 2-9. Enzyme fragment complementation (EFC) technology utilized by HitHunter® cAMP assay. In order to quantify cyclic adenosine monophosphate (cAMP) inhibition, the HitHunter® cAMP assay utilizes a β-galactosidase (β-gal) enzyme split into two fragments, the enzyme donor (ED) and the enzyme acceptor (EA). The ED and EA lack activity on their own but when they complement, they form the active β-gal enzyme. Cellular cAMP and cAMP conjugated with a fragment of the ß-gal enzyme (ED-cAMP) compete for binding to an anti-cAMP antibody (anti-cAMP Ab). When there are low levels of cellular cAMP (A), most of the ED-cAMP binds to the anti-cAMP Ab, leaving the EA unable to complement with the ED-cAMP to form the active β-gal enzyme. When there are high levels of cellular cAMP (B), the anti-cAMP Ab is saturated with the cellular cAMP, allowing the EA to complement with the ED-cAMP, forming the active β-gal enzyme, which subsequently hydrolyzes a substrate to produce a detectable chemiluminescent signal that is proportional to the amount of cAMP in the cells. Figure obtained from HitHunter® cAMP Assay Kit User Manual[193].

2.3.3 PathHunter® βarrestin assay

βarrestin2 recruitment was assessed using the DiscoverX PathHunter® assay in CHO-K1 CB1R and CB2R βarrestin2 cells (Figure 2-10). Cells were dissociated from 10 cm tissue culture plates using 2 mL 0.5% trypsin-EDTA and replated into white-walled, white-bottom, flat-bottom 96-well tissue culture plates at a density of 160,000 cells/well. Plates were incubated overnight in Opti-MEM™ containing 1% FBS at 37°C and 5% CO_2. Afterwards, cells were treated with 0.1 nM – 10 µM ligands for 90 min at 37°C. Detection solution was then added to cells according to the

manufacturer's directions (DiscoverX) and cells were incubated for 60 min at room temperature. Chemiluminescence was measured on a BioTek Synergy™ HT microplate reader (BioTek Instruments, Winooski, VT, USA) with the following settings: top read, gain 200, integration time 1,000 ms[122,170,189].

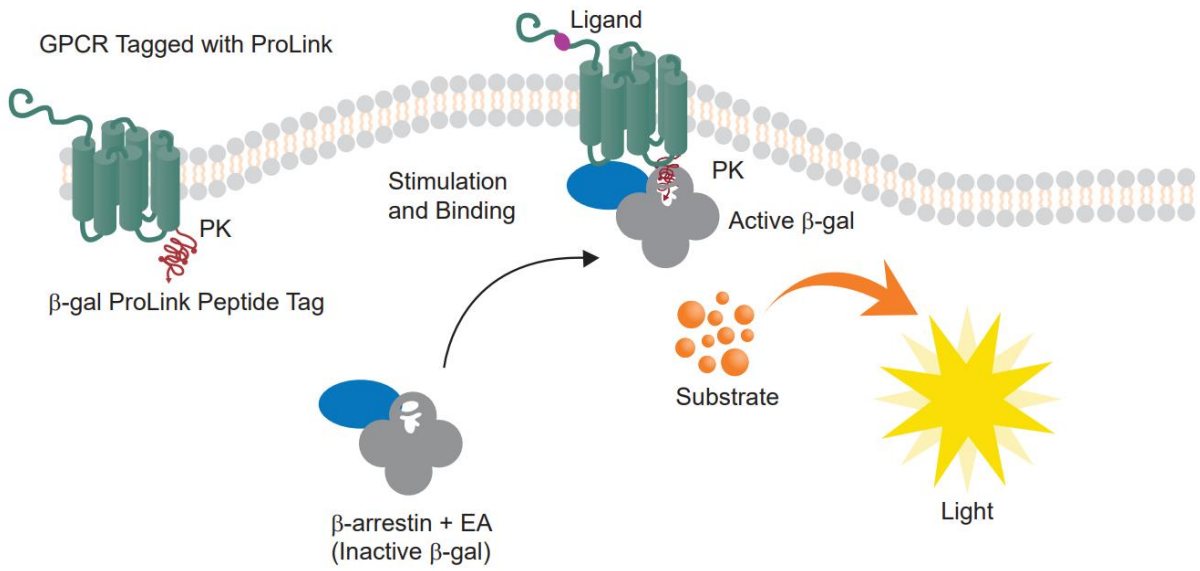

Figure 2-10. Enzyme fragment complementation (EFC) technology utilized by PathHunter® βarrestin assay. In order to quantify βarrestin2 recruitment, the PathHunter® βarrestin assay utilizes a β-galactosidase (β-gal) enzyme split into two fragments, the enzyme donor (ED) and the enzyme acceptor (EA). The ED and EA lack activity on their own but when they complement, they form the active β-gal enzyme. The G protein-coupled receptor (GPCR) of interest is tagged with a fragment of the β-gal called ProLink™ (PK) and functions as the ED while the cells stably express βarrestin2 tagged with the EA. When the GPCR is activated, the EA tagged βarrestin2 binds to the PK-tagged GPCR, allowing for the complementation of the EA and the ED, forming the active β-gal enzyme, which subsequently hydrolyzes a substrate to produce a detectable chemiluminescent signal that is proportional to the level of βarrestin2 recruitment. Figure obtained from PathHunter® Detection Kit User Manual[194].

2.4. Plasmids

*h*CB1R and *h*CB2R plasmids were a gift from Dr. Eileen Denovan-Wright at Dalhousie University (Halifax, NS, Canada). *h*GPR55 plasmids were obtained from the cDNA Resource Centre (Bloomsburg, PA, USA). *h*OX1R and *h*OX2R plasmids were sourced from Proxima Research & Development (Saskatoon, SK, Canada). All plasmids were propagated and sequenced by Proxima Research & Development. For all plasmids, receptor cDNA was inserted into the common pcDNA3.1(+) vector. Receptor plasmids were used in transfection experiments.

2.4.1 Transfections

Receptor plasmids were introduced into CHO-K1 cells using Lipofectamine™ 3000, according to the manufacturer's instructions (Invitrogen™, ThermoFisher Scientific, Waltham, MA, USA). Cells were grown to ~80% confluency in F-12/DMEM containing 1 mM L-glutamine, 10% FBS, and 1% Pen/Strep at 37 °C and 5% CO_2. Cell media was aspirated and cells were washed with 2 mL 1X PBS. Cells were then incubated in serum-free media for 30 min at 37 °C. Lipofectamine™ 3000 solution was prepared by diluting Lipofectamine™ 3000 reagent in Opti-MEM™. Plasmid solution was prepared by diluting plasmid DNA in Opti-MEM™ and P3000™ reagent. Diluted Lipofectamine™ 3000 reagent was then added to the diluted plasmid solution and the resultant solution was incubated for 15 min at room temperature. Following this, the Lipofectamine™ plasmid solution was added to the cells and cells were incubated for 24-48h at 37°C and 5% CO_2 prior to conducting experiments[195].

2.5 Statistical analyses

Statistical analyses were conducted using GraphPad Prism 9.0 (GraphPad Software Inc., San Diego, CA, USA). Data for ERK phosphorylation, cAMP inhibition, and βarrestin2 recruitment are represented as % of the maximal response of the reference agonist CP55,940 or fold over vehicle, as indicated in the figure descriptions. Concentration-response curves (CRCs) were fit using non-linear regression (3-parameters; Hill slope constrained to 1). Hill slope was constrained to 1 because this constraint produced the best-fit data and reduced the standard error of the regression, whereas variable slope nonlinear regression fits are often more appropriate for curves fit with more datapoints than our experiments included (GraphPad, Prism v. 9.0). CRCs were used to estimate EC_{50} and E_{max} values. The potency of a ligand is represented by its EC_{50} value, which is the concentration of ligand required to produce 50% of its maximal response in a given signaling pathway. The efficacy of a ligand is represented by its E_{max} value, which is the maximal response of a ligand in a given signaling pathway[131]. Based off of the CRCs and E_{max} values, ligands were defined as either full agonists, partial agonists, inactive (i.e. potential neutral antagonists) or inverse agonists (Figure 2-11).

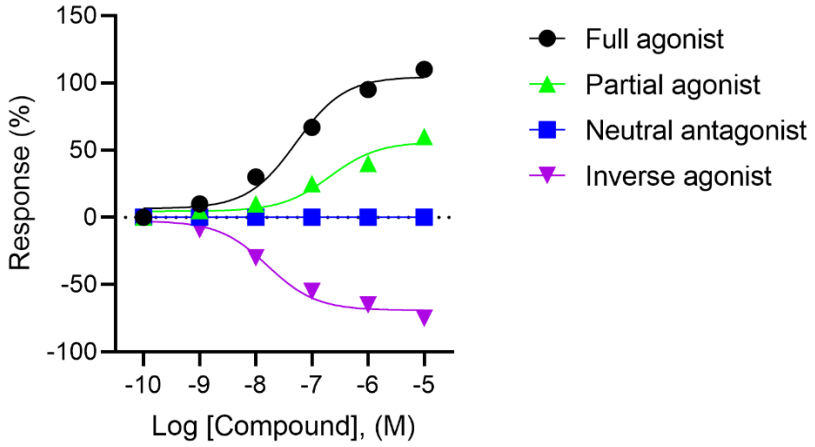

Figure 2-11. Pharmacological classification of ligands. A full agonist is a ligand which activates a given receptor to produce a maximal response. A partial agonist is a ligand which activates a given receptor to produce a submaximal response. A neutral antagonist is a ligand which occupies the binding site of a given receptor and inhibits the binding of other ligands, but itself lacks activity at the receptor. An inverse agonist is a ligand which occupies the binding site of a given receptor and reduces the constitutive activity of the receptor[74]. Figure generated by author in GraphPad Prism 9.0.

Statistical analyses were conducted by one-way analysis of variance (ANOVA) or two-way ANOVA, as indicated in the figure and table descriptions. *Post-hoc* analyses were performed using Tukey's test. For bias analyses, data were also fit to the operational model of Black and Leff to calculate signal bias ($\Delta\Delta$LogR) (Equation 2-1)[196]. All values are expressed as the mean ± the standard error of the mean (SEM) or 95% confidence interval (CI), as indicated. p values < 0.05 were considered to be significant.

$$E = \frac{E_{\max}[\mathrm{A}]^n \tau^n}{[\mathrm{A}]^n \tau^n + (K_\mathrm{A} + [\mathrm{A}])^n}$$

Equation 2-1. Operational model of Black and Leff. E is the response, E_{max} is the maximal response of the system, [A] is the agonist concentration, n is the transducer slope, τ is the efficacy/operational efficacy of the agonist in the receptor system and K_A is the agonist equilibrium dissociation constant[196].

Chapter 3: Results

3.1 Experiment 1: Pharmacological properties of novel GPR55 ligands

3.1.1 Phosphorylation of ERK1/2 at GPR55

The phosphorylation of ERK1/2 is observed for many GPCRs downstream of receptor activation and may be mediated by $G\alpha_{i/o}$ or βarrestins[191]. Here, ERK1/2 phosphorylation was quantified to determine the pharmacological activity of ligands downstream of GPR55. CC-17, CC-28, CC-38, CC-66, CC-67, CC-81a, and CC-81b were assessed for their ability to induce phosphorylation of ERK1/2 through the in-cell western assay using CHO cells transfected with *h*GPR55. The non-selective orthosteric cannabinoid receptor agonist CP55,940 was used as a reference compound. All of the novel GPR55 ligands were agonists of ERK1/2 phosphorylation at GPR55, with CC-17, CC-28, CC-38 and CC-81b producing strong, full agonist responses. CC-67 was also a full agonist of GPR55, but this only became apparent at higher concentrations. CC-66 and CC-81a were not as efficacious as the reference ligand CP55,940 (Figure 3-1; Table 3-1). Nevertheless, they acted as partial agonists of ERK1/2 phosphorylation at GPR55. Many of these ligands displayed favorable potencies at GPR55, as evidenced by their relatively low EC_{50} values. For example, CC-28, one of the most efficacious ligands in the series ($E_{max(CC\text{-}28)}$ =1.5 ± 0.06) had an EC_{50} of 6.4 (0.38 – 48) nM while the partial agonist CC-66 displayed one of the highest potencies ($EC_{50(CC\text{-}66)}$ = 2.9 [0.24 – 63] nM) (Table 3-1).

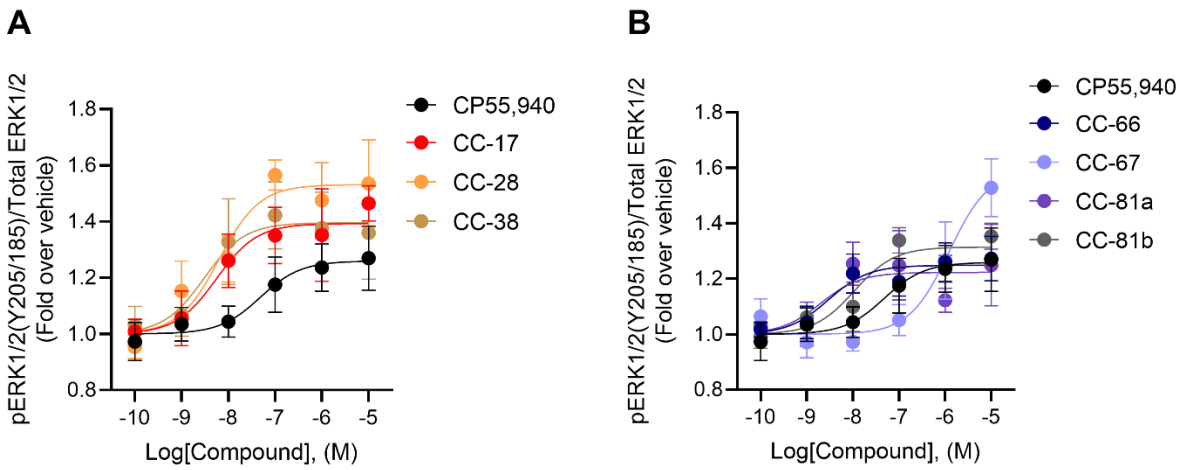

Figure 3-1. GPR55-dependent phosphorylation of ERK1/2 for CC series of GPR55 ligands. CHO cells expressing *h*GPR55 were treated with 0.1 nM – 10 μM CC-17, CC-28, and CC-38 (A) or CC-66, CC-67, CC-81a, and CC-81b (B) for 10 min to measure ERK1/2 phosphorylation. Data were fit to a 3-parameter non-linear regression and are represented as fold over vehicle. Data are mean ± SEM from n = 6 independent experiments performed in duplicate.

Compound	**ERK1/2 phosphorylation**	
	EC_{50} (nM)	**E_{max} (Fold)**
CP55,940	48 (0.65 – 2,100)	1.3 ± 0.06
CC-17	5.6 (0.28 – 220)	1.4 ± 0.07
CC-28	6.4 (0.38 – 48)	1.5 ± 0.06
CC-38	< 0.1	1.4 ± 0.05
CC-66	2.9 (0.24 – 63)	1.2 ± 0.04
CC-67	> 10,000	1.5 ± 0.04*
CC-81a	n.c	1.2 ± 0.06
CC-81b	11 (1.0 – 56)	1.3 ± 0.03

Table 3-1. GPR55-dependent phosphorylation of ERK1/2 for CC series of GPR55 ligands. Data were fit to a 3-parameter non-linear regression to estimate potency (EC_{50}) and efficacy (E_{max}) values. Data are expressed as mean with 95% CI (EC_{50}) or mean ± SEM (E_{max}). n = 6 independent experiments performed in duplicate. If potency could not be estimated (*i.e.* < 0.1 nM or > 10,000 nM), then E_{max} is reported as the mean of the greatest response observed. Statistical analyses were by one-way ANOVA followed by Tukey's *post-hoc* test. *p < 0.05 relative to CP55,940. n.c – not converged.

3.1.2 $G\alpha_{i/o}$-mediated inhibition of FSK-stimulated cAMP at CB2R

To assess whether the GPR55 ligands were truly selective for GPR55, the ability of the compounds to induce downstream signaling at other cannabinoid receptors, specifically at CB2R, was assessed. CB2R is a $G\alpha_{i/o}$-coupled GPCR whose activation leads to the inhibition of AC and reduced accumulation of cAMP. CC-17, CC-28, CC-38, CC-66, CC-67, CC-81a, and CC-81b were evaluated for their ability to inhibit the production of FSK-stimulated cAMP in CHO cells expressing *h*CB2R. CP55,940 was used as a reference compound. Despite being designed as GPR55-selective agonists, many of the compounds also displayed activity at CB2R. While none of the compounds displayed full agonist activity, CC-66 and CC-67 acted as weak partial agonists of cAMP inhibition at CB2R ($E_{max(CC\text{-}66)} = 14 \pm 15\%$; $E_{max(CC\text{-}67)} = 27 \pm 26\%$) (Figure 3-2; Table 3-2). Interestingly, the CRCs for CC-17, CC-28, CC-38, CC-81a, and CC-81b trended below the x-axis, consistent with the activity of an inverse agonist (Figure 3-2). This is further reflected by the negative efficacy values for these compounds ($E_{max(CC\text{-}17)} = -67 \pm 4.2\%$; $E_{max(CC\text{-}28)} = -70 \pm 4.5\%$; $E_{max(CC\text{-}38)} = -58 \pm 6.4\%$; $E_{max(CC\text{-}81a)} = -40 \pm 5.5\%$; $E_{max(CC\text{-}81b)} = -45 \pm 7.3\%$) (Table 3-2).

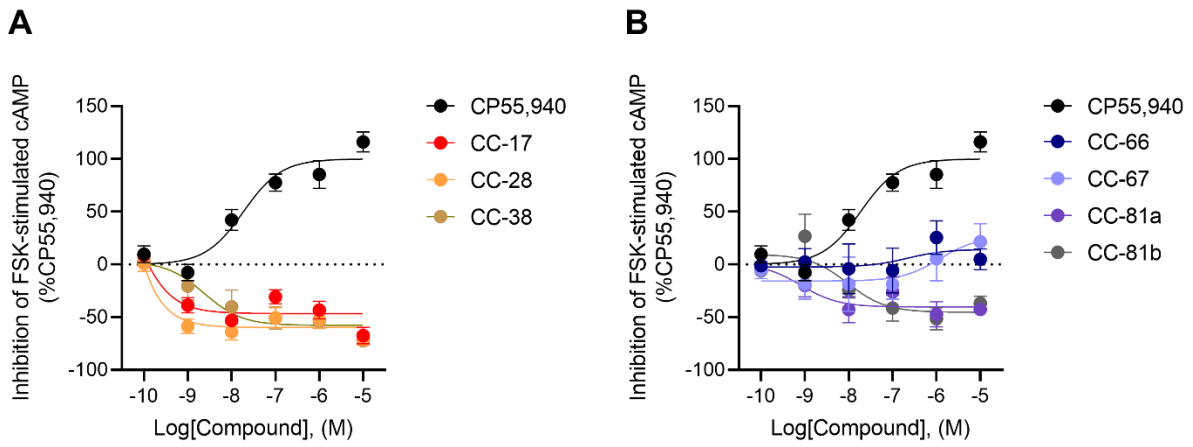

Figure 3-2. CB2R-dependent inhibition of FSK-stimulated cAMP for CC series of GPR55 ligands. CHO cells expressing *h*CB2R were treated with 10 µM FSK and 0.1 nM – 10 µM CC-17, CC-28, and CC-38 (A) or CC-66, CC-67, CC-81a, and CC-81b (B) for 90 min to measure cAMP inhibition. Data were fit to a 3-parameter non-linear regression and are represented as % of the maximal response of CP55,940. Data are mean ± SEM from n = 6 independent experiments performed in duplicate.

3.1.3 βarrestin2 recruitment at CB2R

Since ligands can activate receptors through different signaling pathways, testing novel ligands in more than one functional assay can help provide a more comprehensive understanding of their activity at a given receptor. For this reason, CC-17, CC-28, CC-38, CC-66, CC-67, CC-81a, and CC-81b were evaluated for their ability to recruit βarrestin2 in CHO cells expressing *h*CB2R since CB2R can associated with βarrestin2, leading to receptor desensitization and internalization[58]. CP55,940 was used as a reference compound. Most of the GPR55 ligands were unable to effectively recruit βarrestin2 to CB2R. The exception being CC-17 and CC-28 ($E_{max(CC-17)}$ = 13 ± 4.5%; $E_{max(CC-28)}$ = 24 ± 1.1%), which acted as weak partial agonists of βarrestin2 recruitment at CB2R though this was only evident at higher concentrations (e.g. 10,000 nM) (Figure 3-3; Table 3-2).

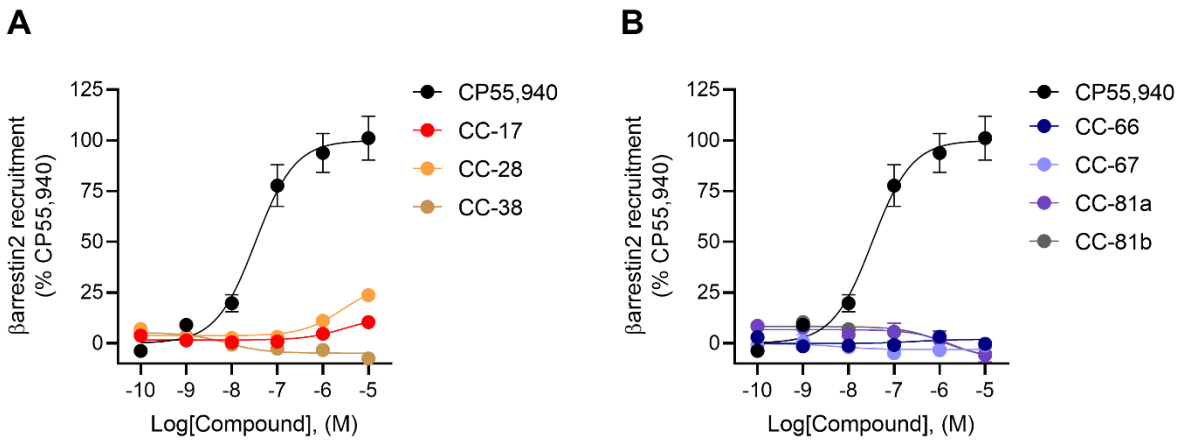

Figure 3-3. CB2R-dependent recruitment of βarrestin2 for CC series of GPR55 ligands. CHO cells expressing *h*CB2R were treated with 0.1 nM – 10 μM CC-17, CC-28, and CC-38 (A) or CC-66, CC-67, CC-81a, and CC-81b (B) for 90 min to measure βarrestin2 recruitment. Data were fit to a 3-parameter non-linear regression and are represented as % of the maximal response of CP55,940. Data are mean ± SEM from n = 6 independent experiments performed in duplicate.

Compound	**cAMP inhibition**		**βarrestin2 recruitment**	
	EC_{50} (nM)	**E_{max} (%)**	**EC_{50} (nM)**	**E_{max} (%)**
CP55,940	19 (7.0 – 65)	100 ± 6.7	33 (16 – 70)	100 ± 5.4
CC-17	< 0.1	-67 ± 4.2****	n.c	13 ± 4.5****
CC-28	< 0.1	-70 ± 4.5****	> 10,000	24 ± 1.1****
CC-38	2.4 (0.22 – 42)	-58 ± 6.4****	7.6 (0.31 – 1,100)	-4.9 ± 1.6****
CC-66	n.c	14 ± 15****	n.c	1.9 ± 3.1****
CC-67	n.c	27 ± 26***	n.c	-3.1 ± 1.5****
CC-81a	n.c	-40 ± 5.5****	n.c	-8.1 ± 6.1****
CC-81b	9.5 (1.9 – 70)	-45 ± 7.3****	n.c	-6.8 ± 4.2****

Table 3-2. CB2R-dependent inhibition of FSK-stimulated cAMP and recruitment of βarrestin2 for CC series of GPR55 ligands. Data were fit to a 3-parameter non-linear regression to estimate potency (EC_{50}) and efficacy (E_{max}) values. Data are expressed as mean with 95% CI (EC_{50}) or mean ± SEM (E_{max}). n = 6 independent experiments performed in duplicate. If potency could not be estimated (*i.e.* < 0.1 nM or > 10,000 nM), then E_{max} is reported as the mean of the greatest response observed. Statistical analyses were by one-way ANOVA followed by Tukey's *post-hoc* test. ***p < 0.001, ****p < 0.0001 relative to CP55,940. n.c – not converged.

Although the CC series of GPR55 ligands were assessed in both cAMP inhibition and βarrestin2 recruitment assays at CB2R, bias factors (ΔΔLogR) were not calculated for these compounds. Firstly, many compounds (e.g. CC-38, CC-66, CC-67, CC-81a, and CC-81b), were inactive in the βarrestin2 recruitment assay so bias factors could not be calculated for these compounds (Figure 3-3; Table 3-2). Furthermore, while CC-17 and CC-28 displayed activity in both cAMP inhibition and βarrestin2 recruitment assays, as inverse agonists and weak partial agonists respectively, it might be beyond our understanding of biased agonism to conduct and interpret bias analyses for these ligands (Figure 3-2; Figure 3-3; Table 3-2).

3.2 Experiment 2: Pharmacological properties of novel CB2R ligands

3.2.1 FD series

3.2.1.1 $G\alpha_{i/o}$-mediated inhibition of FSK-stimulated cAMP at CB2R

The CB2R bitopic ligands FD-22a, FD-24a, FD-25a, FD-27a, and FD-32a, and their parent orthosteric and allosteric ligands FM-6b and EC-21a, were assessed in the cAMP inhibition assay using CHO cells expressing *h*CB2R. CP55,940 was used as a reference compound. The orthosteric parent ligand FM-6b was a potent and efficacious partial agonist of cAMP inhibition at CB2R ($E_{max(FM\text{-}6b)}$ = 76 ± 10%; $EC_{50(FM\text{-}6b)}$ = 20 [0.10 – 1,500]nM) (Figure 3-4A; Table 3-3). The allosteric parent ligand EC-21a displayed no response in the cAMP inhibition assay ($E_{max(EC\text{-}21a)}$ = 0.12 ± 2.2%), which was expected given its allosteric nature (Figure 3-4A; Table 3-3). Among the CB2R bitopic ligands, FD-22a and FD-24a represented the most efficacious and potent compounds, respectively ($E_{max(FD\text{-}22a)}$ = 45 ± 3.4%; $EC_{50(FD\text{-}24a)}$ = 10 [1.0 – 140] nM) (Figure 3-4B; Table 3-3). FD-25a, FD-27a, and FD-32a displayed low potencies and efficacies (Figure 3-4B; Table 3-3).

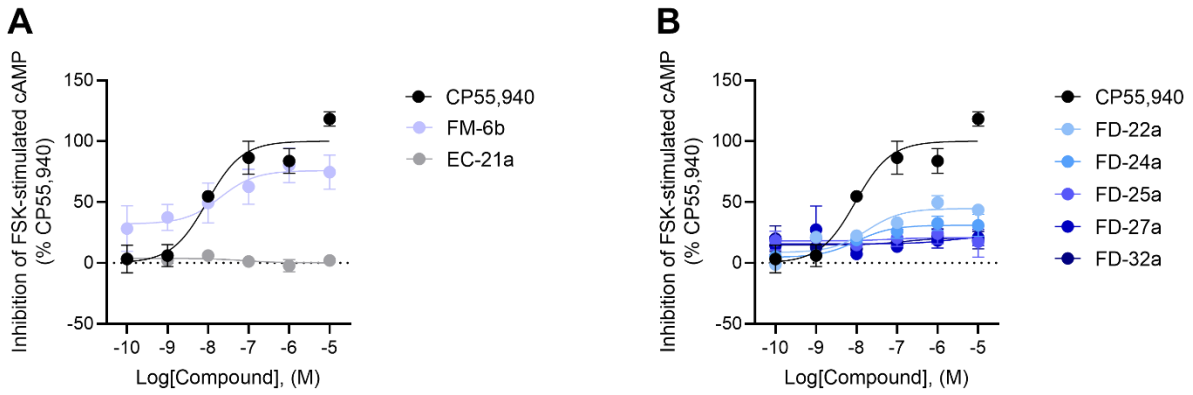

Figure 3-4. CB2R-dependent inhibition of FSK-stimulated cAMP for FD series of CB2R ligands. CHO cells expressing *h*CB2R were treated with 10 μM FSK and 0.1 nM – 10 μM parent ligands of the FD series (A) or FD series ligands (B) for 90 min to measure cAMP inhibition. Data were fit to a 3-parameter non-linear regression and are represented as % of the maximal response of CP55,940. Data are mean ± SEM from n = 4-6 independent experiments performed in triplicate.

3.2.1.2 βarrestin2 recruitment at CB2R

FD-22a, FD-24a, FD-25a, FD-27a, and FD-32a, and their parent ligands were also evaluated in the βarrestin2 recruitment assay using CHO cells expressing *h*CB2R. CP55,940 was used as a reference compound. As with the cAMP inhibition experiment, the parent ligands displayed similar activity with regard to βarrestin2 recruitment: FM-6b was a potent partial agonist of βarrestin2 recruitment ($E_{max(FM\text{-}6b)}$ = 45 ± 1.5%; $EC_{50(FM\text{-}6b)}$ = 63 [36 – 100]nM) at CB2R whereas EC-21a was inactive (Figure 3-5A; Table 3-3). Most of the FD series ligands displayed efficacies similar to the orthosteric parent FM-6b ($E_{max(FD\text{-}24a)}$ = 43 ± 2.3%; $E_{max(FD\text{-}25a)}$ = 46 ± 1.6%; $E_{max(FD\text{-}27a)}$ = 41 ± 1.1%; $E_{max(FD\text{-}32a)}$ = 53 ± 1.4%) though they were much less potent in this regard ($EC_{50(FD\text{-}24a)}$ = 2,600 [1,800 – 4,000]nM; $EC_{50(FD\text{-}25a)}$ = 1,200 [890 – 1,600]nM; $EC_{50(FD\text{-}27a)}$ = 860 [670 – 1,100]nM; $EC_{50(FD\text{-}32a)}$ = 560 [400 – 760]nM) (Figure 3-5B; Table 3-3).

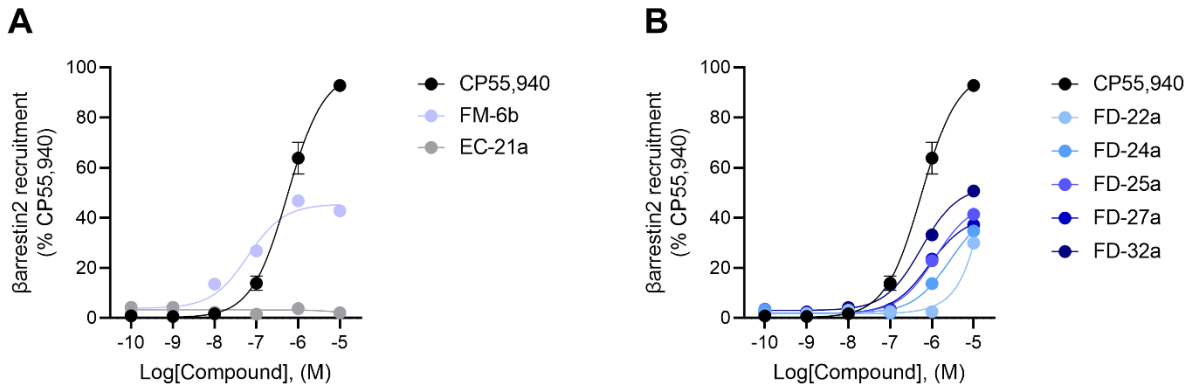

Figure 3-5. CB2R-dependent recruitment of βarrestin2 for FD series of CB2R ligands. CHO cells expressing *h*CB2R were treated with 0.1 nM – 10 μM parent ligands of the FD series (A) or FD series ligands (B) for 90 min to measure βarrestin2 recruitment. Data were fit to a 3-parameter non-linear regression and are represented as % of the maximal response of CP55,940. Data are mean ± SEM from n = 6 independent experiments performed in triplicate.

Compound	**cAMP inhibition**		**βarrestin2 recruitment**	
	EC_{50} (nM)	**E_{max} (%)**	**EC_{50} (nM)**	**E_{max} (%)**
CP55,940	9.4 (3.4 – 29)	100 ± 6.4	560 (410 – 760)	98 ± 3.4
FM-6b	20 (0.10 – 1,500)	76 ± 10***	63 (36 – 100)	45 ± 1.5****
EC-21a	n.c	0.12 ± 2.2***	> 10,000	2.1 ± 0.30****
FD-22a	18 (0.34 – 150)	45 ± 3.4***	> 10,000	30 ± 2.5****
FD-24a	10 (1.0 – 140)	31 ± 3.4****	2,600 (1,800 – 4,000)	43 ± 2.3****
FD-25a	n.c	21 ± 6.0****	1,200 (890 – 1,600)	46 ± 1.6****
FD-27a	n.c	22 ± 1.8****	860 (670 – 1,100)	41 ± 1.1****
FD-32a	n.c	21 ± 0.62****	560 (400 – 760)	53 ± 1.4****

Table 3-3. CB2R-dependent inhibition of FSK-stimulated cAMP and recruitment of βarrestin2 for FD series of CB2R ligands. Data were fit to a 3-parameter non-linear regression to estimate potency (EC_{50}) and efficacy (E_{max}) values. Data are expressed as mean with 95% CI (EC_{50}) or mean ± SEM (E_{max}). n = 4-6 independent experiments performed in triplicate. If potency could not be estimated (*i.e.* > 10,000 nM), then E_{max} is reported as the mean of the greatest response observed. Statistical analyses were by one-way ANOVA followed by Tukey's *post-hoc* test. ***$p < 0.001$, ****$p < 0.0001$ relative to CP55,940. n.c – not converged.

3.2.1.3 Signal bias at CB2R

In order to assess signal bias at CB2R, bias factors (ΔΔLogR) were calculated by fitting data from cAMP inhibition and βarrestin2 recruitment assays to the operational model of Black and Leff. Bias factors were only calculated for compounds which displayed activity in both cAMP inhibition and βarrestin2 recruitment assays. For this reason, bias factors were not calculated for EC-21a as it lacked activity in cAMP inhibition and βarrestin2 recruitment assays (Figure 3-4A; Figure 3-5A; Table 3-3). Similarly, bias factors were not calculated for FD-25a, FD-27a, and FD-32a as these compounds displayed little to no activity in the cAMP inhibition assay (Figure 3-4B; Table 3-3). ΔΔLogR values > 0 indicate bias towards inhibition of FSK-stimulated cAMP, ΔΔLogR values < 0 indicate bias towards βarrestin2 recruitment, and ΔΔLogR values $= 0$ indicate that the ligand did not display bias towards either of the pathways (i.e. balanced ligand). FM-6b, FD-22a and FD-24a were biased towards βarrestin2 recruitment, though this may not be of biological relevance for FM-6b and FD-22a due to the size of their bias factors, which were -0.39 and -0.10 respectively (Figure 3-6)[197]. Conversely, FD-24a displayed a greater level of βarrestin2 recruitment bias, with a bias factor of -5.7 (Figure 3-6).

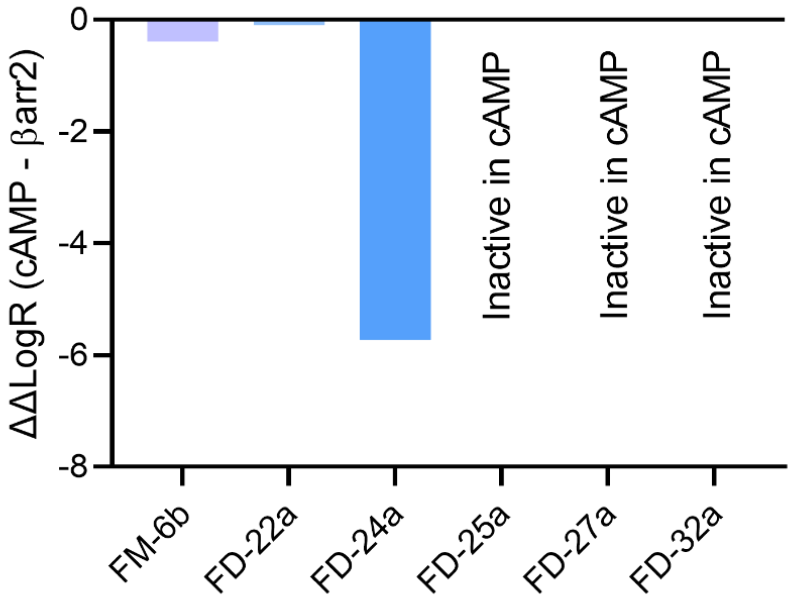

Figure 3-6. Signal bias at CB2R for FD series of CB2R ligands. Data from cAMP inhibition and βarrestin2 recruitment assays were fit to the operational model of Black and Leff to calculate bias factors (ΔΔLogR). Data are from n = 4-6 independent experiments performed in triplicate.

3.2.1.4 $G\alpha_{i/o}$-mediated inhibition of FSK-stimulated cAMP at CB2R in the presence of additional ligands

Given that the FD series of CB2R bitopic ligands were designed by joining the pharmacophoric portions of the orthosteric agonist FM-6b and CB2R PAM EC-21a, the effect of 10 nM FM-6b in combination with 0.1 nM – 10 μM of EC-21a was explored in the cAMP inhibition assay using CHO cells expressing *h*CB2R. CP55,940 was used as a reference compound. Though the combination of the two compounds lead to a more potent response than FM-6b alone ($EC_{50(\text{FM-6b + EC-21a})}$ = 8.8 [0.63 – 970]nM; $EC_{50(\text{FM-6b})}$ = 20 [0.10 – 1,500]nM), a decrease in efficacy was also observed ($E_{max(\text{FM-6b + EC-21a})}$ = 56 ± 7.0%; $E_{max(\text{FM-6b})}$ = 76 ± 10%) (Figure 3-7; Table 3-4).

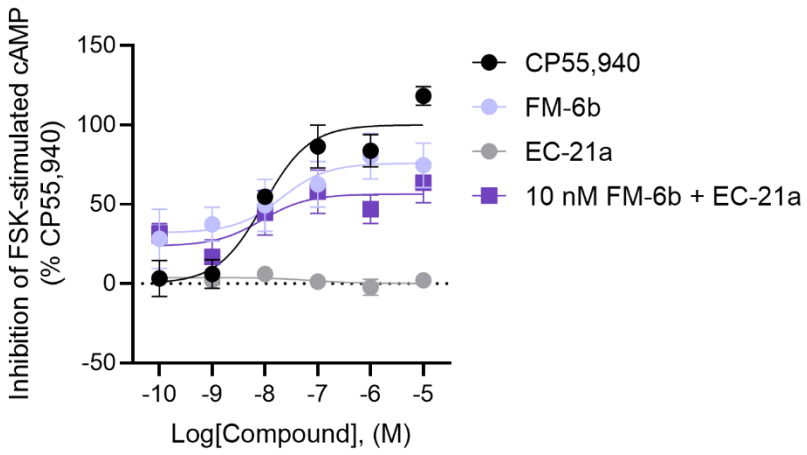

Figure 3-7. CB2R-dependent inhibition of FSK-stimulated cAMP for combination experiments with orthosteric and allosteric parent ligands of the FD series of CB2R ligands. CHO cells expressing *h*CB2R were treated with 10 μM FSK, 10 nM FM-6b and 0.1 nM – 10 μM EC-21a for 90 min to measure cAMP inhibition. Data were fit to a 3-parameter non-linear regression and are represented as % of the maximal response of CP55,940. Data are mean ± SEM from n = 6 independent experiments performed in triplicate.

Preliminary assessment of the FD series uncovered FD-22a and FD-24a as the most promising ligands of the FD series (Figure 3-4B; Table 3-3). These ligands, at their approximated EC_{50} values, were subsequently assessed in combination with 0.1 nM – 10 μM EC-21a in the cAMP inhibition assay using CHO cells expressing *h*CB2R. CP55,940 was used as a reference compound. While the combination of FD-22a and EC-21a resulted in a decrease in efficacy compared to FD-22a alone ($E_{max(FD\text{-}22a\ +\ EC\text{-}21a)}$ = 20 ± 4.9%; $E_{max(FD\text{-}22a)}$ = 45 ± 3.4%), the combination of FD-24a and EC-21a produced a more efficacious response than FD-24a alone ($E_{max(FD\text{-}24a\ +\ EC\text{-}21a)}$ = 89 ± 33%; $E_{max(FD\text{-}24a)}$ = 31 ± 3.4 %) (Figure 3-8; Table 3-4).

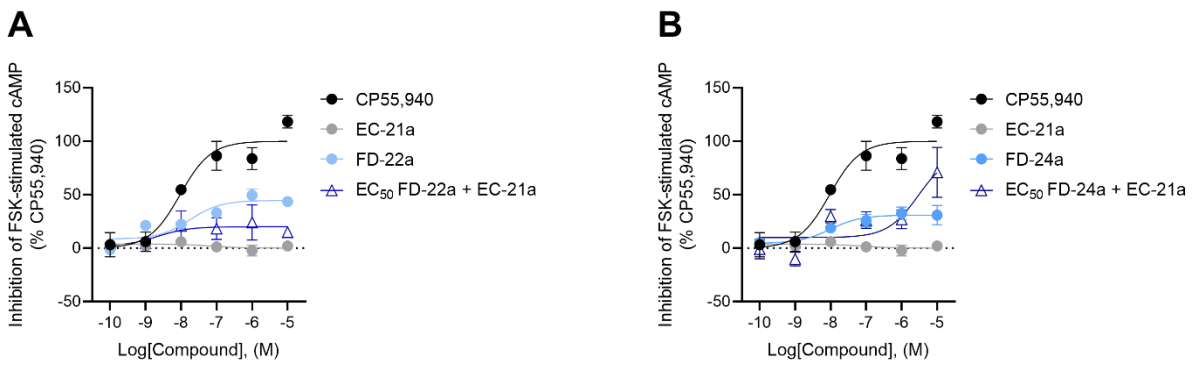

Figure 3-8. CB2R-dependent inhibition of FSK-stimulated cAMP for combination experiments with the allosteric parent ligand and select bitopic ligands of the FD series of CB2R ligands. CHO cells expressing *h*CB2R were treated with 10 µM FSK, 0.1 nM – 10 µM EC-21a and 50 nM FD-22a (A) or 5 nM FD-24a (B) for 90 min to measure cAMP inhibition. Data were fit to a 3-parameter non-linear regression and are represented as % of the maximal response of CP55,940. Data are mean ± SEM from n = 4-6 independent experiments performed in triplicate.

To confirm whether these ligands mediated their signaling through CB2R, 0.1 nM – 10 µM FD-22a and FD-24a were tested in combination with 100 nM of the CB2R antagonist/inverse agonist SR144528 in the cAMP inhibition assay using CHO cells expressing *h*CB2R. CP55,940 was used as a reference compound. For both FD-22a and FD-24a, the presence of SR144528 resulted in a downward shift of their CRCs, compared to those of either bitopic ligand alone (Figure 3-9). However, as the concentration of FD-22a or FD-24a increased, these ligands effectively competed off SR144528 from the orthosteric binding site, thereby removing the inhibition of CB2R and producing efficacy values similar to that of FD-22a or FD-24a alone ($E_{max(SR144528 + FD\text{-}22a)}$ = 39 ± 12%; $E_{max(FD\text{-}22a)}$ = 45 ± 3.4%); $E_{max(SR144528 + FD\text{-}24a)}$ = 34 ± 8.1%; $E_{max(FD\text{-}24a)}$ = 31 ± 3.4%) (Figure 3-9; Table 3-4).

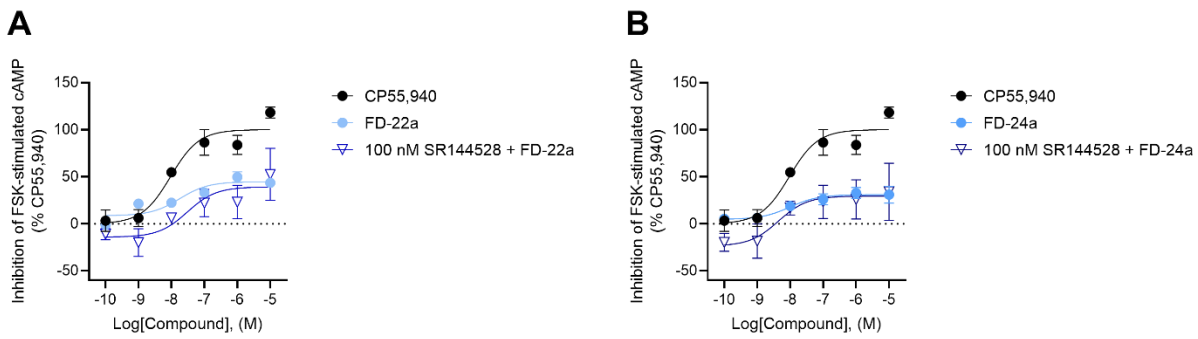

Figure 3-9. CB2R-dependent inhibition of FSK-stimulated cAMP for combination experiments with SR144528 and select bitopic ligands of the FD series of CB2R ligands. CHO cells expressing *h*CB2R were treated with 10 μM FSK, 100 nM SR144528 and 0.1 nM – 10 μM FD-22a (A) or FD-24a (B) for 90 min to measure cAMP inhibition. Data were fit to a 3-parameter non-linear regression and are represented as % of the maximal response of CP55,940. Data are mean ± SEM from n = 4-6 independent experiments performed in triplicate.

Compound	**cAMP inhibition**	
	EC_{50} (nM)	**E_{max} (%)**
CP55,940	9.4 (3.4 – 29)	100 ± 6.4
FM-6b	20 (0.10 – 1,500)	76 ± 10***
EC-21a	n.c	0.12 ± 2.2***
10 nM FM-6b + EC-21a	8.8 (0.63 – 970)	56 ± 7.0**
FD-22a	18 (0.34 – 150)	45 ± 3.4***
EC_{50} FD-22a + EC-21a	n.c	20 ± 4.9****
100 nM SR144528 + FD-22a	n.c	39 ± 12****
FD-24a	10 (1.0 – 140)	31 ± 3.4****
EC_{50} FD-24a + EC-21a	n.c	89 ± 33
100 nM SR144528 + FD-24a	< 0.1	34 ± 8.1****

Table 3-4. CB2R-dependent inhibition of FSK-stimulated cAMP for combination experiments with FD series of CB2R ligands. Data were fit to a 3-parameter non-linear regression to estimate potency (EC_{50}) and efficacy (E_{max}) values. Data are expressed as mean with 95% CI (EC_{50}) or mean ± SEM (E_{max}). n = 4-6 independent experiments performed in triplicate. If potency could not be estimated (*i.e.* < 0.1 nM), then E_{max} is reported as the mean of the greatest response observed. Statistical analyses were by one-way ANOVA followed by Tukey's *post-hoc* test. **p < 0.01, ***p < 0.001, ****p < 0.0001 relative to CP55,940. n.c – not converged.

3.2.2 FG series

3.2.2.1 $G\alpha_{i/o}$-mediated inhibition of FSK-stimulated cAMP at CB2R

The synthetic CB2R ligand LV-62 and its derivatives, FG-158a, FG-160a, and FG-161a, were assessed in the cAMP inhibition assay using CHO cells expressing *h*CB2R. CP55,940 was used as a reference compound. LV-62 proved to be the most efficacious and most potent among the series of ligands, producing a response similar to the reference compound CP55,940 ($E_{max(LV\text{-}62)}$ = 110 ± 8.8%; $E_{max(CP55,940)}$ = 100 ± 6.4%) (Figure 3-10; Table 3-5). FG-158a, FG-160a, and FG-161a also activated the cAMP inhibition pathway albeit at a lower potency and efficacy than their parent ligand LV-62 ($E_{max(FG\text{-}158a)}$ = 94 ± 48%; $EC_{50(FG\text{-}158a)}$ = not converged; $E_{max(FG\text{-}160a)}$ = 96 ± 19%; $EC_{50(FG\text{-}160a)}$ = 600 [73 – 6,100] nM; $E_{max(FG\text{-}161a)}$ = 83 ± 11%; $EC_{50(FG\text{-}161a)}$ = 760 [150 – 2,900] nM; $EC_{50(LV\text{-}62)}$ = 34 [3.9 – 220] nM) (Figure 3-10; Table 3-5). As seen in the CRCs, the efficacy of FG-158a, FG-160a, and FG-161a becomes more apparent at higher concentrations (Figure 3-10).

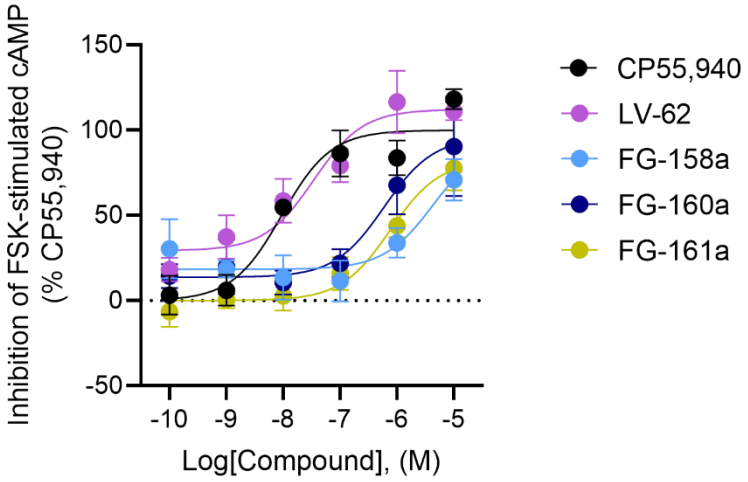

Figure 3-10. CB2R-dependent inhibition of FSK-stimulated cAMP for FG series of CB2R ligands. CHO cells expressing *h*CB2R were treated with 10 µM FSK and 0.1 nM – 10 µM compounds for 90 min to measure cAMP inhibition. Data were fit to a 3-parameter non-linear regression and are represented as % of the maximal response of CP55,940. Data are mean ± SEM from *n* = 6 independent experiments performed in triplicate.

3.2.2.2 βarrestin2 recruitment at CB2R

LV-62 and its derivatives FG-158a, FG-160a, and FG-161a were evaluated for their ability to enhance βarrestin2 recruitment to CB2R using CHO cells expressing *h*CB2R. CP55,940 was used as a reference compound. LV-62 enhanced βarrestin2 recruitment to CB2R, although with less efficacy than the reference compound ($E_{max(LV\text{-}62)}$ = 65 ±1.4%; $E_{max(CP55,940)}$ = 98 ± 3.4%) (Figure 3-11; Table 3-5). Despite this, LV-62 displayed greater potency than CP55,940 ($EC_{50(LV\text{-}62)}$ = 63 [49 – 82] nM; $EC_{50(CP55,940)}$ = 560 [410 – 760] nM) (Table 3-5). The FG series exhibited reduced efficacies in the βarrestin2 recruitment assay ($E_{max(FG\text{-}158a)}$ = 46 ±1.8%; $E_{max(FG\text{-}160a)}$ = 41 ± 1.0%; $E_{max(FG\text{-}161a)}$ = 47 ±1.8%) (Figure 3-11; Table 3-5). As seen in the cAMP inhibition experiments, these ligands were also less potent than the parent ligand LV-62 ($EC_{50(FG\text{-}158a)}$ = 1,100 [820 – 1,600] nM; $EC_{50(FG\text{-}160a)}$ = 870 [690 – 1,100] nM; $EC_{50(FG\text{-}161a)}$ = 1,300 [950 – 1,800] nM; $EC_{50(LV\text{-}62)}$ = 63 [49 – 82] nM) (Table 3-5).

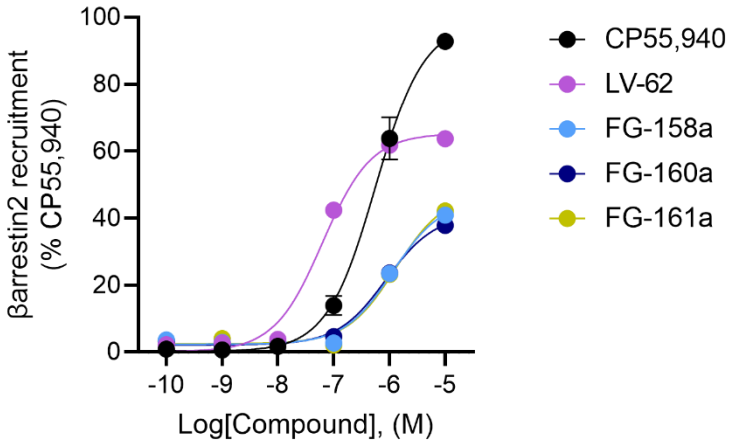

Figure 3-11. CB2R-dependent recruitment of βarrestin2 for FG series of CB2R ligands. CHO cells expressing *h*CB2R were treated with 0.1 nM – 10 μM compounds for 90 min to measure βarrestin2 recruitment. Data were fit to a 3-parameter non-linear regression and are represented as % of the maximal response of CP55,940. Data are mean ± SEM from *n* = 6 independent experiments performed in triplicate.

Compound	cAMP inhibition		βarrestin2 recruitment	
	EC_{50} (nM)	**E_{max} (%)**	**EC_{50} (nM)**	**E_{max} (%)**
CP55,940	9.4 (3.4 – 29)	100 ± 6.4	560 (410 – 760)	98 ± 3.4
LV-62	34 (3.9 – 220)	110 ± 8.8	63 (49 – 82)	65 ± 1.4*
FG-158a	n.c	94 ± 48	1,100 (820 – 1,600)	46 ± 1.8*
FG-160a	600 (73 – 6,100)	96 ± 19	870 (690 – 1,100)	41 ± 1.0*
FG-161a	760 (150 – 2,900)	83 ± 11	1,300 (950 – 1,800)	47 ± 1.8*

Table 3-5. CB2R-dependent inhibition of FSK-stimulated cAMP and recruitment of βarrestin2 for FG series of CB2R ligands. Data were fit to a 3-parameter non-linear regression to estimate potency (EC_{50}) and efficacy (E_{max}) values. Data are expressed as mean with 95% CI (EC_{50}) or mean ± SEM (E_{max}). $n = 6$ independent experiments performed in triplicate. Statistical analyses were by one-way ANOVA followed by Tukey's *post-hoc* test. *$p < 0.05$ relative to CP55,940. n.c – not converged.

3.2.2.3 Signal bias at CB2R

In order to assess signal bias at CB2R, bias factors (ΔΔLogR) were calculated for LV-62, FG-158a, FG-160a, and FG-161a, by fitting data from cAMP inhibition and βarrestin2 recruitment assays to the operational model of Black and Leff. ΔΔLogR values > 0 indicate bias towards inhibition of FSK-stimulated cAMP, ΔΔLogR values < 0 indicate bias towards βarrestin2 recruitment, and ΔΔLogR values = 0 indicate that the ligand did not display bias towards either of the pathways (i.e. balanced ligand). LV-62, FG-158a, FG-160a, and FG-161a were all modestly biased towards βarrestin2 recruitment with biases between -1.7 and -0.18, which indicates some degree of bias but likely not enough to be of biological relevance (Figure 3-12)[197].

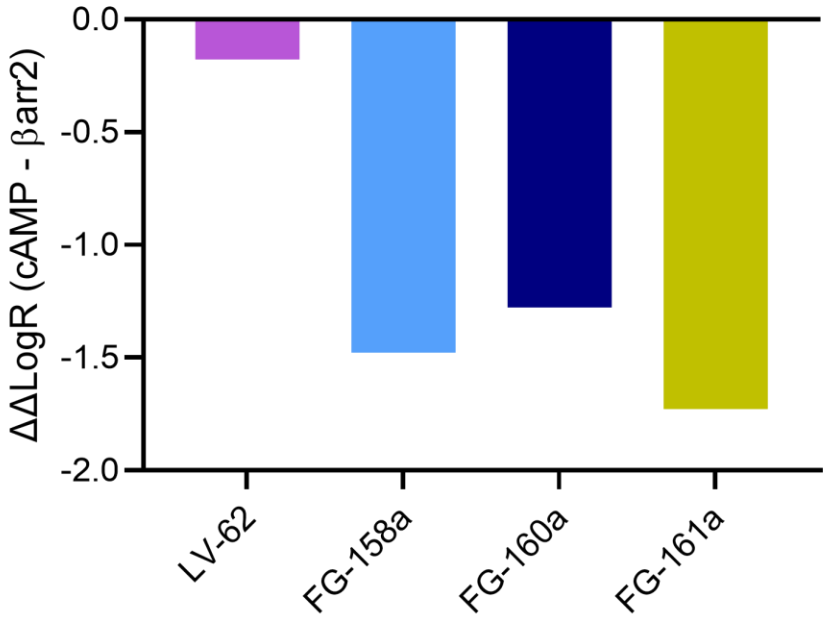

Figure 3-12. Signal bias at CB2R for FG series of CB2R ligands. Data from cAMP inhibition and βarrestin2 recruitment assays were fit to the operational model of Black and Leff to calculate bias factors (ΔΔLogR). Data are from *n* = 4-6 independent experiments performed in triplicate.

3.2.3 JR series

3.2.3.1 $G\alpha_{i/o}$-mediated inhibition of FSK-stimulated cAMP at CB2R

The JR series, consisting of JR-14a, JR-16a, JR-22a, JR-26a, JR-58a, JR-60a, JR-61a, and JR-64a, along with their parent ligands LV-62 and EC-21a were evaluated for their ability to inhibit FSK-stimulated cAMP production in CHO cells expressing *h*CB2R. CP55,940 was used as a reference compound. As indicated previously, the orthosteric parent ligand LV-62 was a potent full agonist of cAMP inhibition at CB2R ($E_{max(LV-62)}$ = 110 ± 8.8%) while the allosteric parent EC-21a was inactive (Figure 3-13A; Table 3-6). All ligands of series A and series B of the JR series displayed partial agonist activity in the cAMP inhibition assay at CB2R (Figure 3-13B-D; Table 3-6). JR-

14a and JR-64a were of particular interest as they represented the most potent ligands of series B and series A, respectively ($EC_{50(JR\text{-}14a)}$ = 150 [5.0 – 2,200] nM; $EC_{50(JR\text{-}64a)}$ = 11 [0.84 – 200] nM) (Table 3-6).

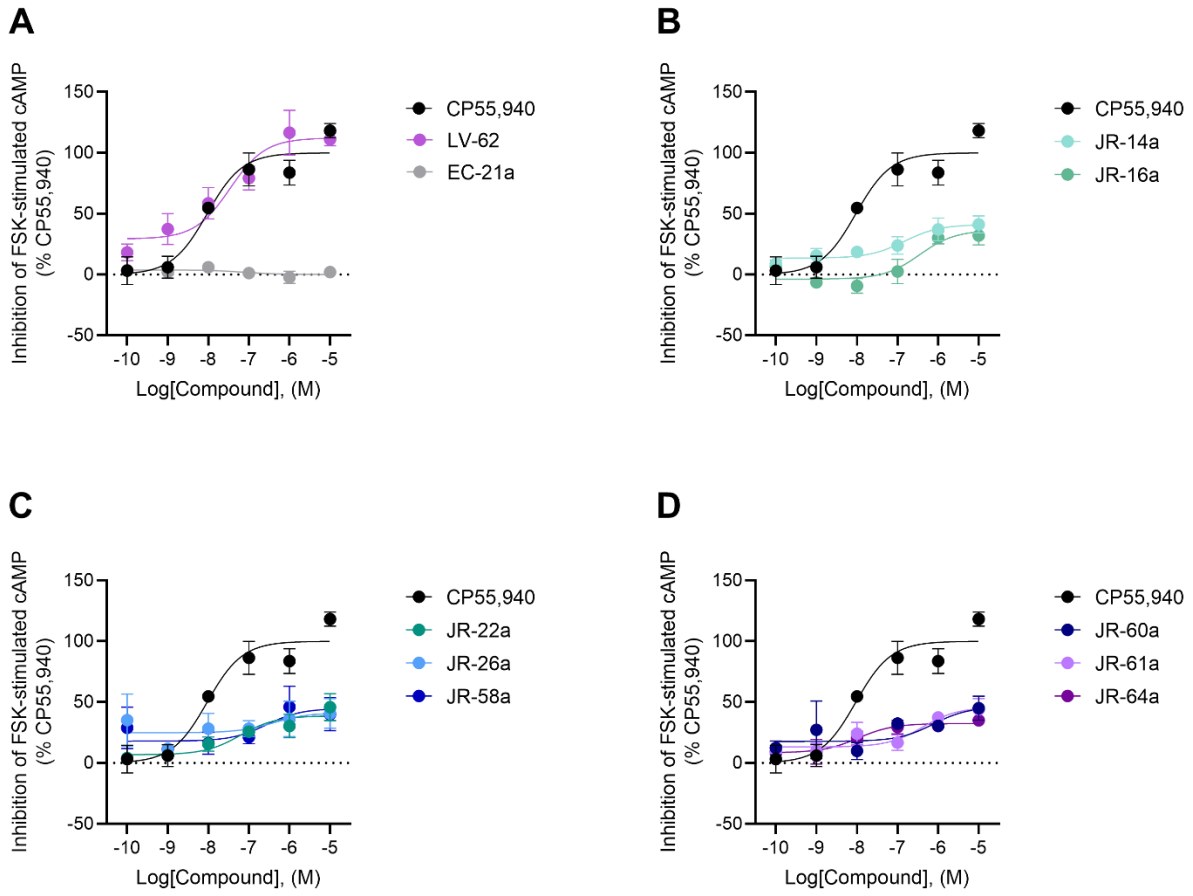

Figure 3-13. CB2R-dependent inhibition of FSK-stimulated cAMP for JR series of CB2R ligands. CHO cells expressing *h*CB2R were treated with 10 µM FSK and 0.1 nM – 10 µM parent ligands of the JR series (A), series B ligands of the JR series (B), or series A ligands of the JR series (C, D) for 90 min to measure cAMP inhibition. Data were fit to a 3-parameter non-linear regression and are represented as % of the maximal response of CP55,940. Data are mean ± SEM from n = 6 independent experiments performed in triplicate.

3.2.3.2 βarrestin2 recruitment at CB2R

The same compounds were also assessed in the βarrestin2 recruitment assay using CHO cells expressing *h*CB2R. CP55,940 was used as a reference compound. As with the cAMP inhibition assay, LV-62 was capable of activating the βarrestin2 recruitment signaling pathway, although it did so as a partial agonist rather than a full agonist ($E_{max(LV\text{-}62)}$ = 65 ±1.4%) (Figure 3-14A; Table 3-6). As expected for an allosteric ligand, EC-21a was inactive in this assay (Figure 3-14A; Table 3-6). Though less efficacious than its orthosteric parent ligand, JR-14a was a potent partial agonist of βarrestin2 recruitment at CB2R ($E_{max(JR\text{-}14a)}$ = 39 ± 0.93%; $EC_{50(JR\text{-}14a)}$ = 25 [16 – 39] nM) (Figure 3-14B; Table 3-6). Interestingly JR-16a was inactive in the βarrestin2 recruitment assay (Figure 3-14B; Table 3-6). The JR ligands of series A displayed low potencies and as evidenced by their CRCs, their ability to recruit βarrestin2 to CB2R only became apparent at higher concentrations (Figure 3-14C-D; Table 3-6).

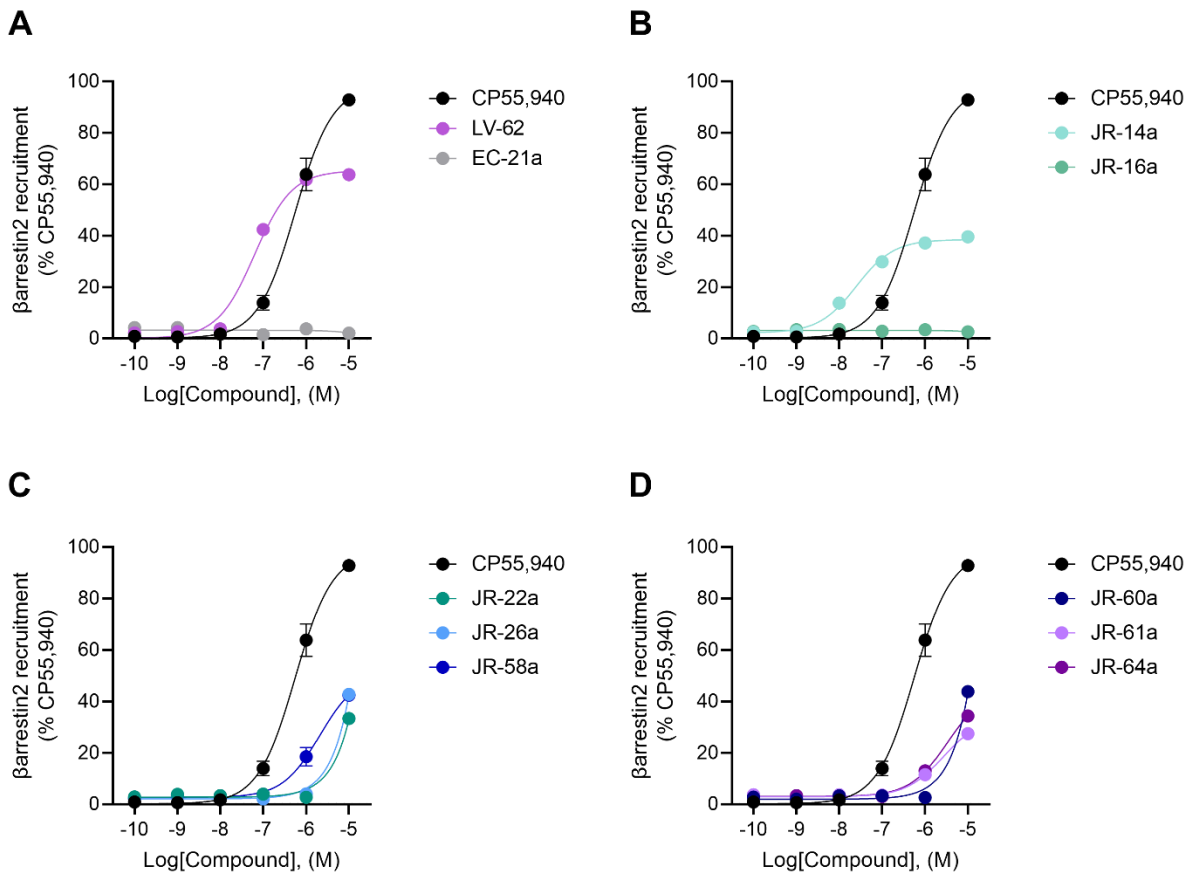

Figure 3-14. CB2R-dependent recruitment of βarrestin2 for JR series of CB2R ligands. CHO cells expressing *h*CB2R were treated with 0.1 nM – 10 μM parent ligands of the JR series (A), series B ligands of the JR series (B), or series A ligands of the JR series (C, D) for 90 min to measure βarrestin2 recruitment. Data were fit to a 3-parameter non-linear regression and are represented as % of the maximal response of CP55,940. Data are mean ± SEM from n = 6 independent experiments performed in triplicate.

Compound	cAMP inhibition		βarrestin2 recruitment	
	EC_{50} (nM)	**E_{max} (%)**	**EC_{50} (nM)**	**E_{max} (%)**
CP55,940	9.4 (3.4 – 29)	100 ± 6.4	560 (410 – 760)	98 ± 3.4
LV-62	34 (3.9 – 220)	110 ± 8.8	63 (49 – 82)	65 ± 1.4*
EC-21a	n.c	0.12 ± 2.2***	> 10,000	2.1 ± 0.30****
JR-14a	150 (5.0 – 2,200)	41 ± 5.7*	25 (16 – 39)	39 ± 0.93*
JR-16a	350 (71 – 1,900)	36 ± 8.6*	> 10,000	2.7 ± 0.25*
JR-22a	62 (2.6 – 4,100)	39 ± 5.5*	> 10,000	33 ± 2.7*
JR-26a	n.c	41 ± 15*	> 10,000	43 ± 3.6*
JR-58a	n.c	45 ± 12*	2,100 (1,400 – 3,300)	51 ± 2.8*
JR-60a	n.c	46 ± 17*	> 10,000	44 ± 3.7*
JR-61a	420 (14 – 4,600)	46 ± 7.7*	2,700 (1,700 – 4,800)	34 ± 2.2*
JR-64a	11 (0.84 – 200)	32 ± 4.0*	3,300 (2,300 – 5,100)	45 ± 2.4*

Table 3-6. CB2R-dependent inhibition of FSK-stimulated cAMP and recruitment of βarrestin2 for JR series of CB2R ligands. Data were fit to a 3-parameter non-linear regression to estimate potency (EC_{50}) and efficacy (E_{max}) values. Data are expressed as mean with 95% CI (EC_{50}) or mean ± SEM (E_{max}). $n = 6$ independent experiments performed in triplicate. If potency could not be estimated (*i.e.* > 10,000 nM), then E_{max} is reported as the mean of the greatest response observed. Statistical analyses were by one-way ANOVA followed by Tukey's *post-hoc* test. *$p < 0.05$, ***$p < 0.001$, ****$p < 0.0001$ relative to CP55,940. n.c – not converged.

3.2.3.3 Signal bias at CB2R

In order to assess signal bias at CB2R, bias factors (ΔΔLogR) were calculated by fitting data from cAMP inhibition and βarrestin2 recruitment assays to the operational model of Black and Leff. Bias factors were only calculated for compounds which displayed activity in both cAMP inhibition and βarrestin2 recruitment assays. As previously mentioned, bias factors were not calculated for EC-21a as it was inactive in cAMP inhibition and βarrestin2 recruitment assays (Figure 3-13A; Figure 3-14A; Table 3-6). Additionally, bias factors were not calculated for JR-16a, JR-22a, JR-

61a and JR-64a. JR-16a lacked activity in the βarrestin2 recruitment assay while JR-22a, JR-61a and JR-64a displayed low activity (Figure 3-14B-D; Table 3-6). ΔΔLogR values > 0 indicate bias towards inhibition of FSK-stimulated cAMP, ΔΔLogR values < 0 indicate bias towards βarrestin2 recruitment, and ΔΔLogR values = 0 indicate that the ligand did not display bias towards either of the pathways (i.e. balanced ligand). LV-62, JR-14a, JR-58a, and JR-60a were biased towards βarrestin2 recruitment, with bias factors ranging from -3.0 to -0.18 (Figure 3-15). With a bias factor of 0.44, JR-26a displayed slight bias towards cAMP inhibition (Figure 3-15).

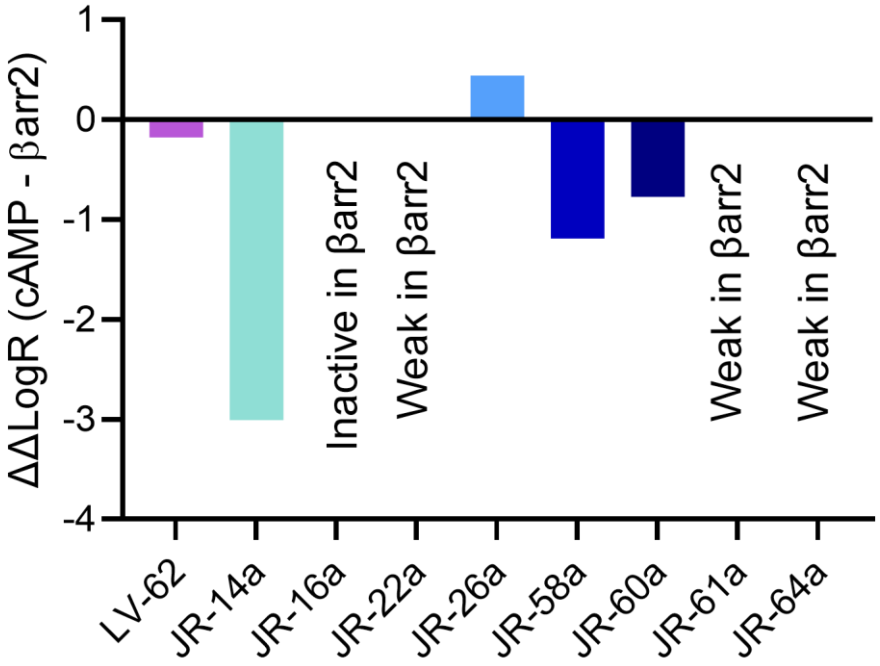

Figure 3-15. Signal bias at CB2R for JR series of CB2R ligands. Data from cAMP inhibition and βarrestin2 recruitment assays were fit to the operational model of Black and Leff to calculate bias factors (ΔΔLogR). Data are from *n* = 4-6 independent experiments performed in triplicate.

3.2.3.4 $G\alpha_{i/o}$-mediated inhibition of FSK-stimulated cAMP at CB2R in the presence of additional ligands

The JR series of CB2R bitopic ligands were designed by joining the pharmacophoric portions of the CB2R agonist LV-62 and the CB2R PAM EC-21a. Thus, the combination of 10 nM LV-62 with 0.1 nM – 10 μM of EC-21a was explored in the cAMP inhibition assay using CHO cells expressing *h*CB2R. CP55,940 was used as a reference compound. Though less efficacious than LV-62 alone ($E_{max(LV\text{-}62 + EC\text{-}21a)}$ = 55 ± 5.2%; $E_{max(LV\text{-}62)}$ = 110 ± 8.8%), the combination of LV-62 and EC-21a produced a more potent response ($EC_{50(LV\text{-}62 + EC\text{-}21a)}$ = 4.3 [0.57 – 34]nM; $EC_{50(LV\text{-}62)}$ = 34 [3.9 – 220]nM) (Figure 3-16; Table 3-7).

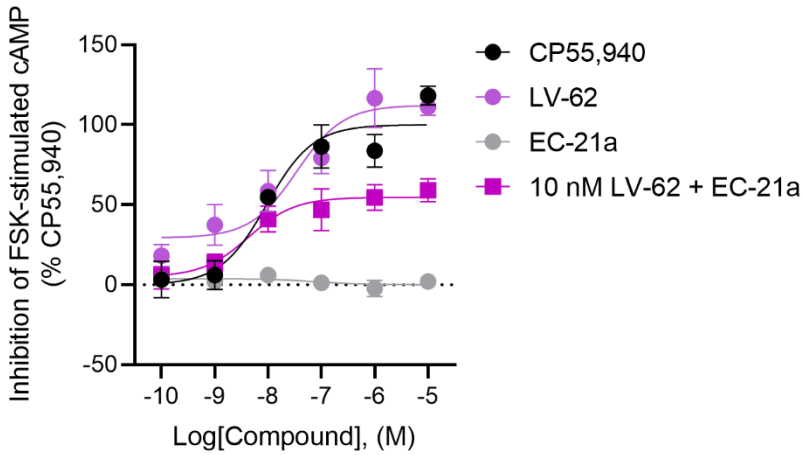

Figure 3-16. CB2R-dependent inhibition of FSK-stimulated cAMP for combination experiments with orthosteric and allosteric parent ligands of the JR series of CB2R ligands. CHO cells expressing *h*CB2R were treated with 10 μM FSK, 10 nM LV-62 and 0.1 nM – 10 μM EC-21a for 90 min to measure cAMP inhibition. Data were fit to a 3-parameter non-linear regression and are represented as % of the maximal response of CP55,940. Data are mean ± SEM from *n* = 6 independent experiments performed in triplicate.

Following preliminary assessment of the JR series, JR-14a and JR-64a were identified as the most promising ligands of series B and A, respectively (Figure 3-13B; Figure 3-13D; Table 3-6). Thus, these ligands, at their approximated EC_{50} values, were tested in combination with 0.1 nM – 10 μM EC-21a in the cAMP inhibition assay using CHO cells expressing *h*CB2R. CP55,940 was used as a reference compound. The combination of JR-14a and EC-21a produced a more efficacious response than JR-14a alone with similar potency ($E_{max(JR\text{-}14a + EC\text{-}21a)}$ = 84 ± 11%; $E_{max(JR\text{-}14a)}$ = 41 ± 5.7%); ($EC_{50(JR\text{-}14a + EC\text{-}21a)}$ = 140 [3.5 – 3,200]nM; $EC_{50(JR\text{-}14a)}$ = 150 [5.0 – 2,200]nM) (Figure 3-17A; Table 3-7). The combination of JR-64a with EC-21a also produced a more efficacious response than JR-64a alone ($E_{max(JR\text{-}64a + EC\text{-}21a)}$ = 96 ± 12%; $E_{max(JR\text{-}64a)}$ = 32 ± 4.0%) though there was a reduction in potency ($EC_{50(JR\text{-}64a + EC\text{-}21a)}$ = 84 [5.6 – 1,100]nM; $EC_{50(JR\text{-}64a)}$ = 11 [0.84 – 200]nM) (Figure 3-17B; Table 3-7).

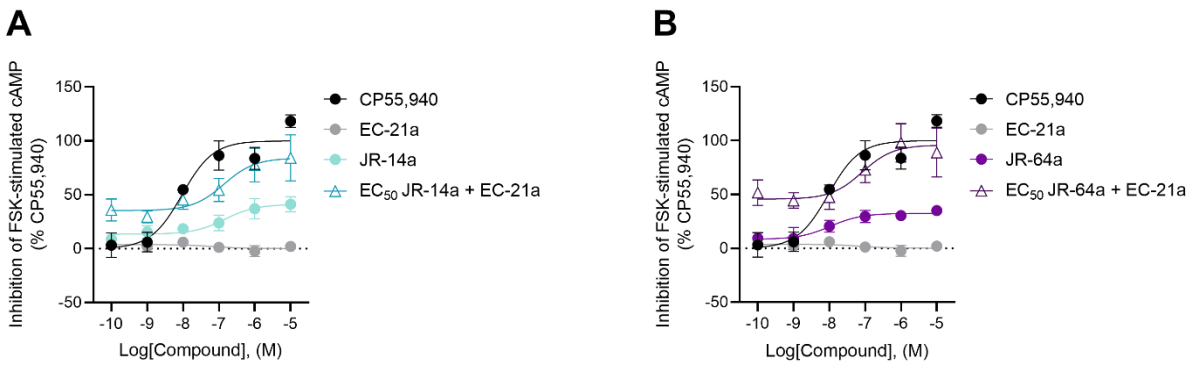

Figure 3-17. CB2R-dependent inhibition of FSK-stimulated cAMP for combination experiments with the allosteric parent ligand and select bitopic ligands of the JR series of CB2R ligands. CHO cells expressing *h*CB2R were treated with 10 μM FSK, 0.1 nM – 10 μM EC-21a and 53 nM JR-14a (A) or 75 nM JR-64a (B) for 90 min to measure cAMP inhibition. Data were fit to a 3-parameter non-linear regression and are represented as % of the maximal response of CP55,940. Data are mean ± SEM from *n* = 6 independent experiments performed in triplicate.

To confirm whether these ligands mediated their signaling through CB2R, 0.1 nM – 10 μM JR-14a and JR-64a were tested in combination with 100 nM of the CB2R antagonist/inverse agonist SR144528 in the cAMP inhibition assay using CHO cells expressing *h*CB2R. CP55,940 was used as a reference compound. At lower concentrations of JR-14a or JR-64a, the presence of SR144528 led to a downward shift in the CRCs of these ligands (Figure 3-18). As the concentration of either JR-14a or JR-64a increased, the inhibitory effect of SR144528 on cAMP inhibition at CB2R was removed, and these bitopic ligands were capable of modulating the cAMP inhibition signaling pathway with efficacies similar to that of JR-14a or JR-64a alone ($E_{max(SR144528 + JR\text{-}14a)} = 30 \pm 12\%$; $E_{max(JR\text{-}14a)} = 41 \pm 5.7\%$; $E_{max(SR144528 + JR\text{-}64a)} = 43 \pm 9.0\%$; $E_{max(JR\text{-}64a)} = 32 \pm 4.0\%$) (Figure 3-18; Table 3-7).

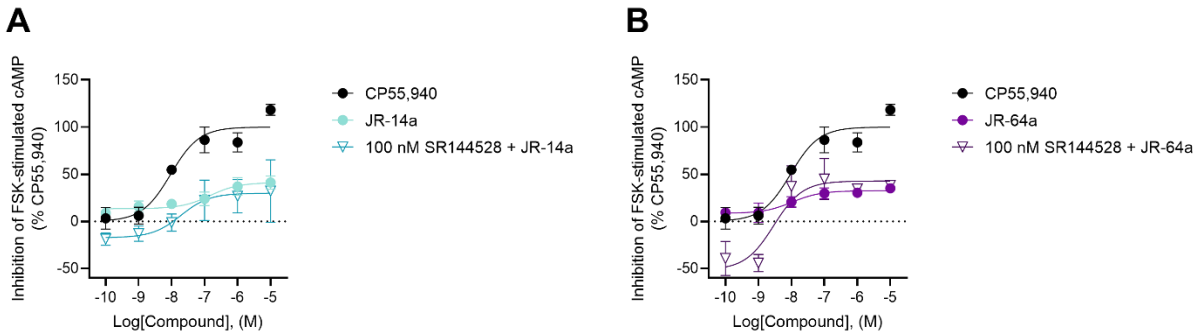

Figure 3-18. CB2R-dependent inhibition of FSK-stimulated cAMP for combination experiments with SR144528 and select bitopic ligands of the JR series of CB2R ligands. CHO cells expressing *h*CB2R were treated with 10 μM FSK, 100 nM SR144528 and 0.1 nM – 10 μM JR-14a (A) or JR-64a (B) for combination experiments for 90 min to measure cAMP inhibition. Data were fit to a 3-parameter non-linear regression and are represented as % of the maximal response of CP55,940. Data are mean ± SEM from $n = 6$ independent experiments performed in triplicate.

Compound	cAMP inhibition	
	EC_{50} (nM)	**E_{max} (%)**
CP55,940	9.4 (3.4 – 29)	100 ± 6.4
LV-62	34 (3.9 – 220)	110 ± 8.8
EC-21a	n.c	0.12 ± 2.2***
10 nM LV-62 + EC-21a	4.3 (0.57 – 34)	55 ± 5.2*
JR-14a	150 (5.0 – 2,200)	41 ± 5.7*
EC_{50} JR-14a + EC-21a	140 (3.5 – 3,200)	84 ± 11
100 nM SR144528 + JR-14a	n.c	30 ± 12***
JR-64a	11 (0.84 – 200)	32 ± 4.0*
EC_{50} JR-64a + EC-21a	84 (5.6 – 1,100)	96 ± 12
100 nM SR144528 + JR-64a	2.9 (0.72 – 12)	43 ± 9.0

Table 3-7. CB2R-dependent inhibition of FSK-stimulated cAMP for combination experiments with JR series of CB2R ligands. Data were fit to a 3-parameter non-linear regression to estimate potency (EC_{50}) and efficacy (E_{max}) values. Data are expressed as mean with 95% CI (EC_{50}) or mean ± SEM (E_{max}). n = 4-6 independent experiments performed in triplicate. Statistical analyses were by one-way ANOVA followed by Tukey's *post-hoc* test. *$p < 0.05$, ***$p < 0.001$ relative to CP55,940. n.c – not converged.

3.3 Experiment 3: GPCR interactions with cannabinoid receptors

In order to explore the potential interactions between cannabinoid receptors and orexin receptors, CHO cells expressing *h*CB1R or *h*CB2R were transfected with increasing amounts of *h*OX1R or *h*OX2R plasmid (0.10 µg, 0.25 µg, and 0.50 µg) and assessed for their ability to inhibit cAMP production and to enhance βarrestin2 recruitment to CB1R or CB2R. Cells were either untreated or treated with vehicle (10% DMSO in 1X PBS) or CP55,940, as indicated. CB1R or CB2R cells with 0.00 µg OX1R or 0.00 µg OX2R (i.e. untransfected cells) were used as a control.

3.3.1 $G\alpha_{i/o}$-mediated inhibition of FSK-stimulated cAMP in CB1R-OX1R transfected cells

In untreated cells, increasing the amount of OX1R produced a greater reduction in FSK-stimulated cAMP (Figure 3-19A). In vehicle-treated cells, a similar effect was seen, although cells transfected with 0.10 µg OX1R inhibited cAMP production to a lesser extent than untransfected cells (Figure 3-19A). As the amount of OX1R increased, CP55,940's potency decreased while its efficacy increased, though cells transfected with 0.50 µg OX1R exhibited reduced efficacy which may indicate that the system is oversaturated at plasmid levels above 0.25 µg OX1R (Figure 3-19B; Table 3-8; Table 3-12). Overall, these data suggest that OX1R enhances CB1R-dependent cAMP inhibition.

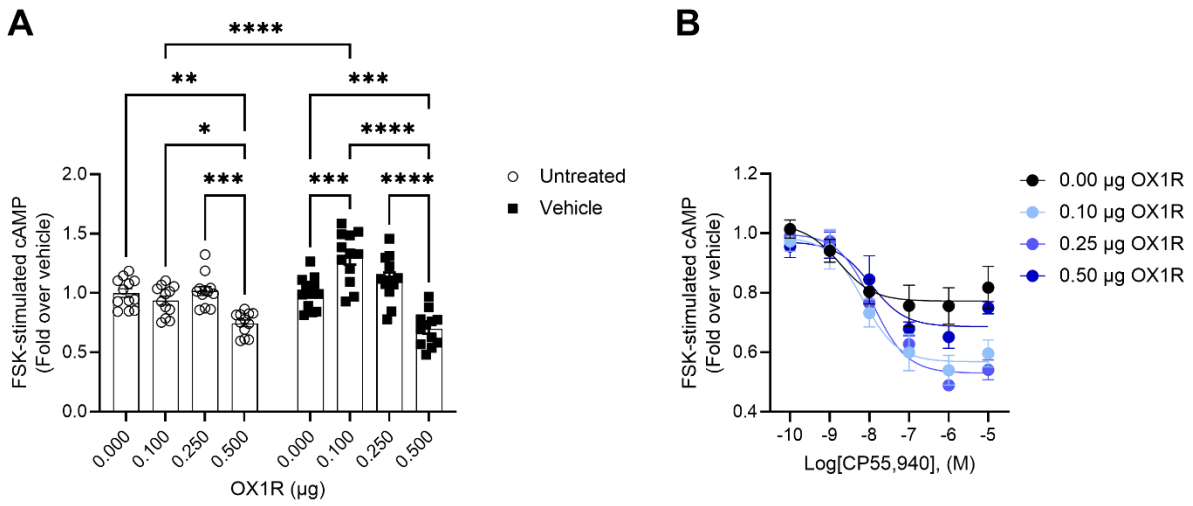

Figure 3-19. CB1R-dependent inhibition of FSK-stimulated cAMP in CB1R-OX1R cells. CHO cells stably expressing *h*CB1R and transiently expressing *h*OX1R were treated with 10 µM FSK and 0.1 nM – 10 µM CP55,940 for 90 min to measure cAMP inhibition. Data were fit to a 3-parameter non-linear regression and are represented as fold over vehicle. Data are mean ± SEM from $n = 4$ independent experiments performed in triplicate for baseline data (A) and 4-8 independent experiments performed in triplicate for concentration-response data (B). *$p < 0.05$, **$p < 0.01$, ***$p < 0.001$, ****$p < 0.0001$ as determined by two-way ANOVA followed by Tukey's *post-hoc* test.

3.3.2 βarrestin2 recruitment in CB1R-OX1R transfected cells

In both untreated and vehicle-treated cells, OX1R generally enhanced CB1R-dependent βarrestin2 recruitment, though in both treatment groups, cells transfected with 0.10 µg OX1R exhibited reduced βarrestin2 recruitment compared to untransfected cells (Figure 3-20A). Potency could not be determined for untransfected cells as the data did not produce either a CRC or a clear maximum plateau and therefore EC_{50} could not be estimated (Figure 3-20B; Table 3-8). The potency of CP55,940 among transfected cells, however, appeared to increase as the amount of OX1R increased (Table 3-8; Table 3-12). The presence of OX1R also reduced CP55,940's efficacy in the βarrestin2 recruitment assay (Table 3-8; Table 3-12). These data suggest that the effect of OX1R on CB1R-dependent βarrestin2 recruitment may depend on the specific treatment the cells are exposed to: βarrestin2 recruitment was improved in untreated and vehicle-treated cells while CP55,940-treated cells exhibited reduced βarrestin2 recruitment.

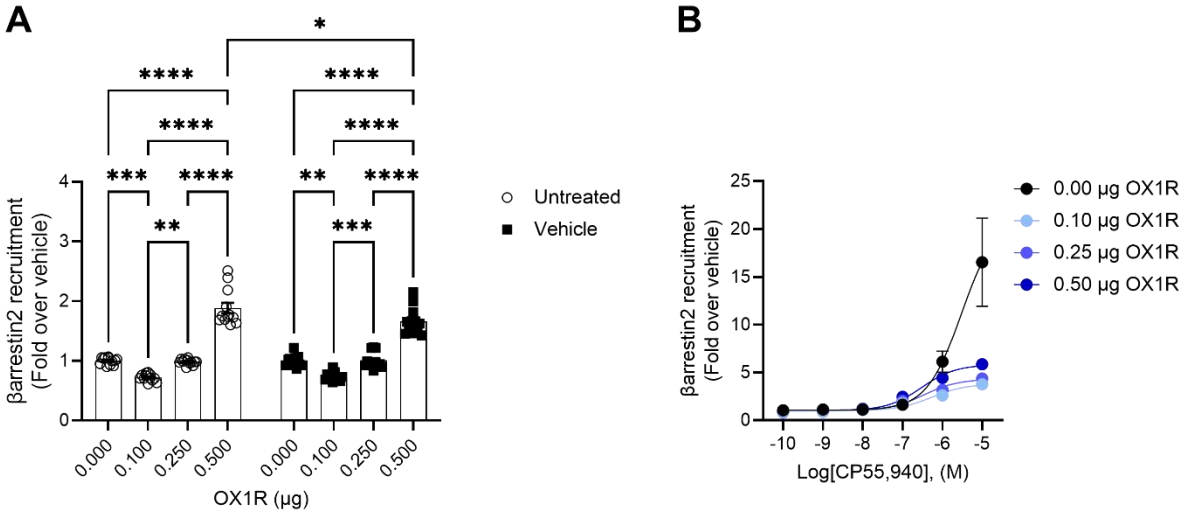

Figure 3-20. CB1R-dependent recruitment of βarrestin2 in CB1R-OX1R cells. CHO cells stably expressing *h*CB1R and transiently expressing *h*OX1R were treated with 0.1 nM – 10 µM CP55,940 for 90 min to measure βarrestin2 recruitment. Data were fit to a 3-parameter non-linear regression and are represented as fold over vehicle. Data are mean ± SEM from $n = 4$ independent experiments performed in triplicate for baseline data (A) and 4-8 independent experiments performed in triplicate for concentration-response data (B). *$p < 0.05$, **$p < 0.01$, ***$p < 0.001$, ****$p < 0.0001$ as determined by two-way ANOVA followed by Tukey's *post-hoc* test.

[OX1R] (µg)	cAMP		βarrestin2	
	EC_{50} (nM)	E_{max} (Fold)	EC_{50} (nM)	E_{max} (Fold)
0.00	1.7 (0.13 – 16)	0.77 ± 0.03	n.c	21 ± 4.9
0.10	6.8 (2.0 – 23)	0.57 ± 0.03***	540 (140 – 1,500)	3.8 ± 0.25*
0.25	12 (6.2 – 25)	0.53 ± 0.02***	340 (180 – 650)	4.3 ± 0.15*
0.50	11 (2.3 – 47)	0.69 ± 0.03	300 (210 – 420)	5.8 ± 0.13

Table 3-8. CB1R-dependent inhibition of FSK-stimulated cAMP and recruitment of βarrestin2 in CB1R-OX1R cells. Data were fit to a 3-parameter non-linear regression to estimate potency (EC_{50}) and efficacy (E_{max}) values. Data are expressed as mean with 95% CI (EC_{50}) or mean ± SEM (E_{max}). n = 4-8 independent experiments performed in triplicate. Statistical analyses were by one-way ANOVA followed by Tukey's *post-hoc* test. *$p < 0.05$, ***$p < 0.001$ relative to CP55,940. n.c – not converged.

3.3.3 $G\alpha_{i/o}$-mediated inhibition of FSK-stimulated cAMP in CB1R-OX2R transfected cells

In untreated cells, no significant difference was observed in the level of CB1R-mediated cAMP inhibition as the amount of OX2R increased (Figure 3-21A). In vehicle-treated cells however, the presence of OX2R led to an increased amount of FSK-stimulated cAMP (i.e. reduced level of cAMP inhibition) (Figure 3-21A). The presence of OX2R enhanced both the potency and efficacy of CP55,940, with a statistically significant effect of increasing plasmid concentration on efficacy (Figure 3-21B; Table 3-9; Table 3-12). These data suggest that OX2R enhances CP55,940-mediated cAMP inhibition via CB1R while having an opposite effect in vehicle-treated cells.

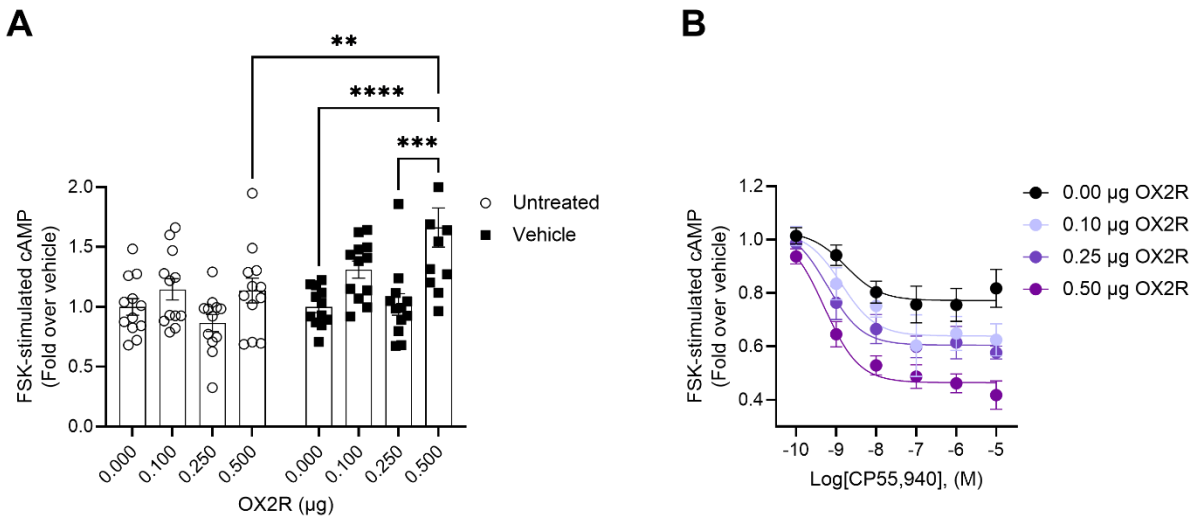

Figure 3-21. CB1R-dependent inhibition of FSK-stimulated cAMP in CB1R-OX2R cells. CHO cells stably expressing *h*CB1R and transiently expressing *h*OX2R were treated with 10 µM FSK and 0.1 nM – 10 µM CP55,940 for 90 min to measure cAMP inhibition. Data were fit to a 3-parameter non-linear regression and are represented as fold over vehicle. Data are mean ± SEM from n = 4 independent experiments performed in triplicate for baseline data (A) and 4-8 independent experiments performed in triplicate for concentration-response data (B). $^{**}p < 0.01$, $^{***}p < 0.001$, $^{****}p < 0.0001$ as determined by two-way ANOVA followed by Tukey's *post-hoc* test.

3.3.4 βarrestin2 recruitment in CB1R-OX2R transfected cells

In both untreated and vehicle-treated cells, transfection with 0.25 µg OX2R resulted in reduced βarrestin2 recruitment, which was statistically significant (Figure 3-22A). However, no difference was observed for cells transfected with 0.10 µg or 0.50 µg OX2R (Figure 3-22A). Potency could not be determined for untransfected cells as the concentration-response data were too variable (Figure 3-22B; Table 3-9). The potency of CP55,940 in transfected cells did not appear to follow a particular trend, though all transfection groups demonstrated relatively high EC_{50} values (Table 3-9; Table 3-12). A statistically significant increase in the efficacy of CP55,940 was observed for all transfection groups (Table 3-9; Table 3-12). These data suggest that OX2R can either reduce

or improve CB1R-mediated βarrestin2 recruitment: untreated or vehicle-treated cells exhibit reduced βarrestin2 recruitment, CP55,940-treated cells display increased levels of βarrestin2 recruitment.

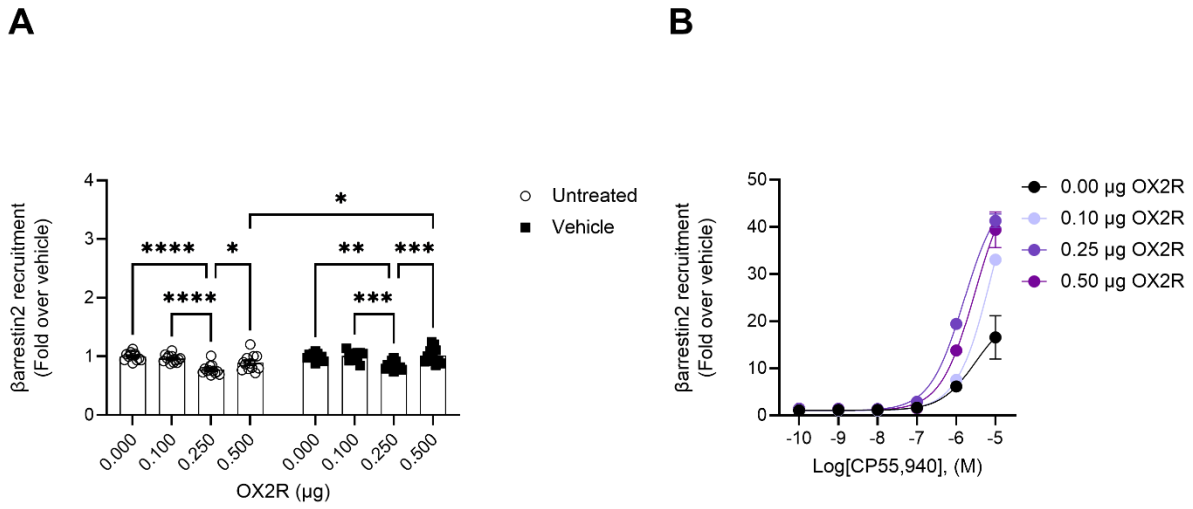

Figure 3-22. CB1R-dependent recruitment of βarrestin2 in CB1R-OX2R cells. CHO cells stably expressing *h*CB1R and transiently expressing *h*OX2R were treated with 0.1 nM – 10 μM CP55,940 for 90 min to measure βarrestin2 recruitment. Data were fit to a 3-parameter non-linear regression and are represented as fold over vehicle. Data are mean ± SEM from $n = 4$ independent experiments performed in triplicate for baseline data (A) and 4-8 independent experiments performed in triplicate for concentration-response data (B). *$p < 0.05$, **$p < 0.01$, ***$p < 0.001$, ****$p < 0.0001$ as determined by two-way ANOVA followed by Tukey's *post-hoc* test.

[OX2R] (µg)	cAMP		βarrestin2	
	EC_{50} (nM)	E_{max} (Fold)	EC_{50} (nM)	E_{max} (Fold)
0.00	1.7 (0.13 – 16)	0.77 ± 0.03	n.c	21 ± 4.9
0.10	< 0.1	0.62 ± 0.04*	> 10,000	33 ± 2.4***
0.25	< 0.1	0.58 ± 0.03**	1,600 (1,300 – 1,900)	48 ± 1.1**
0.50	0.51 (0.12 – 1.4)	0.46 ± 0.02****	3,000 (1,800 – 5,600)	51 ± 3.9**

Table 3-9. CB1R-dependent inhibition of FSK-stimulated cAMP and recruitment of βarrestin2 in CB1R-OX2R cells. Data were fit to a 3-parameter non-linear regression to estimate potency (EC_{50}) and efficacy (E_{max}) values. Data are expressed as mean with 95% CI (EC_{50}) or mean ± SEM (E_{max}). n = 4-8 independent experiments performed in triplicate. Statistical analyses were by one-way ANOVA followed by Tukey's *post-hoc* test. *$p < 0.05$, **$p < 0.01$, ***$p < 0.001$, ****$p < 0.0001$ relative to CP55,940. n.c – not converged.

3.3.5 $G\alpha_{i/o}$-mediated inhibition of FSK-stimulated cAMP in CB2R-OX1R transfected cells

No statistical difference was detected between untreated and vehicle-treated cells (Figure 3-23A). While no difference in cAMP inhibition was observed among untreated cells, in vehicle-treated cells, the presence of 0.10 µg OX1R led to a significant reduction in cAMP production, but no difference was observed for cells transfected with 0.25 µg or 0.50 µg OX1R (Figure 3-23A). This may suggest that the system is oversaturated at plasmid levels above 0.10 µg OX1R. Potency could not be determined for cells transfected with 0.25 µg or 0.50 µg OX1R as the concentration-response data were too variable (Figure 3-23B; Table 3-10; Table 3-12). The efficacy of CP55,940 decreased as the concentration of OX1R increased, though this was only statistically significant for cells transfected with 0.10 µg OX1R, which may further support the idea that the system is oversaturated at plasmid levels above 0.10 µg OX1R (Table 3-10; Table 3-12). These data suggest that OX1R enhances CB2R-dependent cAMP inhibition though the system is oversaturated at plasmid levels above 0.10 µg OX1R.

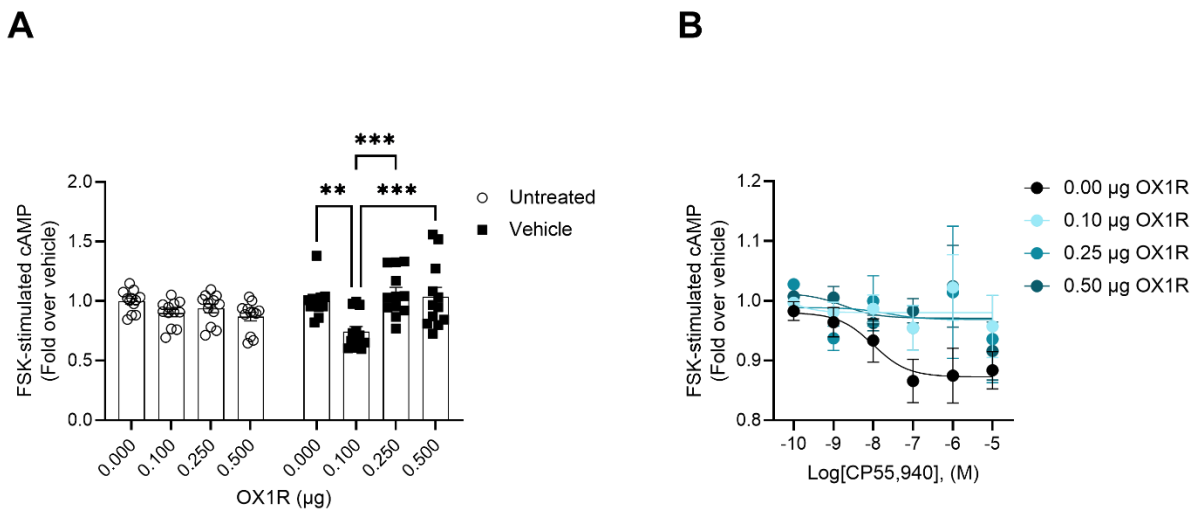

Figure 3-23. CB2R-dependent inhibition of FSK-stimulated cAMP in CB2R-OX1R cells. CHO cells stably expressing *h*CB2R and transiently expressing *h*OX1R were treated with 10 µM FSK and 0.1 nM – 10 µM CP55,940 for 90 min to measure cAMP inhibition. Data were fit to a 3-parameter non-linear regression and are represented as fold over vehicle. Data are mean ± SEM from $n = 4$ independent experiments performed in triplicate for baseline data (A) and 4-8 independent experiments performed in triplicate for concentration-response data (B). $^{**}p < 0.01$, $^{***}p < 0.001$ as determined by two-way ANOVA followed by Tukey's *post-hoc* test.

3.3.6 βarrestin2 recruitment in CB2R-OX1R transfected cells

No statistical difference was detected between untreated and vehicle-treated cells (Figure 3-24A). In both untreated and vehicle-treated cells, a significant difference was detected in all transfection groups, in which the presence of OX1R led to a reduction in CB2R-mediated βarrestin2 recruitment (Figure 3-24A). The potency of CP55,940 did not appear to follow a specific trend (Table 3-10; Table 3-12). However, the efficacy of CP55,940 did increase as the level of OX1R increased up to 0.25 µg OX1R (Figure 3-24B; Table 3-10; Table 3-12). At 0.50 µg OX1R, the efficacy of CP55,940 was not statistically different from that of untransfected cells (Table 3-10). Thus, our system may be oversaturated at plasmid levels above 0.25 µg OX1R. These data suggest

that OX1R enhances CP55,940-dependent βarrestin2 recruitment while reducing βarrestin2 recruitment in untreated and vehicle-treated cells.

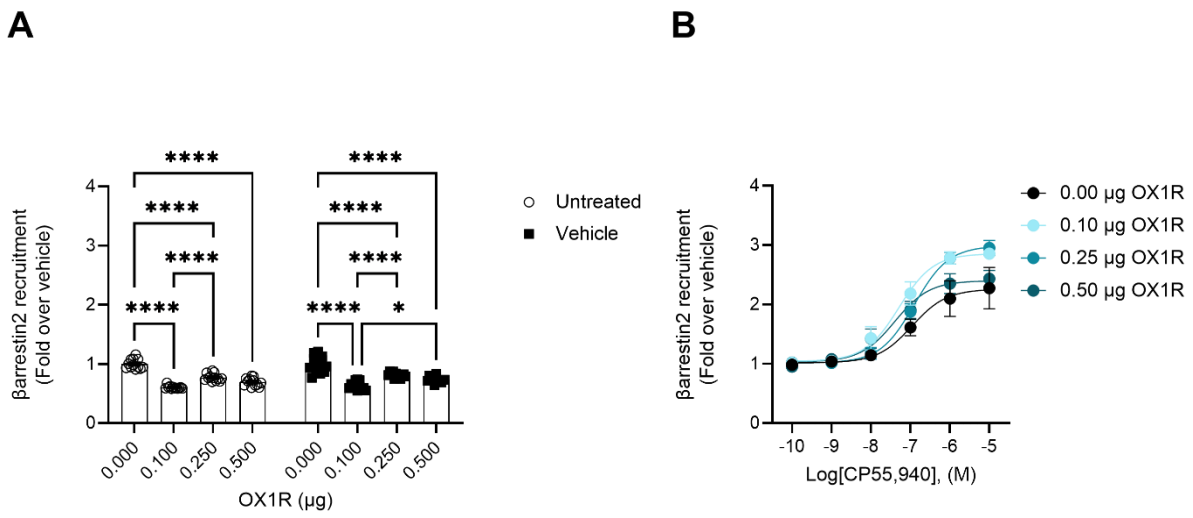

Figure 3-24. CB2R-dependent recruitment of βarrestin2 in CB2R-OX1R cells. CHO cells stably expressing *h*CB2R and transiently expressing *h*OX1R were treated with 0.1 nM – 10 μM CP55,940 for 90 min to measure βarrestin2 recruitment. Data were fit to a 3-parameter non-linear regression and are represented as fold over vehicle. Data are mean ± SEM from $n = 4$ independent experiments performed in triplicate for baseline data (A) and 4-8 independent experiments performed in triplicate for concentration-response data (B). *$p < 0.05$, ****$p < 0.0001$ as determined by two-way ANOVA followed by Tukey's *post-hoc* test.

[OX1R] (µg)	cAMP		βarrestin2	
	EC_{50} (nM)	**E_{max} (Fold)**	**EC_{50} (nM)**	**E_{max} (Fold)**
0.00	10 (0.21 – 190)	0.87 ± 0.02	110 (20 – 620)	2.3 ± 0.16
0.10	< 0.1	0.96 ± 0.01*	51 (24 – 100)	2.9 ± 0.09*
0.25	n.c	0.97 ± 0.04	130 (80 – 200)	3.0 ± 0.08*
0.50	n.c	0.97 ± 0.02	41 (12 – 120)	2.4 ± 0.10

Table 3-10. CB2R-dependent inhibition of FSK-stimulated cAMP and recruitment of βarrestin2 in CB2R-OX1R cells. Data were fit to a 3-parameter non-linear regression to estimate potency (EC_{50}) and efficacy (E_{max}) values. Data are expressed as mean with 95% CI (EC_{50}) or mean ± SEM (E_{max}). n = 4-8 independent experiments performed in triplicate. Statistical analyses were by one-way ANOVA followed by Tukey's *post-hoc* test. *$p < 0.05$ relative to CP55,940. n.c – not converged.

3.3.7 $G\alpha_{i/o}$-mediated inhibition of FSK-stimulated cAMP in CB2R-OX2R transfected cells

No statistical differences were observed among untreated cells (Figure 3-25A). In vehicle-treated cells, increasing the amount of OX2R led to reduced cAMP inhibition (Figure 3-25A). While the potency of CP55,940 was diminished by the presence of OX2R, CP55,940's efficacy significantly increased in all transfection groups (Figure 3-25B; Table 3-11; Table 3-12). These data suggest that OX2R facilitates CB2R-dependent cAMP inhibition in CP55,940-treated cells but not in vehicle-treated cells.

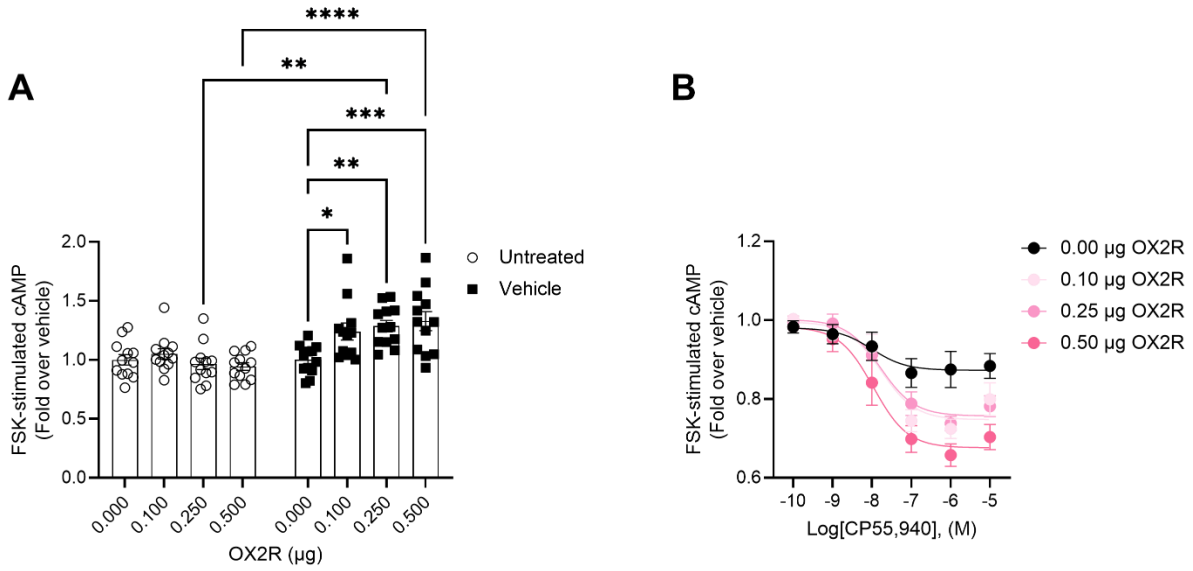

Figure 3-25. CB2R-dependent inhibition of FSK-stimulated cAMP in CB2R-OX2R cells. CHO cells stably expressing *h*CB2R and transiently expressing *h*OX2R were treated with 10 µM FSK and 0.1 nM – 10 µM CP55,940 for 90 min to measure cAMP inhibition. Data were fit to a 3-parameter non-linear regression and are represented as fold over vehicle. Data are mean ± SEM from n = 4 independent experiments performed in triplicate for baseline data (A) and 4-8 independent experiments performed in triplicate for concentration-response data (B). *p < 0.05, **p < 0.01, ***p < 0.001, ****p < 0.0001 as determined by two-way ANOVA followed by Tukey's *post-hoc* test.

3.3.8 βarrestin2 recruitment in CB2R-OX2R transfected cells

In untreated cells, the presence of OX2R led to a significant increase in βarrestin2 recruitment in cells transfected with 0.10 µg and 0.25 µg OX2R but not in cells transfected with 0.50 µg OX2R, which may suggest that our system is oversaturated at plasmid levels above 0.25 µg OX2R (Figure 3-26A). In vehicle-treated cells, a similar effect was seen, in which cells transfected with 0.10 µg and 0.25 µg OX2R exhibited significant increases in βarrestin2 recruitment (Figure 3-26A). Unlike in untreated cells, vehicle-treated cells transfected with 0.50 µg OX2R demonstrated a significant

improvement in βarrestin2 recruitment (Figure 3-26A). CP55,940's potency was improved in the presence of OX2R, although its efficacy significantly decreased in cells transfected with 0.10 µg and 0.50 µg OX2R (Figure 3-26B; Table 3-11; Table 3-12). Overall, OX2R enhances CB2R-mediated βarrestin2 recruitment in untreated and vehicle-treated cells but not in CP55,940-treated cells.

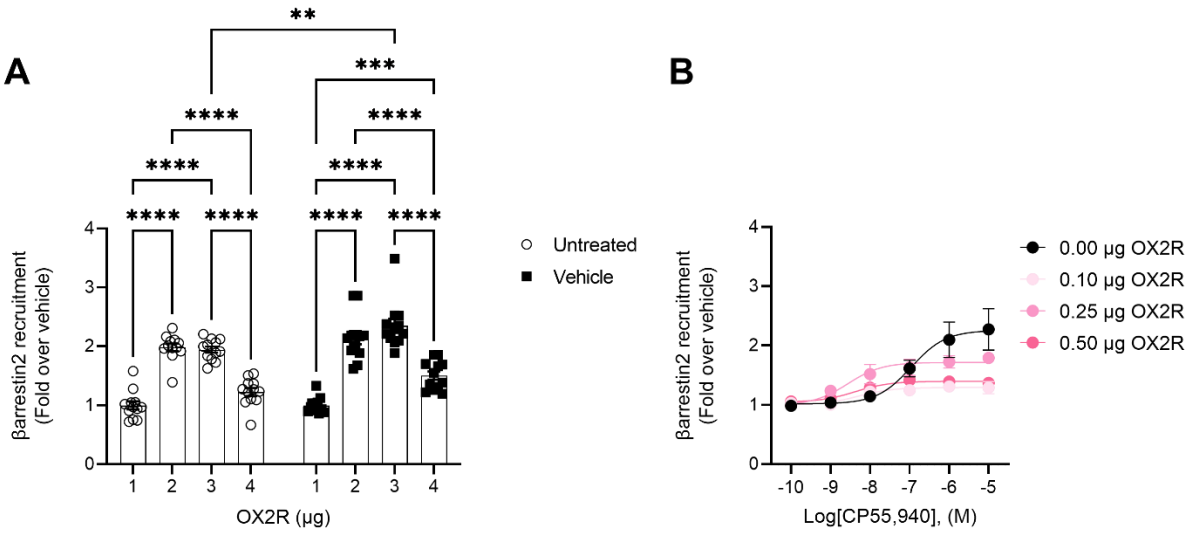

Figure 3-26. CB2R-dependent recruitment of βarrestin2 in CB2R-OX2R cells. CHO cells stably expressing *h*CB2R and transiently expressing *h*OX2R were treated with 0.1 nM – 10 µM CP55,940 for 90 min to measure βarrestin2 recruitment. Data were fit to a 3-parameter non-linear regression and are represented as fold over vehicle. Data are mean ± SEM from $n = 4$ independent experiments performed in triplicate for baseline data (A) and 4-8 independent experiments performed in triplicate for concentration-response data (B). $^{**}p < 0.01$, $^{***}p < 0.001$, $^{****}p < 0.0001$ as determined by two-way ANOVA followed by Tukey's *post-hoc* test.

[OX2R] (μg)	cAMP		βarrestin2	
	EC_{50} (nM)	**E_{max} (Fold)**	**EC_{50} (nM)**	**E_{max} (Fold)**
0.00	10 (0.21 – 190)	0.87 ± 0.02	110 (20 – 620)	2.3 ± 0.16
0.10	17 (5.6 – 49)	0.75 ± 0.02**	5.0 (0.59 – 75)	1.3 ± 0.04***
0.25	16 (7.0 – 40)	0.76 ± 0.01**	2.7 (0.41 – 23)	1.7 ± 0.06
0.50	11 (3.5 – 34)	0.68 ± 0.02****	4.2 (0.97 – 17)	1.4 ± 0.03**

Table 3-11. CB2R-dependent inhibition of FSK-stimulated cAMP and recruitment of βarrestin2 in CB2R-OX2R cells. Data were fit to a 3-parameter non-linear regression to estimate potency (EC_{50}) and efficacy (E_{max}) values. Data are expressed as mean with 95% CI (EC_{50}) or mean ± SEM (E_{max}). n = 4-8 independent experiments performed in triplicate. Statistical analyses were by one-way ANOVA followed by Tukey's *post-hoc* test. $^{**}p < 0.01$, $^{***}p < 0.001$, $^{****}p < 0.0001$ relative to CP55,940.

	***h*CB1R**		***h*CB2R**	
	cAMP	**βarrestin2**	**cAMP**	**βarrestin2**
***h*OX1R**	Potency ↓ Efficacy ↑	Potency ? Efficacy ↓	Potency ↑ Efficacy ↓	Potency ? Efficacy ↑
***h*OX2R**	Potency ↑ Efficacy ↑	Potency ? Efficacy ↑	Potency ↓ Efficacy ↑	Potency ↑ Efficacy ↓

Table 3-12. Summary of potency and efficacy trends for cannabinoid-orexin receptor experiments. Data from cAMP inhibition and βarrestin2 recruitment assays were fit to a 3-parameter non-linear regression to estimate potency (EC_{50}) and efficacy (E_{max}) values. n = 4-8 independent experiments performed in triplicate. Due to variable data, trends in potency could not be established for all groups.

3.4 Experiment 4: Pharmacological properties of metabolites from *C. sativa*

3.4.1 $G\alpha_{i/o}$-mediated inhibition of FSK-stimulated cAMP at CB1R

Five phytocannabinoid metabolites, namely 11-OH-THC, COOH-THC, 6-OH-CBD, 7-OH-CBD, and COOH-CBD, were assessed in the cAMP inhibition assay using CHO cells expressing *h*CB1R. CP55,940 was used as a reference compound. Among the hydroxylated phytocannabinoid metabolites, 11-OH-THC and 6-OH-CBD acted as partial agonists of cAMP inhibition at CB1R ($E_{max(11\text{-}OH\text{-}THC)}$ = 47 ± 5.8%; $E_{max(6\text{-}OH\text{-}CBD)}$ = 47 ± 9.0%), while 7-OH-CBD was a full agonist ($E_{max(7\text{-}OH\text{-}CBD)}$ = 130 ± 11%) (Figure 3-27A; Table 3-13). For the carboxylated metabolites, COOH-THC and COOH-CBD exhibited full agonist responses at CB1R ($E_{max(COOH\text{-}THC)}$ = 310 ± 40%; $E_{max(COOH\text{-}CBD)}$ = 470 ± 320%), though COOH-CBD's full agonist response only became apparent at the highest concentration tested (i.e. 10,000 nM) (Figure 3-27B; Table 3-13). These data suggest that phytocannabinoid metabolites are agonists of CB1R-dependent cAMP inhibition.

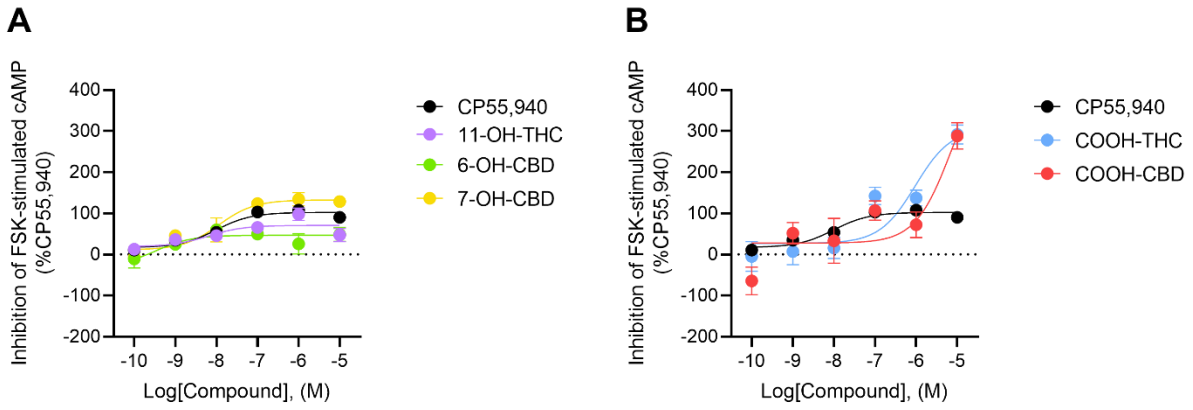

Figure 3-27. CB1R-dependent inhibition of FSK-stimulated cAMP for phytocannabinoid metabolites. CHO cells expressing *h*CB1R were treated with 10 µM FSK and 0.1 nM – 10 µM hydroxylated metabolites of Δ^9-THC and CBD (A) or carboxylated metabolites of Δ^9-THC and CBD (B) for 90 min to measure cAMP inhibition. Data were fit to a 3-parameter non-linear regression and are represented as % of the maximal response of CP55,940. Data are mean ± SEM from *n* = 4 independent experiments performed in triplicate.

3.4.2 βarrestin2 recruitment at CB1R

In order to obtain a comprehensive understanding of their pharmacological activity at CB1R, 11-OH-THC, COOH-THC, 6-OH-CBD, 7-OH-CBD, and COOH-CBD were also assessed in the βarrestin2 recruitment assay using CHO cells expressing *h*CB1R. CP55,940 was used as a reference compound. Apart from 11-OH-THC, which displayed weak partial agonist activity ($E_{max(11\text{-}OH\text{-}THC)}$ = 14 ± 0.73%), the remaining metabolites were unable to effectively recruit βarrestin2 to CB1R (Figure 3-28; Table 3-13).

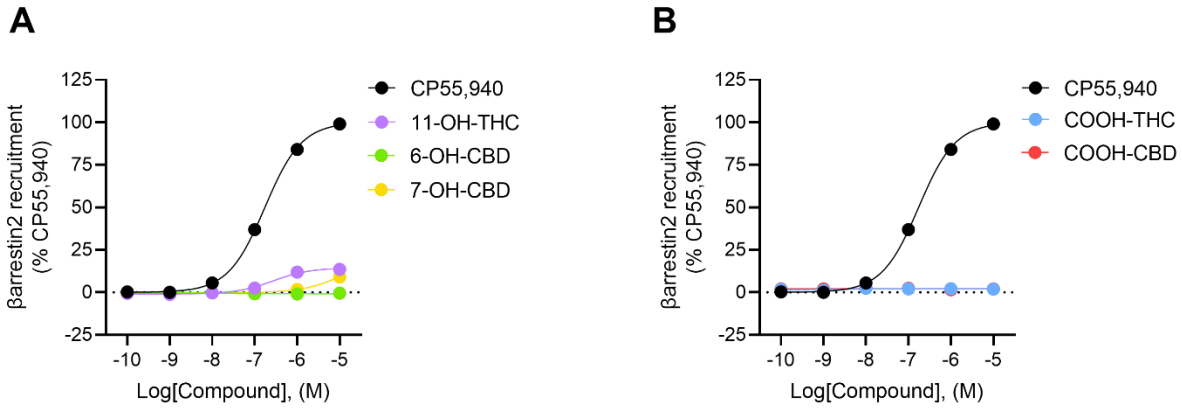

Figure 3-28. CB1R-dependent recruitment of βarrestin2 for phytocannabinoid metabolites. CHO cells expressing *h*CB1R were treated with 0.1 nM – 10 μM hydroxylated metabolites of Δ^9-THC and CBD (A) or carboxylated metabolites of Δ^9-THC and CBD (B) for 90 min to measure βarrestin2 recruitment. Data were fit to a 3-parameter non-linear regression and are represented as % of the maximal response of CP55,940. Data are mean ± SEM from *n* = 3 independent experiments performed in triplicate.

Compound	cAMP		βarrestin2	
	EC_{50} (nM)	**E_{max} (%)**	**EC_{50} (nM)**	**E_{max} (%)**
CP55,940	9.9 (3.0 – 27)	100 ± 6.0	170 (150 – 200)	100 ± 1.2
11-OH-THC	< 0.1	47 ± 5.8	270 (170 – 430)	14 ± 0.73****
COOH-THC	960 (21 – 5,600)	310 ± 40	n.c	2.2 ± 0.23****
6-OH-CBD	n.c	47 ± 9.0	n.c	-0.76 ± 0.42****
7-OH-CBD	11 (1.4 – 52)	130 ± 11	n.c	17 ± 9.4****
COOH-CBD	n.c	470 ± 320	n.c	2.2 ± 0.20****

Table 3-13. CB1R-dependent inhibition of FSK-stimulated cAMP and recruitment of βarrestin2 for phytocannabinoid metabolites. Data were fit to a 3-parameter non-linear regression to estimate potency (EC_{50}) and efficacy (E_{max}) values. Data are expressed as mean with 95% CI (EC_{50}) or mean ± SEM (E_{max}). n = 3-4 independent experiments performed in triplicate. Statistical analyses were by one-way ANOVA followed by Tukey's *post-hoc* test. ****$p < 0.0001$ relative to CP55,940. n.c – not converged.

3.4.3 $G\alpha_{i/o}$-mediated inhibition of FSK-stimulated cAMP at CB2R

As demonstrated in previous studies, the activity of phytocannabinoids can depend on the specific cannabinoid receptor subtype[170]. This may also apply to phytocannabinoid metabolites. Thus 11-OH-THC, COOH-THC, 6-OH-CBD, 7-OH-CBD, and COOH-CBD were also tested at CB2R. The compounds were assessed in the cAMP inhibition assay using CHO cells expressing *h*CB2R. CP55,940 was used as a reference compound. Among the hydroxylated metabolites, 11-OH-THC exhibited partial agonist activity ($E_{max(11\text{-}OH\text{-}THC)}$ = 33 ± 13%), 6-OH-CBD appeared to act as an inverse agonist ($E_{max(6\text{-}OH\text{-}CBD)}$ = -120 ± 40%), and 7-OH-CBD was inactive ($E_{max(7\text{-}OH\text{-}CBD)}$ = -9.2 ± 11%) at CB2R (Figure 3-29A; Table 3-14). Both carboxylated metabolites acted as agonists of cAMP inhibition at CB2R, with COOH-THC producing a full agonist response ($E_{max(COOH\text{-}THC)}$ = 130 ± 21%) while COOH-CBD displayed partial agonist activity ($E_{max(COOH\text{-}CBD)}$ = 85 ± 93%)

(Figure 3-29B; Table 3-14). Overall, the phytocannabinoid metabolites displayed a range of activity in the cAMP inhibition assay at CB2R.

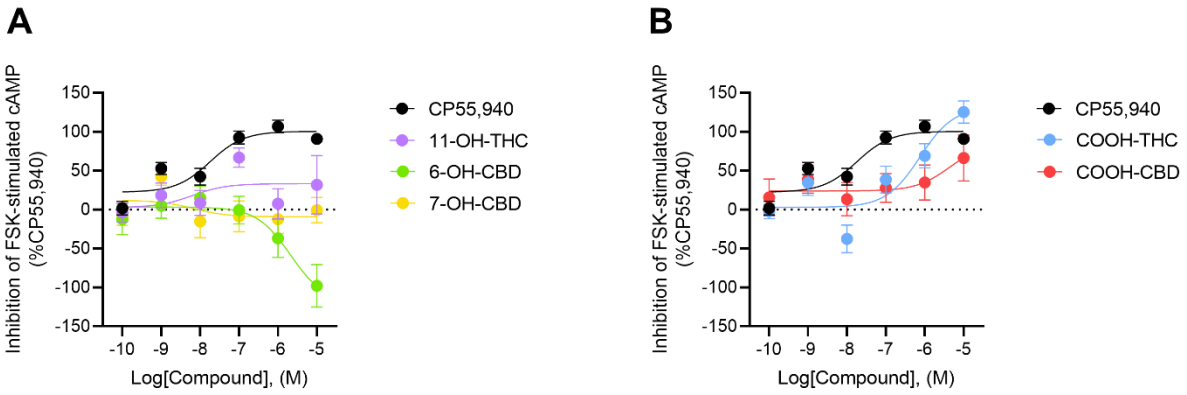

Figure 3-29. CB2R-dependent inhibition of FSK-stimulated cAMP for phytocannabinoid metabolites. CHO cells expressing *h*CB2R were treated with 10 µM FSK and 0.1 nM – 10 µM hydroxylated metabolites of Δ^9-THC and CBD (A) or carboxylated metabolites of Δ^9-THC and CBD (B) for 90 min to measure cAMP inhibition. Data were fit to a 3-parameter non-linear regression and are represented as % of the maximal response of CP55,940. Data are mean ± SEM from n = 6 independent experiments performed in triplicate.

3.4.4 βarrestin2 recruitment at CB2R

11-OH-THC, COOH-THC, 6-OH-CBD, 7-OH-CBD, and COOH-CBD were also assessed for their ability to recruit βarrestin2 to CB2R using CHO cells expressing *h*CB2R. CP55,940 was used as a reference compound. Most metabolites lacked activity in the βarrestin2 recruitment signaling pathway, the exception being the CBD metabolite 7-OH-CBD (Figure 3-30; Table 3-14). 7-OH-CBD acted as a full agonist at CB2R, displaying efficacy and potency similar to that of CP55,940 ($E_{max(7\text{-OH-CBD})}$ = 96 ± 12%; $E_{max(CP55,940)}$ = 96 ± 4.4%; $EC_{50(7\text{-OH-CBD})}$ = 480 [60 – 2,500]nM; $EC_{50(CP55,940)}$ = 530 [360 – 770]nM) (Figure 3-30A; Table 3-14).

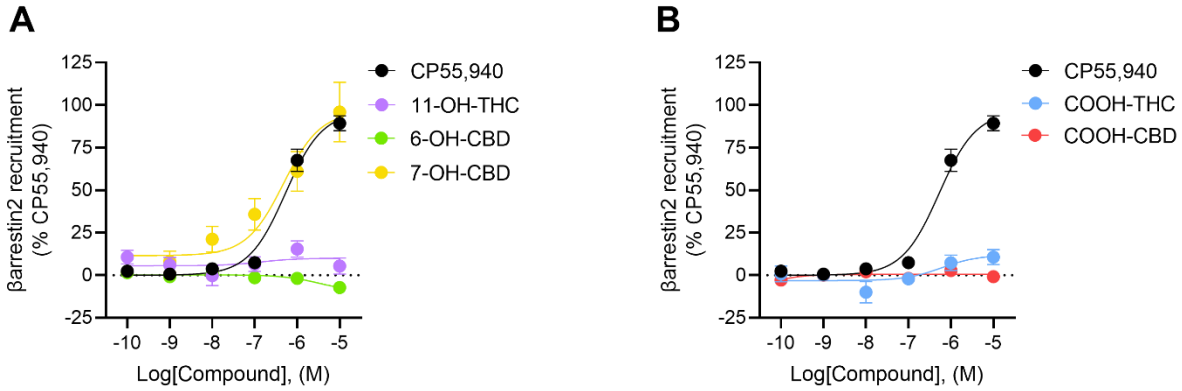

Figure 3-30. CB2R-dependent recruitment of βarrestin2 for phytocannabinoid metabolites. CHO cells expressing *h*CB2R were treated with 0.1 nM – 10 μM hydroxylated metabolites of Δ^9-THC and CBD (A) or carboxylated metabolites of Δ^9-THC and CBD (B) for 90 min to measure βarrestin2 recruitment. Data were fit to a 3-parameter non-linear regression and are represented as % of the maximal response of CP55,940. Data are mean ± SEM from *n* = 4 independent experiments performed in triplicate.

Compound	**cAMP**		**βarrestin2**	
	EC_{50} (nM)	**E_{max} (%)**	**EC_{50} (nM)**	**E_{max} (%)**
CP55,940	18 (5.0 – 54)	100 ± 6.0	530 (360 – 770)	96 ± 4.4
11-OH-THC	n.c	33 ± 13****	n.c	10 ± 4.2
COOH-THC	760 (110 – 4,100)	130 ± 21****	n.c	12 ± 5.5
6-OH-CBD	n.c	-120 ± 40****	n.c	-9.7 ± 4.9***
7-OH-CBD	n.c	-9.2 ± 11	480 (60 – 2,500)	96 ± 12
COOH-CBD	n.c	85 ± 93****	n.c	0.55 ± 1.0

Table 3-14. CB2R-dependent inhibition of FSK-stimulated cAMP and recruitment of βarrestin2 for phytocannabinoid metabolites. Data were fit to a 3-parameter non-linear regression to estimate potency (EC_{50}) and efficacy (E_{max}) values. Data are expressed as mean with 95% CI (EC_{50}) or mean ± SEM (E_{max}). *n* = 4-6 independent experiments performed in triplicate. Statistical analyses were by one-way ANOVA followed by Tukey's *post-hoc* test. ***$p < 0.001$, ****$p < 0.0001$ relative to CP55,940. n.c – not converged.

Chapter 4: Discussion

The aims of this work were: (1) to characterize the pharmacology of novel GPR55 and CB2R ligands; (2) to understand how cannabinoid receptor signaling is influenced by orexin receptors; and (3) to investigate the pharmacological activity of phytocannabinoid metabolites. Regarding these aims, we hypothesized that (a) novel synthetic GPR55- and CB2R-specific ligands could be developed using iterative pharmacological data and drug design; (b) OX1R and OX2R would increase the potency and efficacy of agonists at CB1R and CB2R; and (c) at CB1R and CB2R, Δ^9-THC metabolites would act as agonists while CBD metabolites would lack activity.

4.1 Novel GPR55 ligands are active at GPR55

The modulation of ERK1/2 by GPR55 has been reported previously[198,199]. In this study, ERK1/2 phosphorylation was quantified for the CC series of GPR55 ligands as a measure of GPR55 activation. It was revealed that all ligands of the series were agonists of GPR55, with many ligands displaying potent, full agonist activity (Figure 3-1; Table 3-1). These data support our hypothesis that pharmacologically active GPR55 ligands can be created using rational drug design based on iterative modifications to previously identified ligands. Our novel GPR55 agonists were modified from a class of 3-substituted coumarins which functioned as antagonists of βarrestin2 recruitment at GPR55[185,200]. In addition to these coumarin-based agonists and antagonists, coumarin scaffolds have also been used to develop GPR55 ligands with inverse agonist activity[201]. Thus, coumarin derivatives may represent a class of GPR55 ligands with a range of pharmacological activity. GPR55 has been proposed as a therapeutic target in the treatment of

neuropathic pain, osteoporosis, cancer, and inflammation[98,202]. However, potent and selective GPR55 ligands, which are required to thoroughly investigate GPR55's function and to facilitate the development of novel therapeutics, are limited[203,204]. Our novel GPR55 agonists could therefore be used as tool compounds in this regard. Additionally, our GPR55 agonists could function as starting points in the development of other GPR55 ligands in the future. The utility of our GPR55 ligands in these avenues, though, depends on the fundamental property of receptor selectivity.

4.2 Novel GPR55 ligands are not GPR55-selective

To determine the receptor selectivity of our GPR55 ligands, it was essential to test their activity at at least one additional receptor. As a major focus of this work is the identification of CB2R ligands, our GPR55 ligands were evaluated for their ability to facilitate downstream signaling at CB2R. This may also uncover similarities or differences in the binding sites of GPR55 and CB2R. Despite their promising activity at GPR55, experiments quantifying cAMP inhibition and βarrestin2 recruitment at CB2R led to the observation that our GPR55 ligands were not GPR55-selective. Most of the ligands acted as inverse agonists of cAMP inhibition at CB2R (Figure 3-2, Table 3-2). While both agonists and inverse agonists bind to a receptor's orthosteric site to mediate their actions, agonists increase signaling while inverse agonists reduce the basal or constitutive activity of the receptor (Figure 2-11)[17]. Inverse agonists also differ from neutral antagonists, which occupy the orthosteric site, preventing other ligands from binding, but do not affect constitutive receptor activity (Figure 2-11)[31].

It is worth noting that inverse agonism may be more readily detectable in systems where the receptor of interest is overexpressed, as is the case with our experimental model[17]. This is because increased receptor expression is associated with a higher level of constitutive activity[11]. From a therapeutic perspective, the utility of our ligands may be limited as inverse agonists can precipitate tolerance due to receptor upregulation following chronic use[205]. For example, cimetidine and ranitidine, inverse agonists of the histamine H2 receptor, produce an increase in H2 receptor density[206]. Similar effects have been observed among β-blockers that target the β2AR[207]. Nevertheless, conditions characterized by an increase in constitutive receptor activity or in certain types of cancer in which receptors are overexpressed may benefit from treatment with an inverse agonist[208]. More research is required to elucidate the role, if any, of CB2R in pathologies where constitutive receptor activity is involved and if inverse agonism of cAMP inhibition would lead to any therapeutically beneficial effects. In addition to the inverse agonist activity of our GPR55 ligands, some ligands acted as weak partial agonists of cAMP inhibition at CB2R. Finally, most of our GPR55 ligands were unable to recruit βarrestin2 to CB2R, though CC-17 and CC-28 did so as weak partial agonists (Figure 3-3; Table 3-2). As seen with partial agonists of the cannabinoid receptors (e.g. Δ^9-THC), CC-17 and CC-28 may display antagonism when in the presence of full, potent agonists, though further experimentation is required to investigate this[170]. Furthermore, the therapeutic relevance of CB2R partial agonism has yet to be fully elucidated[209].

Although the amino acid similarity between GPR55 and CB2R is low (14.4%), our ligands which were designed to act as GPR55 agonists, also exhibited activity at CB2R[204]. This may be due to the coumarin scaffold employed in the design of these ligands. Various CB1R and CB2R ligands have also been developed using this scaffold[210–212]. Furthermore, coumarin derivatives have been shown to act at the orphan cannabinoid receptor GPR18, and more specifically, these derivatives

were also designed as GPR55 ligands[101]. Thus, while the coumarin scaffold can be employed to design ligands targeting the cannabinoid receptors, careful attention must be paid to ensure that these ligands target one receptor subtype over the other. This does not suggest that the coumarin scaffold should be abandoned completely, rather additional information may be required to improve receptor selectivity. As the crystal structure for GPR55 has yet to be solved, acquiring it could be beneficial for improving our understanding of GPR55's binding sites and in turn allow for the use of structure-based drug design (SBDD) to take place[213,214].

Given that our GPR55 ligands were assessed at CB2R through functional assays measuring two distinct components of GPCR signaling, it may seem reasonable to calculate bias factors for these ligands at CB2R. Doing so may uncover whether these ligands display biased agonism. Bias factors were not calculated primarily for two reasons. First, many ligands were inactive in the βarrestin2 recruitment assay so bias factors could not be calculated for those ligands (Figure 3-3; Table 3-2). Of the two ligands which displayed activity in the βarrestin2 recruitment assay, they were weak partial agonists so it may not be reasonable to calculate their bias factors[215]. Second, many ligands acted as inverse agonists of CB2R in the cAMP inhibition assay (Figure 3-2; Table 3-2). The best way to assess bias for these ligands would require use of another inverse agonist as a reference ligand[197]. However, the reference ligand used in these experiments (i.e. CP55,940) would not be suitable for calculating bias factors of inverse agonists as it is a full agonist of cAMP inhibition at CB2R.

4.3 Novel CB2R ligands display a range of activity at CB2R

4.3.1 FD series

The FD series, which were synthesized by joining the CB1R/CB2R orthosteric agonist FM-6b and the CB2R PAM EC-21a, represents the first class of heterobivalent CB2R bitopic ligands to be developed[186]. The orthosteric and allosteric pharmacophores for this series were chosen following experimentation using an *in vitro* microglial model, in which EC-21a enhanced FM-6b's ability to modulate the release of inflammatory cytokines[216]. In both cAMP inhibition and βarrestin2 recruitment assays, the parent ligands of the series displayed activity in accordance with their pre-existing pharmacological classifications (Figure 3-4A; Figure 3-5A; Table 3-3). Interestingly, FM-6b displayed greater efficacy and potency in the cAMP inhibition assay, which may suggest it functions as a biased agonist at CB2R (Figure 3-4A; Table 3-3). Through the development of biased ligands, it may be possible to "fine tune" the signaling profile elicited, with the ideal biased ligand stabilizing receptor conformations which activate intracellular signaling cascades with therapeutically beneficial effects[7,217]. Thus, with the FD series of bitopic ligands, it would be desirable to retain the pathway selectivity of FM-6b while enhancing receptor selectivity through EC-21a.

Apart from FD-22a and FD-24a, which were the most efficacious and potent ligands of the FD series, most bitopic ligands displayed poor potencies and efficacies in inhibiting the production of FSK-stimulated cAMP (Figure 3-4B; Table 3-3). Additionally, none of the bitopic ligands were as efficacious as the orthosteric parent FM-6b. In the βarrestin2 recruitment assay, most bitopic ligands displayed similar efficacies to FM-6b, though with reduced potency (Figure 3-5B; Table 3-3). Though we anticipated that the FD series of bitopic ligands would resemble some of the aspects of their parent ligands' pharmacological activity, we could not predict how the bitopic

nature would be displayed. Therefore, the present study served as an exploratory study to assess how linking these molecules together might have influenced their pharmacology. The differences in the efficacy and potency of these compounds may be explained by one compound having greater affinity or producing a more favourable receptor conformation to evoke a greater response. The precise interactions of these compounds with their receptors have yet to be determined. Additionally, the modifications applied to FM-6b and EC-21a to generate these bitopic ligands may impact their efficacy or potency. For example, the attachment point of the linker and the length and flexibility of the spacer can impact the affinity and pharmacological properties of a bitopic ligand[106,218,219]. Optimizing these components is critical for the future development of bitopic CB2R ligands with improved pharmacological activity[220].

In cAMP inhibition experiments assessing the co-administration of FM-6b and EC-21a, increasing amounts of EC-21a enhanced the efficacy of FM-6b, although the overall efficacy was less than that of FM-6b alone (Figure 3-7; Table 3-4). The combination of the two compounds also produced a more potent response (Table 3-4). Together these data support the characterization of EC-21a as a CB2R PAM[127].

As the most promising bitopic ligands of the FD series, FD-22a and FD-24a were also subject to co-administration cAMP experiments. In the presence of EC-21a, the efficacy of FD-22a was not affected while FD-24a experienced an increase in efficacy, though only at higher concentrations of EC-21a (Figure 3-8; Table 3-4). These data may reveal information regarding the binding sites of these bitopic ligands. For example, the inability of EC-21a to enhance FD-22a's activity may indicate that EC-21a and FD-22a bind to the same allosteric site. Furthermore, at lower concentrations of EC-21a, EC-21a and FD-24a may compete for the allosteric binding site but at higher concentrations of EC-21a, FD-24a is competed off and EC-21a can function as a PAM and

increase FD-24a's activity. As a crystal structure for CB2R's allosteric binding site has yet to be solved, our ability to investigate these possibilities and validate a binding mode for our bitopic ligands is limited[47]. Computational approaches, such as molecular dynamics (MD) simulations, and site-directed mutagenesis may be useful in determining the binding mode for these ligands[28,137,221]. In the presence of the CB2R antagonist/inverse agonist SR144528, both FD-22a and FD-24a initially experienced a reduction in efficacy which resolved as the concentration of either bitopic ligand increased (Figure 3-9; Table 3-4). The competition between FD-22a/FD-24a and SR144528 indicates that our bitopic ligands can interact with the orthosteric binding site. Overall, these data suggest that our bitopic ligands are capable of binding to the orthosteric and allosteric sites of CB2R.

4.3.2 FG series

Selective, high affinity CB2R ligands have been developed using naphthyridinone scaffolds, including the CB2R agonist LV-62[222,223]. The FG series of LV-62 derivatives were highly efficacious agonists of cAMP inhibition, although none were as efficacious as their parent ligand, which was a full agonist (Figure 3-10; Table 3-5)[187]. In contrast, LV-62 acted as a partial agonist in the recruitment of βarrestin2 as did the FG ligands, though with less efficacy than LV-62 (Figure 3-11; Table 3-5). In both cAMP inhibition and βarrestin2 recruitment assays, all FG ligands displayed reduced potencies compared to LV-62 (Table 3-5). This may suggest that the modifications applied to LV-62, such as the replacement of the hydroxyl group, seem to have reduced agonist potency in all cases. Noticeably, all ligands in this series exhibited greater efficacy in the inhibition of cAMP production, which may suggest a functional selectivity for signaling

through $G\alpha_{i/o}$ G proteins. These results warrant further investigation into the chemical moieties driving this mode of signaling, which could be exploited to develop CB2R ligands with complete selectivity for either cAMP inhibition or βarrestin2 recruitment.

4.3.3 JR series

The JR series of bitopic ligands represent another class of heterobivalent CB2R ligands, consisting of the CB2R agonist LV-62 and CB2R PAM EC-21a[188]. LV-62 was a potent full agonist of cAMP inhibition and a partial agonist of βarrestin2 recruitment (Figure 3-13A; Figure 3-14A; Table 3-6). Given the profile of LV-62 in these assays, one could predict that bitopic ligands containing the LV-62 pharmacophore may have similar activity. In the cAMP inhibition assay, all series A and series B ligands were partial agonists with comparable efficacies (Figure 3-13B-D; Table 3-6). JR-14a and JR-64a were the most potent ligands of series B and series A, respectively, with JR-64a having greater potency than LV-62 (Table 3-6). Most series A ligands poorly recruited βarrestin2 to CB2R at concentrations below 10,000 nM (Figure 3-14C-D; Table 3-6). Among series B ligands, JR-14a was a potent partial agonist of βarrestin2 recruitment while JR-16a was inactive (Figure 3-14B; Table 3-6). Though most JR ligands displayed similar efficacies in the inhibition of cAMP production and the recruitment of βarrestin2, the ligands were generally more potent in cAMP inhibition assays, which may indicate bias towards $G\alpha_{i/o}$ G protein signaling (Table 3-6). This class of ligands should be further explored to determine which chemical modifications may be beneficial or detrimental to the efficacy and/or potency in G protein-dependent and G protein-independent signaling pathways. Furthermore, considering that none of the bitopic ligands were

as efficacious as the parent orthosteric ligand, optimization of the linker and spacer moiety may improve the pharmacological profile of these ligands[220].

Additional cAMP inhibition experiments assessing the effect of EC-21a on LV-62's activity revealed that the efficacy of LV-62 increased as the concentration of EC-21a increased, although the overall efficacy was less than that of LV-62 alone (Figure 3-16; Table 3-7). The potency of LV-62 was enhanced by EC-21a, supporting the role of EC-21a as a CB2R PAM[127] (Table 3-7).

As JR-14a and JR-64a were the most potent ligands of series B and series A in the cAMP inhibition assay, these ligands were further investigated in combination with EC-21a and SR144528. For both JR-14a and JR-64a, EC-21a enhanced their efficacy in a concentration-dependent manner and the efficacy was greater than that of either bitopic ligand alone (Figure 3-17; Table 3-7). The ability of EC-21a to modulate the activity of JR-14a and JR-64a as a PAM may suggest that these bitopic ligands primarily act at CB2R's orthosteric binding site and that they are unable to interact with the allosteric site of CB2R, though further experimentation is required to validate their binding mode. Additionally, SR144528 effectively blocked the activity of JR-14a and JR-64a and this blockade was removed with increasing concentrations of either bitopic ligand, supporting an orthosteric interaction for these ligands (Figure 3-18; Table 3-7). The inability of JR-14a and JR-64a to interact with both orthosteric and allosteric sites of CB2R may be explained by the linker used. For example, if a linker molecule is too short, the ability of the bitopic ligand to simultaneously engage both binding sites is impaired[47].

Overall, these data support the hypothesis that iterative drug design can be employed to develop bitopic ligands with *in vitro* activity at CB2R. The FD series, FG series, and JR series were designed using CB2R ligands which have been validated in previous *in vitro* studies[216,223,224].

Though in many cases, the resultant ligands, whether bitopic or orthosteric, exhibited reduced efficacy and/or potency compared to their orthosteric parent ligands, the ligands described herein can be used as tool compounds to improve our comprehension of CB2R signaling[33]. The FD series and JR series of heterobivalent ligands are especially important as they can be used to investigate the bitopic engagement of CB2R. Though it was also hypothesized that these ligands would display CB2R-specific activity, this was not investigated for all ligands. Apart from FM-6b, EC-21a, and LV-62a, whose receptor specificity has previously been investigated, receptor-specific effects were only established for FD-22a, FD-24a, JR-14a, and JR-64a in this study (Figure 3-9; Figure 3-18; Table 3-4; Table 3-7)[223–225]. This was achieved through experiments with SR144528, which mediates its actions through the orthosteric binding site of CB2R. The observed effects between these bitopic ligands and SR144528 indicate that CB2R-mediated signaling is responsible for the actions of these ligands.

4.4 Novel CB2R ligands display bias towards G protein-independent signaling

Given that many ligands among the FD, FG, and JR series exhibited what appeared to be a bias or preference for signaling through $G\alpha_{i/o}$ G proteins, bias analyses were conducted as a means to compare the performance of select ligands in G protein-dependent and G protein-independent pathways, relative to that of a reference ligand, which in this case was CP55,940[111]. While there are many models which can be used to quantify signal bias, the operational model of Black and Leff was used in this study (Equation 2-1)[196,197,215]. This model is advantageous as it allows for the simultaneous comparison of potency and efficacy and is practical as it can be applied to concentration-response data in non-linear regression programs[107,217]. It is important to note that bias factors were only calculated for ligands which displayed activity in both cAMP inhibition and

βarrestin2 recruitment assays. Among all ligands for which bias factors were calculated, only JR-26a was biased towards the inhibition of cAMP production (i.e. $G\alpha_{i/o}$ G protein-biased) (Figure 3-15). All other ligands were biased towards the recruitment of βarrestin2 (i.e. βarrestin2-biased) (Figure 3-6; Figure 3-12; Figure 3-15). This finding was interesting considering that many ligands which were determined to be βarrestin2-biased displayed greater efficacies and/or potencies in the inhibition of cAMP production (Table 3-3; Table 3-5; Table 3-6). From these bias analyses, we may conclude that many of our novel CB2R ligands display a functional selectivity towards G protein-independent signaling[65]. Since βarrestin2 facilitates receptor internalization and the modulation of other G protein-independent signaling cascades, it will be interesting to see if βarrestin2 bias is required for the anti-inflammatory and anti-nociceptive effects of CB2R activation[7,226]. Though the therapeutic outcomes of biased agonism at the cannabinoid receptors is not fully understood, CB1R-mediated anti-nociception appears to be enhanced in the absence of βarrestin2[110,227]. This coupled with the role of βarrestin2 in the development of tolerance at other GPCRs suggests that G protein-dependent signaling may be associated with reduced side effects[121,228].

Many of our CB2R ligands displayed relatively small bias factors (i.e. less than 2.0)[197]. It is not clear if the size of the bias factor (versus simply the presence of bias) is important for the therapeutic effects of G protein-biased agonists of MOR[217]. Therefore, the bias observed *in vitro* for our CB2R ligands may not translate to a biologically relevant response *in vivo*. Given the complex nature and novelty of bitopic ligands, an extension of the operational model may be more suitable for the calculation of bias, as is the case for allosteric modulators[197]. Allosteric modulators which display signal bias [i.e. biased allosteric modulators (BAMs)] can be determined using extended operational models of allosterism, which has been described in detail by Slosky *et al.*

(2021)[229]. An example of such ligand is ORG27569, a BAM at CB1R[230]. However, the calculation of such bias factors for allosteric ligands requires experimental designs that were not incorporated into our experiments and may be the subject of future, more in-depth, studies.

4.5 Cannabinoid receptor-mediated signaling is influenced by orexin receptors

The shared anatomical distribution of CB1R, OX1R and OX2R in the hypothalamus, mesocorticolimbic system, brainstem, and other regions of the CNS suggests that both endocannabinoid and orexinergic systems may be implicated in the modulation of various physiological processes such as appetite, sleep, nociception, energy homeostasis, and arousal[16,231,232]. Though the presence of CB2R in the CNS is limited, its expression in the amygdala may support a role for its involvement in crosstalk between endocannabinoid and orexinergic systems[16,29]. Given that CB2R and the orexinergic system both modulate inflammation, neuroprotection, and anti-nociception, it is important to establish whether CB2R interacts with orexins and orexin receptors, and if these potential interactions are responsible for these properties[44,160,233–237]. The formation of CB1R-OX1R and CB1R-OX2R heterodimers *in vitro* has previously been established[238]. Little is known about CB2R-OX1R or CB2R-OX2R heterodimers, though CB2R and OX1R may form heterotetramers[239].

Heterodimers may exhibit distinct pharmacological properties from their monomeric GPCRs[142,240]. For example, the CB1R-selective antagonist/inverse agonist SR141716A and the OX1R-selective antagonist SB674042 bind to CB1R-OX1R heterodimers and alter the potency of agonists acting at these receptors. The novel activity exhibited by these antagonists demonstrates that our concept

of receptor selectivity may be impaired by heterodimer formation as these ligands can modulate the activity of receptors for which they lack affinity[76].

The results of our study demonstrate that the introduction of OX1R or OX2R can alter the pharmacological properties (i.e. efficacy, potency) of agonists at CB1R and CB2R (Figures 3-19 – 3-26; Tables 3-8 – 3-12). We hypothesized that orexin receptors would enhance both efficacy and potency of agonists at CB1R and CB2R. While trends in potency could not be established for all cannabinoid-orexin receptor pairings due to variable concentration-response data, trends in efficacy suggest that orexin receptors augment the efficacy of ligands at CB1R and CB2R. OX1R and OX2R enhanced CB1R-mediated inhibition of cAMP production and OX2R, but not OX1R, promoted CB1R-mediated βarrestin2 recruitment. OX2R, but not OX1R, facilitated CB2R-mediated cAMP inhibition and OX1R, but not OX2R, enhanced CB2R-mediated βarrestin2 recruitment (Table 3-12). As these experiments were conducted in cells transfected with orexin receptors, the importance of our findings relies on whether these pairings of cannabinoid receptors and orexin receptors exist on the same cells or tissues and if the formation of heterodimers can be demonstrated *in vivo*[63].

In theory, targeting heterodimers should yield therapeutics with safer side effect profiles as their expression is more restricted than their monomeric counterparts[39]. At the cannabinoid receptors, these types of therapeutics may be beneficial in treating neurodegenerative disorders or cancer, by targeting CB1R-D2 heterodimers or CB2R-GPR55 heterodimers, respectively[10,241]. It is important to determine the specific physiological roles of cannabinoid-orexin receptor heterodimers and this will require the development of heterodimer-specific agonists and antagonists[39,142]. A practical starting point may be the development of bitopic ligands that bind both monomers of a dimer, which have previously been used to study opioid receptor dimers[134,139].

4.6 Metabolites of phytocannabinoids are active at CB1R and CB2R

Δ^9-THC and CBD are the most abundant phytocannabinoids present in *C. sativa*[242]. This coupled with the ongoing investigation into the therapeutic applications of Δ^9-THC and CBD highlights the importance of studying their metabolites[7,243]. Investigating the pharmacological profiles of these metabolites may help explain some of the observed effects associated with Cannabis usage and minimize the occurrence of adverse effects[176,244]. At CB1R, all metabolites tested were agonists of cAMP inhibition, with both partial and full agonists being identified (Figure 3-27; Table 3-13). The E_{max} values obtained for the carboxylic acid metabolites COOH-THC and COOH-CBD would indicate that these ligands are full agonists at CB1R, although as seen in the CRCs, this only became apparent at concentrations above 1,000 nM (Figure 3-27B; Table 3-13) The partial agonist activity of 11-OH-THC may contribute to the biological effects of Δ^9-THC, since 11-OH-THC diffuses more readily into the brain and that the psychoactive effects of Δ^9-THC are mediated by centrally located CB1R[72,245,246]. 7-OH-CBD, which was previously described as an active metabolite of CBD, exhibited a similar CRC to that of the reference compound CP55,940 (Figure 3-27A)[247]. This finding may warrant further investigation into the possible role of 7-OH-CBD in the anti-convulsant effects of CBD, considering that 7-OH-CBD is the second most abundant metabolite present in the blood following treatment with CBD formulations[248,249]. Most metabolites were incapable of effectively recruiting βarrestin2 to CB1R, though the hydroxy-metabolite 11-OH-THC was a weak partial agonist (Figure 3-28; Table 3-13). We previously characterized the pharmacology of various phytocannabinoids, including Δ^9-THC and CBD, at both CB1R and CB2R *in vitro*[170]. In those experiments, we determined that Δ^9-THC and CBD were partial agonists of cAMP inhibition at CB1R, although CBD was less efficacious than Δ^9-THC and its activity was only apparent at 10,000 nM. In βarrestin2 recruitment assays, Δ^9-THC

acted as a partial agonist and CBD displayed no activity. Based on those results, we hypothesized that Δ^9-THC metabolites would be agonists of CB1R and CBD metabolites would be inactive. The results of the current study demonstrate that both Δ^9-THC and CBD metabolites are agonists of CB1R-mediated cAMP inhibition and that most Δ^9-THC and CBD metabolites are poor modulators of CB1R-mediated βarrestin2 recruitment.

At CB2R, a range of activity was observed in the cAMP inhibition assay; 11-OH-THC and COOH-CBD were partial agonists, COOH-THC was a full agonist, 6-OH-CBD was an inverse agonist and 7-OH-CBD was inactive (Figure 3-29; Table 3-14). COOH-THC reportedly has anti-inflammatory and analgesic properties[250]. Though COOH-THC was also a full agonist at CB1R, its activity at CB2R is of particular interest as COOH-THC lacks psychoactivity[245]. Collectively, these findings may indicate a peripheral and/or CB2R-mediated mechanism for COOH-THC, though its brain distribution must first be established to support this theory. Inverse agonism at CB2R may play a role in mediating anti-inflammatory responses[89]. Thus, 6-OH-CBD should be investigated further to determine if it is implicated in CBD's anti-inflammatory properties[251]. As with CB1R, most metabolites lacked activity in the βarrestin2 recruitment assay, except for 7-OH-CBD, which exhibited similar efficacy and potency to CP55,940 (Figure 3-30; Table 3-14). Whether or not this is relevant to the anti-inflammatory effects of 7-OH-CBD is yet to be determined[252]. According to our previous study, Δ^9-THC and CBD are partial agonists of cAMP inhibition at CB2R, though Δ^9-THC had greater efficacy and CBD's activity was only evident at 10,000 nM. Both Δ^9-THC and CBD are partial agonists of βarrestin2 recruitment at CB2R with Δ^9-THC exhibiting greater efficacy[170]. We hypothesized that Δ^9-THC metabolites would be agonists of CB2R and CBD metabolites would be inactive. The results of the current study indicate that most Δ^9-THC and CBD metabolites are agonists of CB2R-mediated cAMP inhibition and that

Δ^9-THC and CBD metabolites are not agonists of CB2R-mediated βarrestin2 recruitment, except for 7-OH-CBD.

4.7 Limitations

There are several limitations which must be considered when interpreting the results of this study and their implications.

Firstly, the pharmacological activity of the ligands in this study was assessed using an *in vitro* model consisting of CHO-K1 cells overexpressing human GPCRs. While cell-based signaling assays allow for the characterization of a large number of compounds with relative ease, the results may not translate to a response *in vivo* as they lack cellular context[240,253]. Though receptor overexpression can facilitate the detection of downstream signaling activity, it may not be reflective of the natural expression levels of the receptor[11,240]. Furthermore, bias detected using such a model may not translate to ligand bias in the natural physiological system in which the receptor of interest is present[197,253]. It is also important to note that these ligands may exhibit different pharmacological profiles when tested in a different species. For example, the synthetic cannabinoid AM1241 is an agonist at human CB2R and an inverse agonist at rodent CB2R[11,62]. These species-dependent effects are important to consider given that while *in vitro* experimentation may use human receptors, rodents are often used for *in vivo* evaluation[7,27,131]. Another caveat is that the PathHunter® βarrestin assay uses a GPCR tagged at the C-terminal with a fragment of the β-gal enzyme in order to quantify βarrestin2 recruitment, as the interaction between the modified GPCR and βarrestin2 produces a chemiluminescent signal indicative of βarrestin2 recruitment[194,254]. It is necessary to consider the implications of this on the signaling

profiles of our ligands given the important role the C-terminal tail plays in βarrestin2 recruitment[50,197,255]. *In vitro* models should therefore be used to identify promising efficacious and/or biased ligands for further experimentation in physiologically relevant *in vivo* systems, rather than being predictive of *in vivo* efficacy and/or bias[11,215,256]. Additionally, since it is difficult to establish complete receptor selectivity for our ligands *in vitro* as non-cannabinoid receptor binding sites may exist, *in vivo* evaluation may reveal off-target effects[62,256].

Secondly, the use of CP55,940 as a reference compound in the experiments quantifying ERK1/2 phosphorylation at GPR55 may have been inappropriate. The reference compound should be a ligand which produces a full agonist response at the receptor of interest as it is used as a comparator for the test compounds. However, considering that most of the novel GPR55 ligands displayed greater efficacies and potencies than our reference ligand, this may suggest that CP55,940 is not an optimal reference ligand. A more appropriate reference ligand may be O-1602, a synthetic analogue of CBD and potent agonist of GPR55[257].

Thirdly, the therapeutic applications of our CB2R bitopic ligands are most likely limited as bitopic ligands tend to have poor pharmacokinetic properties[10]. Furthermore, the advantages conferred to bitopic ligands through the addition of an allosteric component might not be realized, since the rational design of ligands targeting CB2R's allosteric site is impaired by limited knowledge of this site[258]. Thus, our ligands are better suited as pharmacological tools to study the implications of bitopic signaling and biased agonism at CB2R rather than to function as novel therapeutics[33,259].

Fourthly, though bias was determined using the operational model, there is currently no model which can provide an absolute measure of bias[197]. Furthermore, the operational model cannot account for differences in receptor reserve or the level of amplification inherent to the cell

signaling assays used[259]. For example, βarrestin2 recruitment is measured further downstream from cAMP inhibition and, thus, the signal amplification of these pathways may differ[197,256]. As such, our attribution of bias to ligands must be interpreted with caution. Additionally, while several ligands displayed bias towards G protein-dependent and G protein-independent signaling pathways, for this bias to be of therapeutic relevance, it must first be established that distinct signaling pathways are responsible for the separation of beneficial properties versus undesirable side effects[35,111].

Lastly, while this study revealed that OX1R and OX2R can alter CB1R-mediated and CB2R-mediated signaling, we did not conduct any experiments that directly measured transfection efficiency or the expression levels of OX1R or OX2R. That being said, increasing amounts of either receptor did produce a response different from untransfected controls. Additionally, we did not establish the physical interaction of these receptors. Future experiments using co-immunoprecipitation (Co-IP), BRET and/or fluorescence resonance energy transfer (FRET) techniques can be used to investigate this[33,142,260]. It will also be necessary to demonstrate the formation of these heterodimers *in vivo*[139].

4.8 Conclusion

This work allowed for the investigation of various cannabinoid ligands (e.g. orthosteric agonists, allosteric modulators, bitopic ligands, drug metabolites) and receptor interactions, with an overarching focus on CB2R. Based on the findings of this study, we can conclude that: (1) novel synthetic cannabinoids can be developed using iterative pharmacological data and drug design; (2) orexin receptors alter cannabinoid receptor-mediated signaling; and (3) metabolites of the primary

constituents of *C. sativa* are pharmacologically active. These findings are especially important considering the potential role of CB2R as an anti-inflammatory and anti-nociceptive drug target[19,90]. Current treatments for inflammation and pain are less than ideal. Anti-inflammatory agents, such as steroids and non-steroidal anti-inflammatory drugs (NSAIDs) are associated with adverse effects while biologics are costly and increase the risk of infection[261]. Pain management may be achieved using opioids, NSAIDs, tricyclic antidepressants, or anticonvulsants, though the efficacy and side effect profiles of these drugs are poor[90,262]. The urgency to find safer therapeutics for pain is demonstrated by the opioid crisis, as opioids can produce tolerance, physical dependence, respiratory depression and in some cases overdose[77]. Ongoing investigation of tool compounds and signaling paradigms at CB2R is crucial for CB2R ligands to emerge as novel anti-inflammatory and analgesic agents.

References

1. Guindon, J. & Hohmann, A. G. The Endocannabinoid System and Pain. *CNS Neurol. Disord. - Drug Targets* **8**, 403–421 (2009).

2. Baker, D., Pryce, G., Giovannoni, G. & Thompson, A. J. The therapeutic potential of cannabis. *Lancet Neurol.* **2**, 291–298 (2003).

3. Smolyakova, A. M. *et al.* The Endocannabinoid System and Synthetic Cannabinoids in Preclinical Models of Seizure and Epilepsy. *J. Clin. Neurophysiol.* **37**, 15–27 (2020).

4. Cassano, T. *et al.* Cannabinoid receptor 2 signaling in neurodegenerative disorders: From pathogenesis to a promising therapeutic target. *Front. Neurosci.* **11**, 1–10 (2017).

5. Lazarini-Lopes, W., da Silva-Júnior, R. M. P., Servilha-Menezes, G., Do Val-da Silva, R. A. & Garcia-Cairasco, N. Cannabinoid Receptor Type 1 (CB1R) Expression in Limbic Brain Structures After Acute and Chronic Seizures in a Genetic Model of Epilepsy. *Front. Behav. Neurosci.* **14**, 1–15 (2020).

6. Wu, J. Cannabis, cannabinoid receptors, and endocannabinoid system: yesterday, today, and tomorrow. *Acta Pharmacol. Sin.* **40**, 297–299 (2019).

7. Dhopeshwarkar, A. & Mackie, K. CB2 Cannabinoid Receptors as a Therapeutic Target — What Does the Future Hold ? *Mol. Pharmacol.* **86**, 430–437 (2014).

8. Lu, D., Immadi, S. S., Wu, Z. & Kendall, D. A. Translational potential of allosteric modulators targeting the cannabinoid CB 1 receptor. *Acta Pharmacol. Sin.* **40**, 324–335 (2019).

9. Moreno, E. *et al.* Targeting CB2-GPR55 receptor heteromers modulates cancer cell

signaling. *J. Biol. Chem.* **289**, 21960–21972 (2014).

10. Morales, P. & Reggio, P. H. An Update on Non-CB 1 , Non-CB 2 Cannabinoid Related G-Protein-Coupled Receptors. *Cannabis Cannabinoid Res.* **2**, 265–273 (2017).

11. Yao, B. B. *et al.* In vitro pharmacological characterization of AM1241: A protean agonist at the cannabinoid CB 2 receptor? *Br. J. Pharmacol.* **149**, 145–154 (2006).

12. Brown, A. J. Novel cannabinoid receptors. *Br. J. Pharmacol.* **152**, 567–575 (2007).

13. Lauckner, J. E. *et al.* GPR55 is a cannabinoid receptor that increases intracellular calcium and inhibits M current. *Proc. Natl. Acad. Sci. U. S. A.* **105**, 2699–2704 (2008).

14. Kendall, D. A. & Yudowski, G. A. Cannabinoid receptors in the central nervous system: Their signaling and roles in disease. *Front. Cell. Neurosci.* **10**, 1–10 (2017).

15. Quarta, C., Mazza, R., Obici, S., Pasquali, R. & Pagotto, U. Energy balance regulation by endocannabinoids at central and peripheral levels. *Trends Mol. Med.* **17**, 518–526 (2011).

16. Flores, Á., Maldonado, R. & Berrendero, F. Cannabinoid-hypocretin cross-talk in the central nervous system: What we know so far. *Front. Neurosci.* **7**, 1–17 (2013).

17. Mackie, K. Cannabinoid receptors: Where they are and what they do. *J. Neuroendocrinol.* **20**, 10–14 (2008).

18. Manduca, A. *et al.* Interacting cannabinoid and opioid receptors in the nucleus accumbens core control adolescent social play. *Front. Behav. Neurosci.* **10**, 1–17 (2016).

19. Ashton, J. & Glass, M. The Cannabinoid CB2 Receptor as a Target for Inflammation-Dependent Neurodegeneration. *Curr. Neuropharmacol.* **5**, 73–80 (2007).

20. Okamoto, Y., Morishita, J., Tsuboi, K., Tonai, T. & Ueda, N. Molecular Characterization of a Phospholipase D Generating Anandamide and Its Congeners. *J. Biol. Chem.* **279**, 5298–5305 (2004).

21. Murataeva, N., Straiker, A. & Mackie, K. Parsing the players: 2-arachidonoylglycerol synthesis and degradation in the CNS. *Br. J. Pharmacol.* **171**, 1379–1391 (2014).

22. Morena, M., Patel, S., Bains, J. S. & Hill, M. N. Neurobiological Interactions Between Stress and the Endocannabinoid System. *Neuropsychopharmacology* **41**, 80–102 (2016).

23. Verty, A. N. A., Stefanidis, A., McAinch, A. J., Hryciw, D. H. & Oldfield, B. Anti-obesity effect of the CB2 receptor agonist JWH-015 in diet-induced obese mice. *PLoS One* **10**, 1–19 (2015).

24. Callén, L. *et al.* Cannabinoid receptors CB 1 and CB 2 form functional heteromers in brain. *J. Biol. Chem.* **287**, 20851–20865 (2012).

25. Tham, M. *et al.* Allosteric and orthosteric pharmacology of cannabidiol and cannabidiol-dimethylheptyl at the type 1 and type 2 cannabinoid receptors. *Br. J. Pharmacol.* **176**, 1455–1469 (2019).

26. Watanabe, K. *et al.* Cannabidiol metabolism revisited : tentative identification of novel decarbonylated metabolites of cannabidiol formed by human liver microsomes and recombinant cytochrome P450 3A4. *Forensic Toxicol.* **37**, 449–455 (2019).

27. Soethoudt, M. *et al.* Cannabinoid CB2 receptor ligand profiling reveals biased signalling and off-target activity. *Nat. Commun.* **8**, (2017).

28. Navarro, G. *et al.* Design of Negative and Positive Allosteric Modulators of the

Cannabinoid CB2Receptor Derived from the Natural Product Cannabidiol. *J. Med. Chem.* **64**, 9354–9364 (2021).

29. Chen, D. J., Gao, M., Gao, F. F., Su, Q. X. & Wu, J. Brain cannabinoid receptor 2: Expression, function and modulation. *Acta Pharmacol. Sin.* **38**, 312–316 (2017).

30. Nelson, K. M. *et al.* The Essential Medicinal Chemistry of Cannabidiol (CBD). *J. Med. Chem* **63**, 12137−12155 (2020).

31. Mechoulam, R., Hanuš, L. O., Pertwee, R. & Howlett, A. C. Early phytocannabinoid chemistry to endocannabinoids and beyond. *Nat. Rev. Neurosci.* **15**, 757–764 (2014).

32. Buckley, N. E. *et al.* Immunomodulation by cannabinoids is absent in mice deficient for the cannabinoid CB2 receptor. *Eur. J. Pharmacol.* **396**, 141–149 (2000).

33. Hubner, H. *et al.* Structure-guided development of heterodimer-selective GPCR ligands. *Nat. Commun.* **7**, 1–12 (2016).

34. Burgueño, J. *et al.* A Complementary Scale of Biased Agonism for Agonists with Differing Maximal Responses. *Sci. Rep.* **7**, 1–11 (2017).

35. Gottesman-Katz, L., Latorre, R., Vanner, S., Schmidt, B. L. & Bunnett, N. W. Targeting G protein-coupled receptors for the treatment of chronic pain in the digestive system. *Gut* **70**, 970–981 (2021).

36. Wisler, J. W. *et al.* A unique mechanism of β-blocker action: Carvedilol stimulates β-arrestin signaling. *Proc. Natl. Acad. Sci. U. S. A.* **104**, 16657–16662 (2007).

37. Petersen, J. *et al.* Agonist-induced dimer dissociation as a macromolecular step in G protein-coupled receptor signaling. *Nat. Commun.* **8**, (2017).

38. Sengupta, D., Prasanna, X., Mohole, M. & Chattopadhyay, A. Exploring GPCR-Lipid Interactions by Molecular Dynamics Simulations: Excitements, Challenges, and the Way Forward. *J. Phys. Chem. B* **122**, 5727–5737 (2018).

39. Kamal, M. & Jockers, R. Biological significance of GPCR heteromerization in the neuro-endocrine system. *Front. Endocrinol. (Lausanne).* **2**, 1–14 (2010).

40. Oldham, W. M. & Hamm, H. E. Heterotrimeric G protein activation by G-protein-coupled receptors. *Nat. Rev. Mol. Cell Biol.* **9**, 60–71 (2008).

41. Choi, M. *et al.* G protein–coupled receptor kinases (GRKs) orchestrate biased agonism at the 2-adrenergic receptor. *Sci. Signal.* **11**, (2018).

42. Asher, W. B. *et al.* Single-molecule FRET imaging of GPCR dimers in living cells. *Nat. Methods* **18**, 397–405 (2021).

43. Wakefield, A. E., Bajusz, D., Kozakov, D., Keseru, G. M. & Vajda, S. Conservation of Allosteric Ligand Binding Sites in G-Protein Coupled Receptors. *J. Chem. Inf. Model.* **62**, 4937–4954 (2022).

44. Couvineau, A. *et al.* Orexins as Novel Therapeutic Targets in Inflammatory and Neurodegenerative Diseases. *Front. Endocrinol. (Lausanne).* **10**, (2019).

45. Rosenbaum, D. M., Rasmussen, S. G. F. & Kobilka, B. K. The structure and function of G-protein-coupled receptors. *Nature* **459**, 356–363 (2009).

46. Dorsam, R. T. & Gutkind, J. S. G-protein-coupled receptors and cancer. *Nat. Rev. Cancer* **7**, 79–94 (2007).

47. Lane, J. R., Sexton, P. M. & Christopoulos, A. Bridging the gap: Bitopic ligands of G-

protein-coupled receptors. *Trends Pharmacol. Sci.* **34**, 59–66 (2013).

48. Hilger, D., Masureel, M. & Kobilka, B. K. Structure and dynamics of GPCR signaling complexes. *Nat. Struct. Mol. Biol.* **25**, 4–12 (2018).

49. Shenoy, S. K. & Lefkowitz, R. J. B-Arrestin-Mediated Receptor Trafficking and Signal Transduction. *Trends Pharmacol. Sci.* **32**, 521–533 (2011).

50. Smith, J. S., Lefkowitz, R. J. & Rajagopal, S. Biased signalling: From simple switches to allosteric microprocessors. *Nat. Rev. Drug Discov.* **17**, 243–260 (2018).

51. Ge, B. *et al.* Single-molecule imaging reveals dimerization/oligomerization of CXCR4 on plasma membrane closely related to its function. *Sci. Rep.* **7**, 1–9 (2017).

52. Harada, N. *et al.* Identification of G protein-coupled receptor 55 (GPR55) as a target of curcumin. *npj Sci. Food* **6**, (2022).

53. Wootten, D., Christopoulos, A., Marti-Solano, M., Babu, M. M. & Sexton, P. M. Mechanisms of signalling and biased agonism in G protein-coupled receptors. *Nat. Rev. Mol. Cell Biol.* **19**, 638–653 (2018).

54. Gulati, S. *et al.* Targeting G protein-coupled receptor signaling at the G protein level with a selective nanobody inhibitor. *Nat. Commun.* **9**, (2018).

55. Bos, J. L., Rehmann, H. & Wittinghofer, A. GEFs and GAPs: Critical Elements in the Control of Small G Proteins. *Cell* **130**, 385 (2007).

56. Scheffzek, K. & Ahmadian, M. R. GTPase activating proteins: Structural and functional insights 18 years after discovery. *Cell. Mol. Life Sci.* **62**, 3014–3038 (2005).

57. Saroz, Y., Kho, D. T., Glass, M., Graham, E. S. & Grimsey, N. L. Cannabinoid Receptor 2 (CB2) Signals via G-alpha-s and Induces IL-6 and IL-10 Cytokine Secretion in Human Primary Leukocytes. *ACS Pharmacol. Transl. Sci.* **2**, 414–428 (2019).

58. Ibsen, M. S. *et al.* Cannabinoid CB1 and CB2 receptor-mediated arrestin translocation: Species, subtype, and agonist-dependence. *Front. Pharmacol.* **10**, 1–18 (2019).

59. Turcotte, C., Blanchet, M. R., Laviolette, M. & Flamand, N. The CB2 receptor and its role as a regulator of inflammation. *Cell. Mol. Life Sci.* **73**, 4449–4470 (2016).

60. Dhillon, A. S. *et al.* Cyclic AMP-Dependent Kinase Regulates Raf-1 Kinase Mainly by Phosphorylation of Serine 259. *Mol. Cell. Biol.* **22**, 3237–3246 (2002).

61. Zhou, J., Burkovskiy, I., Yang, H., Sardinha, J. & Lehmann, C. CB2 and GPR55 receptors as therapeutic targets for systemic immune dysregulation. *Front. Pharmacol.* **7**, 1–7 (2016).

62. Atwood, B. K. & Mackie, K. CB 2: A cannabinoid receptor with an identity crisis. *Br. J. Pharmacol.* **160**, 467–479 (2010).

63. Hilairet, S., Bouaboula, M., Carrière, D., Le Fur, G. & Casellas, P. Hypersensitization of the orexin 1 receptor by the CB1 receptor: Evidence for cross-talk blocked by the specific CB1 antagonist, SR141716. *J. Biol. Chem.* **278**, 23731–23737 (2003).

64. Panikashvili, D., Mechoulam, R., Beni, S. M., Alexandrovich, A. & Shohami, E. CB1 cannabinoid receptors are involved in neuroprotection via NF-κB inhibition. *J. Cereb. Blood Flow Metab.* **25**, 477–484 (2005).

65. Dhopeshwarkar, A. & Mackie, K. Functional selectivity of CB2 cannabinoid receptor

ligands at a canonical and noncanonical pathways. *J. Pharmacol. Exp. Ther.* **358**, 342–351 (2016).

66. Navarro, G. *et al.* Targeting cannabinoid CB2 receptors in the central nervous system. Medicinal chemistry approaches with focus on neurodegenerative disorders. *Front. Neurosci.* **10**, 1–11 (2016).

67. Shukla, A. K. *et al.* Visualization of arrestin recruitment by a G-protein-coupled receptor. *Nature* **512**, 218–222 (2014).

68. Strachan, R. T. *et al.* Divergent transducer-specific molecular efficacies generate biased agonism at a G protein-coupled receptor (GPCR). *J. Biol. Chem.* **289**, 14211–14224 (2014).

69. Violin, J. D. & Lefkowitz, R. J. β-Arrestin-biased ligands at seven-transmembrane receptors. *Trends Pharmacol. Sci.* **28**, 416–422 (2007).

70. Luttrell, L. M. & Lefkowitz, R. J. The role of β-arrestins in the termination and transduction of G-protein-coupled receptor signals. *J. Cell Sci.* **115**, 455–465 (2002).

71. Maresz, K., Carrier, E. J., Ponomarev, E. D., Hillard, C. J. & Dittel, B. N. Modulation of the cannabinoid CB2 receptor in microglial cells in response to inflammatory stimuli. *J. Neurochem.* **95**, 437–445 (2005).

72. Shao, Z. *et al.* Structure of an allosteric modulator bound to the CB1 cannabinoid receptor. *Nat. Chem. Biol.* **15**, 1199–1205 (2019).

73. Spinelli, F., Capparelli, E., Abate, C., Colabufo, N. A. & Contino, M. Perspectives of Cannabinoid Type 2 Receptor (CB2R) Ligands in Neurodegenerative Disorders:

Structure-Affinity Relationship (SAfiR) and Structure-Activity Relationship (SAR) Studies. *J. Med. Chem.* **60**, 9913–9931 (2017).

74. Laprairie, R. B., Bagher, A. M. & Denovan-Wright, E. M. Cannabinoid receptor ligand bias: implications in the central nervous system. *Curr. Opin. Pharmacol.* **32**, 32–43 (2017).

75. Kargl, J. *et al.* The cannabinoid receptor CB1 modulates the signaling properties of the lysophosphatidylinositol receptor GPR55. *J. Biol. Chem.* **287**, 44234–44248 (2012).

76. Ellis, J., Pediani, J. D., Canals, M., Milasta, S. & Milligan, G. Orexin-1 receptor-cannabinoid CB1 receptor heterodimerization results in both ligand-dependent and -independent coordinated alterations of receptor localization and function. *J. Biol. Chem.* **281**, 38812–38824 (2006).

77. Iyer, V. *et al.* The cannabinoid CB2 receptor agonist LY2828360 synergizes with morphine to suppress neuropathic nociception and attenuates morphine reward and physical dependence. *Eur. J. Pharmacol.* **886**, 173544 (2020).

78. Ward, R. J., Pediani, J. D. & Milligan, G. Heteromultimerization of cannabinoid CB 1 receptor and orexin OX 1 receptor generates a unique complex in which both protomers are regulated by orexin A. *J. Biol. Chem.* **286**, 37414–37428 (2011).

79. Tam, J. *et al.* Peripheral cannabinoid-1 receptor inverse agonism reduces obesity by reversing leptin resistance. *Cell Metab.* **16**, 167–179 (2012).

80. Jones, D. End of the line for cannabinoid receptor 1 as an anti-obesity target? *Nat Rev Drug Discov* **7**, 961–2 (2008).

81. Deng, L. *et al.* Chronic cannabinoid receptor 2 activation reverses paclitaxel neuropathy without tolerance or cannabinoid receptor 1-dependent withdrawal. *Biol. Psychiatry* **77**, 475–487 (2015).

82. Giblin, G. M. P. *et al.* Discovery of 2-[(2,4-Dichlorophenyl)amino]-N-[(tetrahydro- 2H-pyran-4-yl)methyl]-4-(trifluoromethyl)- 5-pyrimidinecarboxamide, a Selective CB2 Receptor Agonist for the Treatment of Inflammatory Pain. *J. Med. Chem* **50**, 2597–2600 (2007).

83. Leach, K., Conigrave, A. D., Sexton, P. M. & Christopoulos, A. Towards tissue-specific pharmacology: Insights from the calcium-sensing receptor as a paradigm for GPCR (patho)physiological bias. *Trends Pharmacol. Sci.* **36**, 215–225 (2015).

84. Atwood, B. K., Wager-Miller, J., Haskins, C., Straiker, A. & Mackie, K. Functional selectivity in CB 2 cannabinoid receptor signaling and regulation: Implications for the therapeutic potential of CB 2 ligands. *Mol. Pharmacol.* **81**, 250–263 (2012).

85. Van Sickle, M. D. *et al.* Neuroscience: Identification and functional characterization of brainstem cannabinoid CB2 receptors. *Science (80-.).* **310**, 329–332 (2005).

86. Mangiatordi, G. F. *et al.* Cannabinoid Receptor Subtype 2 (CB2R) in a Multitarget Approach: Perspective of an Innovative Strategy in Cancer and Neurodegeneration. *J. Med. Chem.* **63**, 14448–14469 (2020).

87. Gutierrez, T., Farthing, J. N., Zvonok, A. M., Makriyannis, A. & Hohmann, A. G. Activation of peripheral cannabinoid CB 1 and CB 2 receptors suppresses the maintenance of inflammatory nociception: A comparative analysis. *Br. J. Pharmacol.* **150**, 153–163

(2007).

88. Han, S., Thatte, J., Buzard, D. J. & Jones, R. M. Therapeutic utility of cannabinoid receptor type 2 (CB2) selective agonists. *J. Med. Chem.* **56**, 8224–8256 (2013).

89. Pertwee, R. G. The diverse CB1 and CB2 receptor pharmacology of three plant cannabinoids: D9-tetrahydrocannabinol, cannabidiol and D9-tetrahydrocannabivarin. *Br. J. Pharmacol.* **153**, 199–215 (2008).

90. Guindon, J. & Hohmann, A. G. Cannabinoid CB 2 receptors: A therapeutic target for the treatment of inflammatory and neuropathic pain. *Br. J. Pharmacol.* **153**, 319–334 (2008).

91. Lin, X., Dhopeshwarkar, A. S., Huibregtse, M., Mackie, K. & Hohmann, A. G. Slowly signaling G protein-biased CB2 cannabinoid receptor agonist LY2828360 suppresses neuropathic pain with sustained efficacy and attenuates morphine tolerance and dependence. *Mol. Pharmacol.* **93**, 49–62 (2018).

92. Hanuš, L. *et al.* HU-308: A specific agonist for CB2, a peripheral cannabinoid receptor. *Proc. Natl. Acad. Sci. U. S. A.* **96**, 14228–14233 (1999).

93. Lin, X. *et al.* A peripheral CB2cannabinoid receptor mechanism suppresses chemotherapy-induced peripheral neuropathy: Evidence from a CB2reporter mouse. *Pain* **163**, 834–851 (2022).

94. Price, D. A. *et al.* WIN55,212-2, a cannabinoid receptor agonist, protects against nigrostriatal cell loss in the 1-methyl-4-phenyl-1,2,3,6-tetrahydropyridine mouse model of Parkinson's disease. *Eur. J. Neurosci.* **29**, 2177–2186 (2009).

95. Whiting, Z. M., Yin, J., de la Harpe, S. M., Vernall, A. J. & Grimsey, N. L. Developing

the Cannabinoid Receptor 2 (CB2) pharmacopoeia: past, present, and future. *Trends Pharmacol. Sci.* **43**, 754–771 (2022).

96. Atwood, B. K., Straiker, A. & Mackie, K. CB2: Therapeutic target-in-waiting. *Prog. Neuro-Psychopharmacology Biol. Psychiatry* **38**, 16–20 (2012).

97. Vitale, R. M. *et al.* Identification and Characterization of Cannabidiol as an OX1R Antagonist by Computational and In Vitro Functional Validation. *Biomolecules* **11**, 1–14 (2021).

98. Fakhouri, L. *et al.* Design, synthesis and biological evaluation of GPR55 agonists. *Bioorganic Med. Chem.* **25**, 4355–4367 (2017).

99. McHugh, D. *et al.* N-arachidonoyl glycine, an abundant endogenous lipid, potently drives directed cellular migration through GPR18, the putative abnormal cannabidiol receptor. *BMC Neurosci.* **11**, (2010).

100. Liu, Y., Wang, L., Lo, K. W. & Lui, V. W. Y. Omics-wide quantitative B-cell infiltration analyses identify GPR18 for human cancer prognosis with superiority over CD20. *Commun. Biol.* **3**, 1–11 (2020).

101. Morales, P. *et al.* Therapeutic Exploitation of GPR18: Beyond the Cannabinoids? *J. Med. Chem.* **63**, 14216–14227 (2020).

102. Overton, H. A. *et al.* Deorphanization of a G protein-coupled receptor for oleoylethanolamide and its use in the discovery of small-molecule hypophagic agents. *Cell Metab.* **3**, 167–175 (2006).

103. Zhao, J., Zhao, Y., Hu, Y. & Peng, J. Targeting the GPR119/incretin axis: a promising

new therapy for metabolic-associated fatty liver disease. *Cell. Mol. Biol. Lett.* **26**, (2021).

104. Overton, H. A., Fyfe, M. C. T. & Reynet, C. GPR119, a novel G protein-coupled receptor target for the treatment of type 2 diabetes and obesity. *Br. J. Pharmacol.* **153**, 76–81 (2008).

105. Ritter, K., Buning, C., Halland, N., Pöverlein, C. & Schwink, L. G Protein-Coupled Receptor 119 (GPR119) Agonists for the Treatment of Diabetes: Recent Progress and Prevailing Challenges. *J. Med. Chem.* **59**, 3579–3592 (2016).

106. Romantini, N. *et al.* Exploring the signaling space of a GPCR using bivalent ligands with a rigid oligoproline backbone. *Proc. Natl. Acad. Sci. U. S. A.* **118**, (2021).

107. Kenakin, T., Watson, C., Muniz-Medina, V., Christopoulos, A. & Novick, S. A simple method for quantifying functional selectivity and agonist bias. *ACS Chem. Neurosci.* **3**, 193–203 (2012).

108. Rajagopal, S., Rajagopal, K. & Lefkowitz, R. J. Teaching old receptors new tricks: Biasing seven-transmembrane receptors. *Nat. Rev. Drug Discov.* **9**, 373–386 (2010).

109. Forster, L. & Pockes, S. Investigating the ligand agonism and antagonism at the D2long receptor by dynamic mass redistribution. *Sci. Rep.* **12**, 1–13 (2022).

110. Manning, J. J., Green, H. M., Glass, M. & Finlay, D. B. Pharmacological selection of cannabinoid receptor effectors: Signalling, allosteric modulation and bias. *Neuropharmacology* **193**, 108611 (2021).

111. Ibsen, M. S., Connor, M. & Glass, M. Cannabinoid CB 1 and CB 2 Receptor Signaling and Bias. *Cannabis Cannabinoid Res.* **2**, 48–60 (2017).

112. Manglik, A. *et al.* Structure-based discovery of opioid analgesics with reduced side effects. *Nature* **537**, 185–190 (2016).

113. Wisler, J. W., Xiao, K., Thomsen, A. R. B. & Lefkowitz, R. J. Recent developments in biased agonism. *Curr. Opin. Cell Biol.* **27**, 18–24 (2014).

114. He, L. *et al.* Pharmacological and genetic manipulations at the μ-opioid receptor reveal arrestin-3 engagement limits analgesic tolerance and does not exacerbate respiratory depression in mice. *Neuropsychopharmacology* **46**, 2241–2249 (2021).

115. Kliewer, A. *et al.* Morphine-induced respiratory depression is independent of β-arrestin2 signalling. *Br. J. Pharmacol.* **177**, 2923–2931 (2020).

116. Conibear, A. E. & Kelly, E. A biased view of μ-Opioid receptors? *Mol. Pharmacol.* **96**, 542–549 (2019).

117. Gillis, A., Sreenivasan, V. & Christie, M. J. Intrinsic efficacy of opioid ligands and its importance for apparent bias, operational analysis, and therapeutic window. *Mol. Pharmacol.* **98**, 410–424 (2020).

118. Wisler, J. W., Rockman, H. A. & Lefkowitz, R. J. Biased G protein-coupled receptor signaling: Changing the paradigm of drug discovery. *Circulation* **137**, 2315–2317 (2018).

119. Monasky, M. M. *et al.* The β-arrestin-biased ligand TRV120023 inhibits angiotensin II-induced cardiac hypertrophy while preserving enhanced myofilament response to calcium. *Am. J. Physiol. - Hear. Circ. Physiol.* **305**, 856–866 (2013).

120. McCorvy, J. D. *et al.* Structural determinants of 5-HT2B receptor activation and biased agonism. *Nat. Struct. Mol. Biol.* **25**, 787–796 (2018).

121. Wouters, E. *et al.* Assessment of Biased Agonism among Distinct Synthetic Cannabinoid Receptor Agonist Scaffolds. *ACS Pharmacol. Transl. Sci.* **3**, 285–295 (2020).

122. Zagzoog, A. *et al.* Assessment of select synthetic cannabinoid receptor agonist bias and selectivity between the type 1 and type 2 cannabinoid receptor. *Sci. Rep.* **11**, 1–18 (2021).

123. Liu, X. *et al.* An allosteric modulator binds to a conformational hub in the β2 adrenergic receptor. *Nat. Chem. Biol.* **16**, 749–755 (2020).

124. Jeffrey Conn, P., Christopoulos, A. & Lindsley, C. W. Allosteric modulators of GPCRs: A novel approach for the treatment of CNS disorders. *Nat. Rev. Drug Discov.* **8**, 41–54 (2009).

125. Foster, D. J. & Conn, P. J. Allosteric Modulation of GPCRs: New Insights and Potential Utility for Treatment of Schizophrenia and Other CNS Disorders. *Neuron* **94**, 431–446 (2017).

126. Conn, P. J., Lindsley, C. W., Meiler, J. & Niswender, C. M. Opportunities and challenges in the discovery of allosteric modulators of GPCRs for treating CNS disorders. *Nat. Rev. Drug Discov.* **13**, 692–708 (2014).

127. Cao, A. M. *et al.* Allosteric modulators enhance agonist efficacy by increasing the residence time of a GPCR in the active state. *Nat. Commun.* **12**, 1–13 (2021).

128. Thal, D. M., Glukhova, A., Sexton, P. M. & Christopoulos, A. Structural insights into G-protein-coupled receptor allostery. *Nature* **559**, 45–53 (2018).

129. Christopoulos, A. Allosteric binding sites on cell-surface receptors: Novel targets for drug discovery. *Nat. Rev. Drug Discov.* **1**, 198–210 (2002).

130. Wacker, D., Stevens, R. C. & Roth, B. L. How Ligands Illuminate GPCR Molecular Pharmacology. *Cell* **170**, 414–427 (2017).

131. Wootten, D., Christopoulos, A. & Sexton, P. M. Emerging paradigms in GPCR allostery: Implications for drug discovery. *Nat. Rev. Drug Discov.* **12**, 630–644 (2013).

132. Lane, J. R. *et al.* A new mechanism of allostery in a G protein-coupled receptor dimer. *Nat. Chem. Biol.* **10**, 745–752 (2014).

133. Pulido, D. *et al.* Heterobivalent Ligand for the Adenosine A2A-Dopamine D2Receptor Heteromer. *J. Med. Chem.* **65**, 616–632 (2022).

134. Portoghese, P. S. From Models to Molecules: Opioid Receptor Dimers, Bivalent Ligands, and Selective Opioid Receptor Probes. *J. Med. Chem.* **44**, 2259–2269 (2001).

135. Vauquelin, G. & Charlton, S. J. Exploring avidity: Understanding the potential gains in functional affinity and target residence time of bivalent and heterobivalent ligands. *Br. J. Pharmacol.* **168**, 1771–1785 (2013).

136. Fernandes, S. M., Lee, Y. S., Gillies, R. J. & Hruby, V. J. Synthesis and evaluation of bivalent ligands for binding to the human melanocortin-4 receptor. *Bioorganic Med. Chem.* **22**, 6360–6365 (2014).

137. Keov, P. *et al.* Molecular mechanisms of bitopic ligand engagement with the M1 muscarinic acetylcholine receptor. *J. Biol. Chem.* **289**, 23817–23837 (2014).

138. Ullmann, T. *et al.* Homobivalent Dopamine D2 Receptor Ligands Modulate the Dynamic Equilibrium of D2Monomers and Homo- And Heterodimers. *ACS Chem. Biol.* **16**, 371–379 (2021).

139. Parmentier, M. GPCRs: Heterodimer-specific signaling. *Nat. Chem. Biol.* **11**, 244–245 (2015).

140. George, S. R. *et al.* Oligomerization of μ- and δ-opioid receptors: Generation of novel functional properties. *J. Biol. Chem.* **275**, 26128–26135 (2000).

141. Kearn, C. S., Blake-Palmer, K., Daniel, E., Mackie, K. & Glass, M. Concurrent stimulation of cannabinoid CB1 and dopamine D2 receptors enhances heterodimer formation: A mechanism for receptor cross-talk? *Mol. Pharmacol.* **67**, 1697–1704 (2005).

142. Hojo, M. *et al.* μ-Opioid receptor forms a functional heterodimer with cannabinoid CB1 receptor: Electrophysiological and fret assay analysis. *J. Pharmacol. Sci.* **108**, 308–319 (2008).

143. George, S. R., O'Dowd, B. F. & Lee, S. P. G-protein-coupled receptor oligomerization and its potential for drug discovery. *Nat. Rev. Drug Discov.* **1**, 808–820 (2002).

144. Ferré, S. *et al.* Building a new conceptual framework for receptor heteromers. *Nat. Chem. Biol.* **5**, 131–134 (2009).

145. Jordan, B. A. & Devi, L. A. G-protein-coupled receptor heterodimerization modulates receptor function. *Nature* **399**, 697–700 (1999).

146. Thompson, M. D., Sakurai, T., Rainero, I., Maj, M. C. & Kukkonen, J. P. Orexin receptor multimerization versus functional interactions: Neuropharmacological implications for opioid and cannabinoid signalling and pharmacogenetics. *Pharmaceuticals* **10**, 1–20 (2017).

147. Bagher, A. M. *et al.* Heteromer formation between cannabinoid type 1 and dopamine type

2 receptors is altered by combination cannabinoid and antipsychotic treatments. *J. Neurosci. Res.* **98**, 2496–2509 (2020).

148. Carriba, P. *et al.* Striatal adenosine A2A and cannabinoid CB1 receptors form functional heteromeric complexes that mediate the motor effects of cannabinoids. *Neuropsychopharmacology* **32**, 2249–2259 (2007).

149. Zou, S., Somvanshi, R. K. & Kumar, U. Somatostatin receptor 5 is a prominent regulator of signaling pathways in cells with coexpression of Cannabinoid receptors 1. *Neuroscience* **340**, 218–231 (2017).

150. Viñals, X. *et al.* Cognitive impairment induced by delta9- tetrahydrocannabinol occurs through heteromers between cannabinoid CB1 and serotonin 5-HT2A receptors. *PLoS Biol.* **13**, 1–40 (2015).

151. Coke, C. J. *et al.* Simultaneous activation of induced heterodimerization between CXCR4 chemokine receptor and cannabinoid receptor 2 (CB2) reveals a mechanism for regulation of tumor progression. *J. Biol. Chem.* **291**, 9991–10005 (2016).

152. Berrendero, F., Flores, Á. & Robledo, P. When orexins meet cannabinoids: Bidirectional functional interactions. *Biochem. Pharmacol.* **157**, 43–50 (2018).

153. Sakurai, T. *et al.* Orexins and orexin receptors: A family of hypothalamic neuropeptides and G protein-coupled receptors that regulate feeding behavior. *Cell* **92**, 573–585 (1998).

154. De Lecea, L. *et al.* The hypocretins: Hypothalamus-specific peptides with neuroexcitatory activity. *Proc. Natl. Acad. Sci. U. S. A.* **95**, 322–327 (1998).

155. Mieda, M. & Yanagisawa, M. Sleep, feeding, and neuropeptides: Roles of orexins and

orexin receptors. *Curr. Opin. Neurobiol.* **12**, 339–345 (2002).

156. Forte, N. *et al.* Orexin-A and endocannabinoids are involved in obesity-associated alteration of hippocampal neurogenesis, plasticity, and episodic memory in mice. *Nat. Commun.* **12**, 1–20 (2021).

157. Sakurai, T. The role of orexin in motivated behaviours. *Nat. Rev. Neurosci.* **15**, 719–731 (2014).

158. Kakizaki, M. *et al.* Differential Roles of Each Orexin Receptor Signaling in Obesity. *iScience* **20**, 1–13 (2019).

159. Yin, J. *et al.* Structure and ligand-binding mechanism of the human OX 1 and OX 2 orexin receptors. *Nat. Struct. Mol. Biol.* **23**, 293–299 (2016).

160. Inutsuka, A. *et al.* The integrative role of orexin/hypocretin neurons in nociceptive perception and analgesic regulation. *Sci. Rep.* **6**, 1–15 (2016).

161. Li, T. *et al.* Orexin A alleviates neuroinflammation via OXR2/CaMKKβ/AMPK signaling pathway after ICH in mice. *J. Neuroinflammation* **17**, 1–15 (2020).

162. Zhou, W. *et al.* Activation of orexin system facilitates anesthesia emergence and pain control. *Proc. Natl. Acad. Sci. U. S. A.* **115**, E10740–E10747 (2018).

163. Equihua, A. C., De La Herrán-Arita, A. K. & Drucker-Colin, R. Orexin receptor antagonists as therapeutic agents for insomnia. *Front. Pharmacol.* **4 DEC**, 1–10 (2013).

164. Yin, J., Mobarec, J. C., Kolb, P. & Rosenbaum, D. M. Crystal structure of the human OX2 orexin receptor bound to the insomnia drug suvorexant. *Nature* **519**, 247–250 (2015).

165. Yang, D. *et al.* G protein-coupled receptors: structure- and function-based drug discovery. *Signal Transduct. Target. Ther.* **6**, (2021).

166. Yamamoto, H. *et al.* OX2R-selective orexin agonism is sufficient to ameliorate cataplexy and sleep/wake fragmentation without inducing drug-seeking behavior in mouse model of narcolepsy. *PLoS One* **17**, 1–17 (2022).

167. Evans, R. *et al.* Orexin 2 receptor–selective agonist danavorexton improves narcolepsy phenotype in a mouse model and in human patients. *Proc. Natl. Acad. Sci. U. S. A.* **119**, 1–10 (2022).

168. Jacobson, L. H., Hoyer, D. & de Lecea, L. Hypocretins (orexins): The ultimate translational neuropeptides. *J. Intern. Med.* **291**, 533–556 (2022).

169. Gülck, T. & Møller, B. L. Phytocannabinoids: Origins and Biosynthesis. *Trends Plant Sci.* **25**, 985–1004 (2020).

170. Zagzoog, A. *et al.* In vitro and in vivo pharmacological activity of minor cannabinoids isolated from Cannabis sativa. *Sci. Rep.* **10**, 1–13 (2020).

171. Citti, C. *et al.* Cannabinoid profiling of hemp seed oil by liquid chromatography coupled to high-resolution mass spectrometry. *Front. Plant Sci.* **10**, 1–17 (2019).

172. Andrenyak, D. M., Moody, D. E., Slawson, M. H., Leary, D. S. O. & Haney, M. Determination of Δ-9-Tetrahydrocannabinol (THC), 11-hydroxy-THC, 11-nor-9-carboxy-THC and Cannabidiol in Human Plasma using Gas Chromatography–Tandem Mass Spectrometry. *J. ofAnalytical Toxicol.* **41**, 277–288 (2017).

173. Britch, S. C., Babalonis, S. & Walsh, S. L. Cannabidiol : pharmacology and therapeutic

targets. *Psychopharmacology (Berl).* **238**, 9–28 (2021).

174. Nadulski, T. *et al.* Simultaneous and sensitive analysis of THC, 11-OH-THC, THC-COOH, CBD, and CBN by GC-MS in plasma after oral application of small doses of THC and cannabis extract. *J. Anal. Toxicol.* **29**, 782–789 (2005).

175. Huestis, M. A. Human Cannabinoid Pharmacokinetics. *Chem Biodivers* **4**, 1770–1804 (2007).

176. Hanuš, L. & Ujváry, I. Human Metabolites of Cannabidiol : A Review on Their Formation, Biological Activity and Relevance in Therapy. *Cannabis Cannabinoid Res.* **1**, 90–101 (2016).

177. Lucas, C. J., Galettis, P. & Schneider, J. The pharmacokinetics and the pharmacodynamics of cannabinoids. *Br J Clin Pharmacol* **84**, 2477–2482 (2018).

178. Yamaori, S., Okamoto, Y., Yamamoto, I. & Watanabe, K. Cannabidiol, a Major Phytocannabinoid, As a Potent Atypical Inhibitor. *Drug Metab. Dispos.* **39**, 2049–2056 (2011).

179. Huestis, M. A. Pharmacokinetics and metabolism of the plant cannabinoids, Δ9-tetrahydrocannibinol, cannabidiol and cannabinol. in *Handbook of Experimental Pharmacology* (ed. Pertwee, R. G.) vol. 168 657–690 (2005).

180. Saenz, S. R., Lewis, R. J., Angier, M. K. & Wagner, J. R. Postmortem Fluid and Tissue Concentrations of THC, 11-OH-THC and THC-COOH. *J. ofAnalytical Toxicol.* **41**, 508–516 (2017).

181. Huestis, M. A., Henningfield, J. E. & Cone, E. J. Blood Cannabinoids: I . Absorption of

THC and Formation of 11-OH-THC and THCCOOH During and After Smoking Marijuana. *J. Anal. Toxicol.* **16**, 276–282 (1992).

182. McCartney, D. *et al.* Cannabidiol and Sports Performance : a Narrative Review of Relevant Evidence and Recommendations for Future Research. *Sport. Med Open* **6**, 27 (2020).

183. Taylor, L., Crockett, J., Tayo, B. & Morrison, G. A Phase 1, Open-Label, Parallel-Group, Single-Dose Trial of the Pharmacokinetics and Safety of Cannabidiol (CBD) in Subjects With Mild to Severe Hepatic Impairment. *J Clin Pharmacol* **59**, 1110–1119 (2019).

184. Kevin, R. C. *et al.* A validated method for the simultaneous quantification of cannabidiol, Δ9-tetrahydrocannabinol, and their metabolites in human plasma and application to plasma samples from an oral cannabidiol open-label trial. *Drug Test. Anal.* **13**, 614–627 (2021).

185. Ceni, C. *et al.* Novel Potent and Selective Agonists of the GPR55 Receptor Based on the 3-Benzylquinolin-2(1H)-One Scaffold. *Pharmaceuticals* **15**, 1–20 (2022).

186. Gado, F. *et al.* Design, Synthesis, and Biological Activity of New CB2 Receptor Ligands: From Orthosteric and Allosteric Modulators to Dualsteric/Bitopic Ligands. *J. Med. Chem.* **65**, 9918–9938 (2022).

187. Gado, F. *et al.* Synthesis and In Vitro Characterization of Selective Cannabinoid CB2 Receptor Agonists: Biological Evaluation against Neuroblastoma Cancer Cells. *Molecules* **27**, (2022).

188. Ferrisi, R. *et al.* Design, synthesis and biological evaluation of novel orthosteric-allosteric

ligands of the cannabinoid receptor type 2 (CB2R). *Front. Chem.* **10**, (2022).

189. Garai, S. *et al.* Application of Fluorine- And Nitrogen-Walk Approaches: Defining the Structural and Functional Diversity of 2-Phenylindole Class of Cannabinoid 1 Receptor Positive Allosteric Modulators. *J. Med. Chem.* **63**, 542–568 (2020).

190. LI-COR. In-Cell Western™ Assay. https://www.licor.com/bio/applications/in-cell-western-assay.

191. Laprairie, R. B., Bagher, A. M., Kelly, M. E. M., Dupré, D. J. & Denovan-Wright, E. M. Type 1 cannabinoid receptor ligands display functional selectivity in a cell culture model of striatal medium spiny projection neurons. *J. Biol. Chem.* **289**, 24845–24862 (2014).

192. Laprairie, R. B. *et al.* Indomethacin Enhances Type 1 Cannabinoid Receptor Signaling. *Front. Mol. Neurosci.* **12**, 1–13 (2019).

193. DiscoverX. HitHunter® cAMP Assay Kit User Manual. https://www.discoverx.com/tools-resources/document-resource-library/documents/user-manual-hithunter-camp-assay-for-small-molecul (2017).

194. DiscoverX. PathHunter®Detection Kit User Manual. https://www.discoverx.com/tools-resources/document-resource-library/documents/user-manual-pathhunter-β-arrestin-assay-for-gpcr-c (2018).

195. Invitrogen. Lipofectamine™ 3000 Reagent Protocol. (2016).

196. Black, J. & Leff, P. Operational models of pharmacological agonism. *Proc. R. Soc. London. Ser. B, Biol. Sci.* **220**, 141–162 (1983).

197. Kolb, P. *et al.* Community guidelines for GPCR ligand bias: IUPHAR review 32. *Br. J.*

Pharmacol. **179**, 3651–3674 (2022).

198. Henstridge, C. M. *et al.* GPR55 ligands promote receptor coupling to multiple signalling pathways. *Br. J. Pharmacol.* **160**, 604–614 (2010).

199. Oka, S., Nakajima, K., Yamashita, A., Kishimoto, S. & Sugiura, T. Identification of GPR55 as a lysophosphatidylinositol receptor. *Biochem. Biophys. Res. Commun.* **362**, 928–934 (2007).

200. Rempel, V. *et al.* Antagonists for the orphan G-protein-coupled receptor GPR55 based on a coumarin scaffold. *J. Med. Chem.* **56**, 4798–4810 (2013).

201. Apweiler, M. *et al.* Targeting oxidative stress: Novel coumarin-based inverse agonists of GPR55. *Int. J. Mol. Sci.* **22**, (2021).

202. Schoeder, C. T. *et al.* Development of chromen-4-one derivatives as (Ant)agonists for the lipid-activated G Protein-Coupled Receptor GPR55 with Tunable Efficacy. *ACS Omega* **4**, 4276–4295 (2019).

203. Kotsikorou, E. *et al.* Identification of the GPR55 antagonist binding site using a novel set of high-potency GPR55 selective ligands. *Biochemistry* **52**, 9456–9469 (2013).

204. Sharir, H. & Abood, M. E. Pharmacological characterization of GPR55, a putative cannabinoid receptor. *Pharmacol. Ther.* **126**, 301–313 (2010).

205. de Ligt, R. A., Kourounakis, A. P. & IJzerman, A. P. Inverse agonism at G protein-coupled receptors: (patho)physiological relevance and implications for drug discovery. *Br J Pharmacol* **130**, 1–12 (2000).

206. Kenakin, T. Inverse, protean, and ligand-selective agonism: matters of receptor

conformation. *FASEB J* **15**, 598–611 (2001).

207. Milligan, G. & Bond, R. A. Inverse agonism and the regulation of receptor number. *Trends Pharmacol. Sci.* **18**, 468–474 (1997).

208. Berg, K. A. & Clarke, W. P. Making sense of pharmacology: Inverse agonism and functional selectivity. *Int. J. Neuropsychopharmacol.* **21**, 962–977 (2018).

209. Uba, A. I., Aluwala, H., Liu, H. & Wu, C. Elucidation of partial activation of cannabinoid receptor type 2 and identification of potential partial agonists: Molecular dynamics simulation and structure-based virtual screening. *Comput. Biol. Chem.* **99**, 107723 (2022).

210. Han, S. *et al.* Design, syntheses, structure - Activity relationships and docking studies of coumarin derivatives as novel selective ligands for the CB2 receptor. *Eur. J. Med. Chem.* **93**, 16–32 (2015).

211. Mohr, F. *et al.* Synthesis and SAR evaluation of coumarin derivatives as potent cannabinoid receptor agonists. *Eur. J. Med. Chem.* **220**, (2021).

212. Behrenswerth, A. *et al.* Synthesis and pharmacological evaluation of coumarin derivatives as cannabinoid receptor antagonists and inverse agonists. *Bioorganic Med. Chem.* **17**, 2842–2851 (2009).

213. Lingerfelt, M. A. *et al.* Identification of Crucial Amino Acid Residues Involved in Agonist Signaling at the GPR55 Receptor. *Biochemistry* **56**, 473–486 (2017).

214. Congreve, M., de Graaf, C., Swain, N. A. & Tate, C. G. Impact of GPCR Structures on Drug Discovery. *Cell* **181**, 81–91 (2020).

215. Kenakin, T. & Christopoulos, A. Signalling bias in new drug discovery: Detection,

quantification and therapeutic impact. *Nat. Rev. Drug Discov.* **12**, 205–216 (2013).

216. Polini, B. *et al.* Positive allosteric modulation of CB1 and CB2 cannabinoid receptors enhances the neuroprotective activity of a dual CB1R/CB2R orthosteric agonist. *Life* **10**, 1–14 (2020).

217. Schmid, C. L. *et al.* Bias Factor and Therapeutic Window Correlate to Predict Safer Opioid Analgesics. *Cell* **171**, 1165.e13-1175.e13 (2017).

218. Shonberg, J., Scammells, P. J. & Capuano, B. Design strategies for bivalent ligands targeting GPCRs. *ChemMedChem* **6**, 963–974 (2011).

219. Hiller, C., Kühhorn, J. & Gmeiner, P. Class A G-protein-coupled receptor (GPCR) dimers and bivalent ligands. *J. Med. Chem.* **56**, 6542–6559 (2013).

220. Battiti, F. O. *et al.* The Significance of Chirality in Drug Design and Synthesis of Bitopic Ligands as D3 Receptor (D3R) Selective Agonists. *J. Med. Chem.* **62**, 6287–6314 (2019).

221. Pandey, P., Roy, K. K. & Doerksen, R. J. Negative allosteric modulators of cannabinoid receptor 2: protein modeling, binding site identification and molecular dynamics simulations in the presence of an orthosteric agonist. *J. Biomol. Struct. Dyn.* **38**, 32–47 (2020).

222. Manera, C. *et al.* Rational design, synthesis, and pharmacological properties of new 1,8-naphthyridin-2(1H)-on-3-carboxamide derivatives as highly selective cannabinoid-2 receptor agonists. *J. Med. Chem.* **52**, 3644–3651 (2009).

223. Lucchesi, V. *et al.* CB2-selective cannabinoid receptor ligands: Synthesis, pharmacological evaluation, and molecular modeling investigation of 1,8-naphthyridin-

2(1 H)-one-3-carboxamides. *J. Med. Chem.* **57**, 8777–8791 (2014).

224. Gado, F. *et al.* Identification of the First Synthetic Allosteric Modulator of the CB 2 Receptors and Evidence of Its Efficacy for Neuropathic Pain Relief. *J. Med. Chem.* **62**, 276–287 (2019).

225. Arena, C. *et al.* The endocannabinoid system dual-target ligand N-cycloheptyl-1,2-dihydro-5-bromo-1-(4-fluorobenzyl)-6-methyl-2-oxo-pyridine-3-carboxamide improves disease severity in a mouse model of multiple sclerosis. *Eur. J. Med. Chem.* **208**, (2020).

226. Latorraca, N. R. *et al.* Molecular mechanism of GPCR-mediated arrestin activation. *Nature* (2018).

227. Nguyen, P. T. *et al.* β-Arrestin2 regulates cannabinoid CB 1 receptor signaling and adaptation in a central nervous system region-dependent manner. *Biol. Psychiatry* **71**, 714–724 (2012).

228. Bohn, L. M., Gainetdinov, R. R., Lin, F.-T., Lefkowitz, R. J. & Caron, M. G. μ-Opioid receptor desensitization by β-arrestin-2 determines morphine tolerance but not dependence. *Nature* **408**, 720–723 (2000).

229. Slosky, L. M., Caron, M. G. & Barak, L. S. Biased Allosteric Modulators: New Frontiers in GPCR Drug Discovery. *Trends Pharmacol. Sci.* **42**, 283–299 (2021).

230. Ahn, K. H., Mahmoud, M. M. & Kendall, D. A. Allosteric modulator ORG27569 induces CB1 cannabinoid receptor high affinity agonist binding state, receptor internalization, and Gi protein-independent ERK1/2 kinase activation. *J. Biol. Chem.* **287**, 12070–12082 (2012).

231. Imperatore, R. *et al.* Overlapping distribution of orexin and endocannabinoid receptors and their functional interaction in the brain of adult zebrafish. *Front. Neuroanat.* **12**, 1–16 (2018).

232. Flores, Á., Julià-Hernández, M., Maldonado, R. & Berrendero, F. Involvement of the orexin/hypocretin system in the pharmacological effects induced by Δ9-tetrahydrocannabinol. *Br. J. Pharmacol.* **173**, 1381–1392 (2016).

233. Ibrahim, M. M. *et al.* CB 2 cannabinoid receptor activation produces antinociception by stimulating peripheral release of endogenous opioids. *PNAS* **22**, 3093–3098 (2005).

234. Okumura, T., Nozu, T., Kumei, S. & Ohhira, M. Role of the cannabinoid signaling in the brain orexin- and ghrelin-induced visceral antinociception in conscious rats. *J. Pharmacol. Sci.* **137**, 230–232 (2018).

235. Ogawa, Y. *et al.* Peripherally administered orexin improves survival of mice with endotoxin shock. *Elife* **5**, 1–18 (2016).

236. Davies, J. *et al.* Orexin receptors exert a neuroprotective effect in Alzheimer's disease (AD) via heterodimerization with GPR103. *Sci. Rep.* **5**, 1–12 (2015).

237. Xin, Q., Xu, F., Taylor, D. H., Zhao, J. fu & Wu, J. The impact of cannabinoid type 2 receptors (CB2Rs) in neuroprotection against neurological disorders. *Acta Pharmacol. Sin.* **41**, 1507–1518 (2020).

238. Jäntti, M. H., Mandrika, I. & Kukkonen, J. P. Human orexin/hypocretin receptors form constitutive homo- and heteromeric complexes with each other and with human CB1 cannabinoid receptors. *Biochem. Biophys. Res. Commun.* **445**, 486–490 (2014).

239. Raïch, I. *et al.* Antagonization of OX1 Receptor Potentiates CB2 Receptor Function in Microglia from APPSw/Ind Mice Model. *Int. J. Mol. Sci.* **23**, 12801 (2022).

240. Ellis, C. & The Nature Reviews Drug Discovery GPCR Questionnaire Participants. The state of GPCR research in 2004. *Nat Rev Drug Discov* **3**, 577–626 (2004).

241. Bagher, A. M., Laprairie, R. B., Toguri, J. T., Kelly, M. E. M. & Denovan-Wright, E. M. Bidirectional allosteric interactions between cannabinoid receptor 1 (CB1) and dopamine receptor 2 long (D2L) heterotetramers. *Eur. J. Pharmacol.* **813**, 66–83 (2017).

242. Corroon, J. & Phillips, J. A. A Cross-Sectional Study of Cannabidiol Users. *Cannabis cannabinoid Res.* **3**, 152–161 (2018).

243. Whiting, P. F. *et al.* Cannabinoids for medical use: A systematic review and meta-analysis. *JAMA - J. Am. Med. Assoc.* **313**, 2456–2473 (2015).

244. Zhang, Z. & Tang, W. Drug metabolism in drug discovery and development. *Acta Pharm. Sin. B* **8**, 721–732 (2018).

245. Baglot, S. L. *et al.* Pharmacokinetics and central accumulation of delta-9-tetrahydrocannabinol (THC) and its bioactive metabolites are influenced by route of administration and sex in rats. *Sci. Rep.* **11**, (2021).

246. Grotenhermen, F. Pharmacokinetics and Pharmacodynamics of Cannabinoids. *Clin Pharmacokinet* **42**, 327–360 (2003).

247. Beers, J. L., Fu, D. & Jackson, K. D. Cytochrome P450–catalyzed metabolism of cannabidiol to the active metabolite 7-hydroxy-cannabidiol. *Drug Metab. Dispos.* **49**, 882–891 (2021).

248. Jones, N. A. *et al.* Cannabidiol displays antiepileptiform and antiseizure properties in vitro and in vivo. *J. Pharmacol. Exp. Ther.* **332**, 569–577 (2010).

249. Pigliasco, F. *et al.* Cannabidiol, Δ9-tetrahydrocannabinol, and metabolites in human blood by volumetric absorptive microsampling and LC-MS/MS following controlled administration in epilepsy patients. *Front. Pharmacol.* **13**, (2022).

250. Ujváry, I. & Grotenhermen, F. 1-Nor-9-carboxy-Δ 9-tetrahydrocannabinol-a ubiquitous yet underresearched cannabinoid. A re-view of the literature. *Cannabinoids* **9**, 1–8 (2014).

251. Lowin, T. *et al.* Cannabidiol (CBD): a killer for inflammatory rheumatoid arthritis synovial fibroblasts. *Cell Death Dis.* **11**, 1–11 (2020).

252. Patricio, F., Morales-Andrade, A. A., Patricio-Martínez, A. & Limón, I. D. Cannabidiol as a Therapeutic Target: Evidence of its Neuroprotective and Neuromodulatory Function in Parkinson's Disease. *Front. Pharmacol.* **11**, (2020).

253. Kenakin, T. Is the quest for signaling bias worth the effort? *Mol. Pharmacol.* **93**, 266–269 (2018).

254. Guo, S., Zhao, T., Yun, Y. & Xie, X. Recent progress in assays for GPCR drug discovery. *Am. J. Physiol. - Cell Physiol.* **323**, C583–C594 (2022).

255. Pedersen, M. H. *et al.* A novel luminescence-based β-arrestin recruitment assay for unmodified receptors. *J. Biol. Chem.* **296**, 100503 (2021).

256. Gundry, J., Glenn, R., Alagesan, P. & Rajagopal, S. A practical guide to approaching biased agonism at G protein coupled receptors. *Front. Neurosci.* **11**, 1–6 (2017).

257. Hill, J. D., Zuluaga-Ramirez, V., Gajghate, S., Winfield, M. & Persidsky, Y. Activation of

GPR55 increases neural stem cell proliferation and promotes early adult hippocampal neurogenesis. *Br. J. Pharmacol.* **175**, 3407–3421 (2018).

258. Yang, X. *et al.* Molecular mechanism of allosteric modulation for the cannabinoid receptor CB1. *Nat. Chem. Biol.* **18**, 831–840 (2022).

259. Rajagopal, S. *et al.* Quantifying ligand bias at seven-transmembrane receptors. *Mol. Pharmacol.* **80**, 367–377 (2011).

260. Balenga, N. A. *et al.* Heteromerization of GPR55 and cannabinoid CB2 receptors modulates signalling. *Br. J. Pharmacol.* **171**, 5387–5406 (2014).

261. Stein, C. Targeting pain and inflammation by peripherally acting opioids. *Front. Pharmacol.* **4**, 1–3 (2013).

262. Roques, B. P., Fournié-Zaluski, M. C. & Wurm, M. Inhibiting the breakdown of endogenous opioids and cannabinoids to alleviate pain. *Nat. Rev. Drug Discov.* **11**, 292–310 (2012).